The University of Calgary

Optimal Control and Optimal Controllers in Vehicle Dynamics

by

Lawrence Gunn

A Thesis
Submitted to the Faculty of Graduate Studies
in Partial Fulfillment of the Requirements for the
Degree of Master of Science

Department of Mechanical Engineering

Calgary, Alberta
June, 1990

ISBN 0-315-61966-X

The University of Calgary
Faculty of Graduate Studies

The undersigned certify that they have read, and recommend to the Faculty of Graduate Studies for acceptance, a thesis entitled, "Optimal Control and Optimal Controllers in Vehicle Dynamics" submitted by Lawrence Gunn in partial fulfillment of the requirements for the degree of Master of Science.

Supervisor
E.C. Mikulcik, Ph.D.
Department of Mechanical Engineering

J.F. Morrall, Ph.D.
Department of Civil Engineering

O. Vinogradov, Ph.D.
Department of Mechanical Engineering

Date July 20, 1990

Abstract

The problem addressed here is to determine, theoretically, the control that a driver might supply to a vehicle to follow a predefined path. The solution method involves determination of the control by optimal control techniques sufficiently general to be applicable to a wide range of dynamic control problems. While optimal control has been applied in the past to linear and simple nonlinear vehicle models, the problem of the general solution for both linear and nonlinear problems has not been adequately analyzed. Here, numerical optimization techniques are adapted for use with linear and nonlinear vehicle models and cost functions. Two approaches are used. The first involves representation of the control as a series of pulses. The second uses a feedback controller which utilizes the vehicle's anticipated error as the input signal to the controller. The controls produced are compared with results from a test vehicle using a driver. The results indicate that the optimization using the controller produces an only slightly inferior cost function value, but the control showed a better correspondence with that produced by the driver. While the steering control inputs differ from one type to another, the trajectory following capabilities are about equal, indicating that there may be more than one way of driving through a manoeuvre successfully. The optimal control techniques produce the same general form of steering input as the driver. More detailed testing using a more accurate vehicle, and driver modelling and testing must be done to confirm this correspondence, and to clarify any dissimilarities.

Acknowledgements

The original idea to make extensive use of optimal control in vehicle dynamics problems came from my thesis supervisor, Dr. E.C. Mikulcik. He tutored me on the basic principals of vehicle dynamics, challenged me in our many discussions, and most importantly, allowed me a great deal of freedom in the direction and scope of my thinking and work. He not only made the thesis possible, but also very enjoyable.

The electronic instrumentation system used for the vehicle testing was designed by Jack Dyck of Valmet Automation Ltd. We had known each other for a few years when I mentioned the need for an inexpensive data acquisition system for my thesis work. Jack volunteered to design a small microprocessor based instrumentation system for me if I would build it. He spent many hours in the design work, tutoring me on digital component construction methods and finally in assisting in the debugging of the system. I am greatly indebted to him, not only for the design work but also for teaching me how to work with and design digital electronic systems.

The actual microprocessor board used was supplied by Valmet Automation Ltd. They supplied me with the CPU card, documentation and diagnostic software. The processor and software worked flawlessly and I am very appreciative of there contribution to this work.

There were many people who helped with this thesis. In particular, Per Nese, Larry Jensen, Warren Flaman, Piotr Grabinski, Arthur Springer and various machinists and technicians in the Faculty of Engineering provided assistance with the experimental or computer work. Technical assistance and many good conversations were had with Brian Will and with Phil Kristensen of AeroTech Specialty Welding and Fabrication Ltd. Cathy Turner was always available to criticize and correct my grammar. To those who helped but are not mentioned here, I offer my apologies and extend my appreciation.

to my mother, Eugenia

Table of Contents

List of Tables

List of Figures

List of Symbols

A	state associated matrix of Rosen's method.
B	control associated matrix of Rosen's method.
c	matrix of Rosen's method associated with initial conditions and nonlinearities.
c	cornering stiffness of tires which is the slope of the side force versus slip angle curve.
$C_{u/o}$	coefficient of understeer/oversteer
c_1, c_2	coefficients used in determining the error function shaped lane change
D	matrix which determines the contribution of a control at any time in Rosen's method.
$F_{fr}, F_{fl}, F_{rr}, F_{rl}$	the lateral tire forces for the front right and left and rear right and left, respectively.
F_l	lateral tire force
$g(), h()$	functions in the cost functions which represent the cost to be integrated for the length of the manoeuvre and part evaluated using end conditions, respectively.
I	Moment of inertia of vehicle about the vertical axis
J, J_D	the cost function value and its discrete approximation counterpart.
k	time interval in discrete analysis
K_α	torsional stiffness of tire
l_f, l_r	distance from vehicle center of mass to front and rear axles
l	length of tire contact patch

m	mass of vehicle
N	the number of time periods into which total time of event is divided.
R_e, R_s	the coefficients for the tracking error and steering magnitude in the cost function.
t, t_o, t_f	time, initial time, and final time.
t_f, t_r	distance from one front wheel to the other and from one rear wheel to the other.
$\mathbf{u}, u$	the control input, typically the steer angle of the front wheel. This can be a continuous input, $\mathbf{u}(t)$, or a vector of discrete values, $\mathbf{u}(k\Delta t)$.
w	width of tire contact patch
$\mathbf{x}, x_n$	the state values
X, x	the global and local coordinate axes used for tire and vehicle models
x'	the coordinate axes attached to the axle, used for tire model
x_H	in Rosen's method, part of solution which does not depend upon control values.
Y, y	the global and local coordinate axes used for tire and vehicle models
y'	the coordinate axes attached to the axle, used for tire model
α	tire slip angle
θ	rotational angle measured as rotation of local coordinate system relative to the global coordinate system.
μ_f, μ_r	tire coefficient of friction
τ_m	shear stress between tire surface and road

1 Introduction

1.1 Vehicle Dynamics

Vehicle dynamics is the study of motion and control of conveyances used on land. Given the history of engineering as a whole, major work in the field is fairly recent, corresponding to the development of motorized vehicles.

Initial models of vehicle motion were quite simple, typically consisting of linear models with linear tire characteristics [1,2,3]. Control systems theory existed to describe the motion and control of linear control systems, providing very useful information about the vehicle's response characteristics and stability from simple models. From this type of analysis such standard vehicle dynamics terms as 'understeer' and 'oversteer' were coined.

Despite their effectiveness on the simpler level, linear models could not describe the behavior of vehicles in which nonlinearities of the system occurred significantly. In general, information on the stability, controllability, or exact motion of nonlinear systems is very difficult to find. However, it is possible to solve for the motion of a vehicle using numerical methods. With the arrival of the digital computer, numerical solutions to the equations of motion became feasible.

The topic of this thesis is the control of vehicles, or, more specifically, simulation of the control applied by a human driver. The ability to simulate driver behavior is of great consequence to the simulation, design, and control of road vehicles, and the design of roadways.

Simulating the driver is useful in computer assisted design of vehicles. For example, a car manufacturer may wish to change some aspect of the tire or suspension geometry. Physically testing the vehicle can be a long and expensive process. Computer simulations could be done to test the motion of the vehicle, but if the driver is not also simulated, tests have limited validity.

Another way of using driver simulation is in the design of roadways. For instance, the length of merge lanes or the curvature of corners should be designed for a certain limit of the driver's ability. Simulation allows consistent, unbiased limits to be maintained. A standard method of roadway design can then be implemented.

A third example is the use of simulation methods to produce control systems capable of driving real vehicles, such as on automated highways. The control of the vehicle is complex, particularly in the event of an emergency. A controller capable of optimal control would be essential to the safety of these highways.

Some recent attempts to approximate the driver's control inputs will be expanded on here, using optimal control and complex control systems produced by the use of optimization methods. The goal is to expand on past techniques to produce a reasonable approximation of human behavior when piloting a vehicle. To measure the success of these methods, the controls will be compared to tests done using a real vehicle and driver.

1.2 Past Use of Optimal Control in Vehicle Dynamics

The majority of work done to simulate the control inputs of drivers has been in deriving feedback controllers for the steering of vehicles. The controller is often designed as a model of the human, and is not so concerned with steering for a particular manoeuvre; therefore its description will be brief, as the use of controllers in this thesis will be primarily in producing a near optimal control for a unique manoeuvre.

Driver models can generally be divided into three main categories: the quasi-linear model, the predictive model, and the optimal control model [4]. The quasi-linear models [5-8] represent the driver with a frequency-dependent gain and phase, based largely upon previously known physiological information. The predictive models [9,10] follow along the same line as the quasi-linear models, but assume that the driver can preview the road ahead of its present position. The third type of model, the optimal control model, is based upon Kalman's optimal control theories [4,11]. There are many other models which combine elements of all of the above [12-14].

For example, MacAdam [14] utilizes a combination of 'cross-over' model (as derived from the quasi-linear model) with an optimal preview control which has a transport delay built into the controller. The general weakness of these models is that they are only designed to follow straight or almost straight line paths.

A model which does not easily fit the above categories is that of Hayhoe [15], who used neurophysiological theory about human motor control to produce a cerebellar model of the driver. Hayhoe used an optimization procedure to change various coefficients in a small simulated cerebellar network. The model was capable of driving through relatively straight manoeuvres and 90° corners.

Unlike controllers, optimal control has seldom been used for vehicles. Optimal control differs from the controllers in that the control is produced by the use of an algorithm, often iterative in nature, and does not use a controller in the standard sense of the word. It often involves complex mathematics requiring exact solutions, difficult or impossible to find, or lengthy numerical solutions to trajectory-oriented problems. The effort required to arrive at these solutions is rewarded by high-quality results. Optimal control has probably proved itself most useful in the areas of aeronautical and aerospace design.

Some of the earliest work was done by Zanten and Krauter [16,17] and covered the optimal control of a tractor-semitrailer truck with emphasis on braking. The results were achieved by variational methods. Work in the area of general optimal control with vehicles has been done by E.C. Mikulcik and his associates. This paper is based on work begun by E.C. Mikulcik using optimal control in the path tracking problem for automobiles. In his early work, he was assisted by H. Hatwal, who used linear optimal control to determine the steering inputs required to drive a linear vehicle model through an obstacle avoidance manoeuvre. He also employed a variational approach which allowed for the use of nonlinear vehicles with well-behaved nonlinear equations of motion [18]. In a subsequent paper [19], the ability to control tractive as well as steering control inputs was included. The primary disadvantage of

the variational method was that its algorithm required complex and tedious manipulations of the equations of motion, often rendering both complex equations of motion and, in particular, complex manoeuvre trajectories unusable.

1.3 Thesis Review

The main goal of this thesis is to develop numerical procedures to determine a control which, when applied to its intended vehicle, allows the vehicle to follow the intended trajectory with reasonable precision. The ideal control is one in which the vehicle follows the trajectory while reasonably representing the control that a driver might have in a similar situation. The desired control is calculated using optimal control methods. Chapter 2 discusses the motivation for using optimal control and why aspects of it may be likened to the driver's determination of the actual control.

Chapters 3 and 4 describe the exact methods of formulating and solving the optimal control problem. The procedure is generally as follows: for a particular manoeuvre, a cost function is set up. The cost is an integral with respect to time, which increases with deviation of the vehicle from the desired path and increase of steering input. A steering input must be determined which minimizes the value of the cost function. The vehicle goes through a manoeuvre with a specified steering input, and from this is determined the cost function value. The steering input is then changed in the hope of minimizing the cost; the manoeuvre is run again and the new cost calculated. This procedure continues until the cost can be decreased no more. This is then considered the optimal steering input. It should be noted that a change in vehicle or manoeuvre will require this procedure to be repeated and a new steering input found.

Because numerical methods are used, the steering must be represented appropriately. This is discussed in chapter 3, first with steering represented as a series of stepped inputs, the optimization procedure determining the height of the steps; secondly, the control is produced by a feedback controller. This is an identical procedure to the first, except that instead of determining step sizes, now the parameters of the controller are determined. The controller is very simple and has no access to information as to the cost value.

Chapter 4 describes the minimization procedures used to find the optimal control, a variety of standard and unusual descent techniques. As well, a method is presented for determining the gradient of the cost function numerically.

In order to determine the degree to which optimal control mirrors human driving patterns, tests were done on a real vehicle being driven through two types of manoeuvres. Details of the vehicle and the manoeuvres are given in chapter 5. The results of these tests are presented in chapter 6. A discussion and comparison of the test results and the optimal control is given in chapter 7. From the conclusions in chapter 8 it becomes apparent that:

1) the optimal control is capable of producing a steering input which will guide the vehicle through the manoeuvres

2) the two ways of representing the optimal control (as a series of pulses and as a controller) produce steering inputs which, while similar, are not exact; both prove able to follow the trajectories equally well

3) the controls produced by optimal control compare favorably with the controls supplied by the driver.

2 Optimal Control Used for Driver Modelling

The equations of motion for a vehicle may be written as

$$\dot{\mathbf{x}} = \mathbf{a}(\mathbf{x}, \mathbf{u}, t) \tag{2.1}$$

where $\mathbf{x}$ is the state vector for the vehicle, $\mathbf{u}$ is the control vector, and t is time. A cost function may be written

$$J = \int_{t_o}^{t_f} g(\mathbf{x}, \mathbf{u}, t)dt \tag{2.2}$$

where $g(\mathbf{x}, \mathbf{u}, t)$ is any function desired and is a measure of performance. There will be a control $\mathbf{u}^*$ which will minimize the cost $\mathbf{J}$. This is referred to as the optimal control.

The intention is to apply the concepts of optimal control to the driving of a vehicle to determine if the optimal control is similar to the control applied by a driver. This section will discuss optimal control and the motivation for using it to simulate a driver.

2.1 Optimal Control

One of the most often used methods for emulating the inputs of a driver is to construct a mathematical model of the driver. For simple or slow manoeuvres this is not difficult, but for faster, more complex manoeuvres the situation changes. The human control system is extremely complicated, capable not only of viewing the desired trajectory ahead of the vehicle, but of bringing to the situation information about past experience which affects interpretation of any control inputs given at that moment. A controller that merely reacts to the present state of the vehicle does not do justice to the complexity of the human.

It is precisely man's complexity that may justify the belief that he is capable of near-optimal control. He is able to drive fairly efficiently through a manoeuvre, keeping to the path he wishes to follow while not expending much more energy than

necessary. We could say that the human is capable of balancing errors in tracking and expenditure of energy. Of course, there are limits; as the speed of response required by a manoeuvre increases, the ability to respond appropriately decreases.

If we accept the idea that the driver uses a near-optimal control, the theory of optimal control may provide the tools necessary to simulate it. It will be optimal in the sense that it will minimize or maximize a cost function. If this cost function can be made to reflect the same performance measure as that of the driver, then the theoretical optimal control should be the same as the actual driver's control.

Given a system of equations describing the vehicle's motion (equation 2.1), the control, $\mathbf{u}^*$, which minimizes the cost function

$$J = \int_{t_o}^{t_f} g(\mathbf{x}, \mathbf{u}, t)dt \tag{2.3}$$

should be the same as the control of the driver if our performance measure, $g(\mathbf{x}, \mathbf{u}, t)$ is the same as that of the driver. Of course, there are performance limits on the control that the driver provides, accounted for in the cost function or in the form of constraints. For the purposes of this thesis we will consider this measure to be quite simple, concerned only with tracking accuracy and amount of steering input. Undoubtedly, the driver's real performance measure is more complex than is indicated by this cost function.

3 Representation of an Optimal Control

When the term 'optimization' is used with respect to control systems, it usually refers to the existence of the control or controls u^* which, when applied to a system, either minimizes or maximizes a cost function J. For complex systems (those with nonlinear equations of motion), determining an exact solution to the minimization problem is difficult or impossible, so one must resort to numerical methods. There are two distinctions to the solution method: the representation of the control, and how to minimize using that representation. The former will be dealt with in this chapter.

3.1 Segmented Optimal Control

A standard method of approximating a continuous control function is to represent it as a series of pulses defined by their magnitude, the time of their initiation, and their final time. If the initial and final times are not variable, then finding an optimal control means merely determining the magnitudes of the various pulses. As the number of pulses increases, the approximation of the continuous control improves.

Implementing this method in an optimal control problem is straightforward and leaves much room for variations of technique, allowing for higher accuracy with less computational effort. For instance, if there is a time when the rate of change in control value is small, then there may be fewer pulses per unit time. At times when the control's rate of change is large, there may be many. Another alternative is to smooth the function so that the optimal control is continuous, but its derivatives are not. Also, interpolation functions may be employed to give a smooth first or second derivative. Simple pulses will be used exclusively here.

3.2 Controllers Designed Using Optimal Procedures

Complex control systems have some type of controller which receives a signal and has a control value as its output. Often the output state of the system is fed back to the input of the controller, where it is subtracted from a signal containing the

desired trajectory. This signal is then used to calculate the output control. A feedback controller can be used to drive a vehicle along a specified trajectory. In the simplest case, the error signal input into the controller is the distance between the desired trajectory and the actual position. The controller, for which the output is the steering angle, is proportional, the error signal being multiplied by a constant and the resulting value output as the control. The gain of the proportional control must, of course, be determined. More complex controllers require that more than one parameter be determined.

The parameters defining the controller can be determined using an optimization procedure similar to that used for finding an optimal control. Suppose we are given a manoeuvre which the vehicle must negotiate and a cost function which sums the tracking error over the interval of time required to complete the manoeuvre. The controller has a set of parameters which affect how the vehicle is steered. The optimization procedure changes the values of the parameters affecting the controller in a manner which decreases the cost function. The changes continue until a set of parameter values is found; any change in these values causes the cost function to increase. Hence this controller is optimized for this manoeuvre for the cost function used. The controller so produced will be referred to as an optimal controller.

In general, the control produced by an optimized controller is not the optimal control $\mathbf{u}^*$. However, as the complexity of the controller increases, control will likely be closer to optimal. As the optimization procedures used here do not require linearity, any imaginable control structure is possible, though some controllers will be superior to others.

Because a vehicle requires a certain amount of time to respond to a control input, the control produced by a single proportional controller taking its error from the current position alone is very poor. A variation is to take the expected error at some distance in the future as the input signal. This is referred to as 'preview control'. As an example, the error may be calculated by projecting the present direction of travel to a point some distance ahead, determining the distance from this point to the desired trajectory, and using the distance between these values as the input to the controller.

The controller then produces a control for the time that the error is expected to occur. Usually, utilizing the future error greatly improves the quality of the control. The controller employed here senses the error at several distances in the future. Each error is then multiplied by a separate constant and the values summed.

One of the primary advantages of the optimized controller is that only a small number of parameters need be optimized. An optimized controller using only a few parameters may produce a control which is equivalent to an optimal control solution having hundreds of segments. Not only is the solution found sooner, but computer memory requirements are significantly reduced. Also, as will be shown later, the optimized controller generally produces a control that is more like the driver than does the optimal control.

3.3 Combining Optimal Control, Controllers and Parameter Optimization

Optimal control is very flexible, with many variations possible. Different techniques may be used simultaneously. Because both the optimal control and optimized controllers depend only on parameters, they may both be used in the same optimization. For example, an optimized controller may be used to determine the steering, while optimal control defines the use of tractive forces.

One further application which could be helpful when designing a vehicle is to optimize the vehicle's parameters while finding the optimal control. For example, to find the position of the center of gravity of a vehicle to allow it to travel through a certain manoeuvre at maximum possible speed, it is only a matter of including the position of the center of gravity as a parameter to be optimized along with the control values. The possible applications of optimization are limited mostly by the user's ingenuity.

4 Numerical Optimization Methods

The previous chapter discussed how the control $\mathbf{u}(t)$ can be represented as a series of discrete numerical values $\mathbf{u}(k\Delta t)$ or can be the output of a controller. In order to find the control which is optimal using these representations, appropriate numerical optimization techniques must be employed. In this chapter, numerical methods will be discussed which will minimize the cost function J where $J = f(\mathbf{u}(t))$ or $J \approx f(\mathbf{u}(k\Delta t))$.

A number of methods for the numerical solution of optimal control problems were originally considered, and computer programs were constructed using the more promising methods. The advantages and disadvantages of these and for vehicle dynamics problems are presented below. These methods form the basis of the numerical results outlined later.

4.1 Gradient Optimization

A common method of minimizing a function is to utilize the gradient of the cost function, $\partial J/\partial \mathbf{u}$. Such gradient methods use the information contained in the gradient to estimate the direction to search for the minimum and its distance. The simplest way of performing a gradient optimization is to invoke an iterative approach where, at the beginning of each iteration, the gradient of the cost function in terms of the discrete control values, $\partial J/\partial \mathbf{u}(k\Delta t) \quad k = 1,2,\ldots,N$, is determined. The second part of the iteration involves finding the minimum in the direction of the gradient, i.e. doing a line minimization. These two procedures continue until an appropriate stopping criterion is fulfilled. The minimum should be located at this point.

The above approach is seldom used without modification. The problem is that the minimum is not always located in the direction of the gradient. If line minimization has just been performed, the new gradient of the cost function will be perpendicular to the direction of the last gradient and, as such, will not generally lead to the minimum. However, as more iterations are performed, information can be gained as to the nature of the cost function's topology. Many methods have been devised which

take advantage of this information to change the direction of the line minimization and make it more optimal. Typical examples of good algorithms are the Fletcher-Reeves conjugate gradient or the Davidson-Fletcher-Powell variable metric methods.

The line minimizations are done in the direction of the gradient, but only require cost function values. Typically the minimum will first be bracketed, then the minimum inside the bracket found by a form of bisection. Finding the gradient is not so simple. For nonlinear functions a numerical approximation is usually necessary, often quite a complex procedure taking almost as long to compute as it takes to perform the line minimization.

If calculating the gradient is not possible or too difficult, there are some methods related to those above which gain information about the cost function's topology by performing line minimizations in N directions, rather than performing any gradient calculations. A good example of this type of method is Powell's direction set method for multidimensions [20]. However, it is not recommended because of its inefficiency in terms of number of function evaluations and their high accuracy requirements. If accuracy is not a high priority, then the method will work quite well.

4.2 Rosen's Technique for Gradient Estimation

The previous section describes gradient optimization algorithms. This section deals with the accurate approximation of the gradient for use with optimal control. For complex systems, this is not a small matter. Estimating the gradient of the cost function $\partial J/\partial \mathbf{u}_k$ can be done by changing each u_k by some small amount Δu and determine the new value of the cost function. The gradient then becomes

$$\frac{\partial J}{\partial \mathbf{u}_k} \approx \frac{J(\mathbf{u}_k + \Delta \mathbf{u}_k) - J(\mathbf{u}_k)}{\Delta \mathbf{u}_k}. \tag{4.1}$$

This works well provided that the integration used to calculate J is sufficiently accurate. In many cases the integration is too long and an alternative method must be

used.

A method devised by Rosen circumvents the accuracy problem by breaking up an integration into small sections corresponding to the control segments. The cost function value is then approximated by the values of the states and controls at these points. Through a series of mathematical manipulations, it is possible to determine the states solely as functions of the control values. The method follows.

The system given is in the form

$$\dot{\mathbf{x}}(t) = \mathbf{a}(\mathbf{x}(t), \mathbf{u}(t)) \tag{4.2}$$

and we wish to find the minimum of a cost function which has the form

$$J = h(\mathbf{x}(t_f)) + \int_{t_o}^{t_f} g(\mathbf{x}(t), \mathbf{u}(t))dt \ . \tag{4.3}$$

Rosen begins by using the simplest approximating difference equation

$$\mathbf{x}(t + \Delta t) = \mathbf{x}(t) + \mathbf{a}(\mathbf{x}(t), \mathbf{u}(t)) \cdot \Delta t \ . \tag{4.4}$$

Assuming that the control is changed and the state observed at $t = 0, \Delta t, 2\Delta t, \ldots, N\Delta t$, we can define $t = k\Delta t$ and the difference equations become

$$\mathbf{x}((k+1)\Delta t) = \mathbf{x}(k\Delta t) + \mathbf{a}(\mathbf{x}(k\Delta t), \mathbf{u}(k\Delta t)) \cdot \Delta t \tag{4.5}$$

or, more simply,

$$\mathbf{x}(k+1) = \mathbf{x}(k) + \mathbf{a}(\mathbf{x}(k), \mathbf{u}(k)) \cdot \Delta t \ . \tag{4.6}$$

The performance measure may be written as

$$J_D \approx h(\mathbf{x}(\mathbf{N})) + \Delta t \sum_{k=0}^{\mathbf{N}-1} g(\mathbf{x}(k), \mathbf{u}(k)) . \tag{4.7}$$

Rosen's method assumes the use of an approximating difference equation. It is also possible to integrate the equations so that equation (4.6) becomes

$$\mathbf{x}(t+\Delta t) = \int_t^{t+\Delta t} \mathbf{a}(\mathbf{x}(t), \mathbf{u}(t))dt \tag{4.8}$$

where the integration can be done numerically. Although this involves more computational work, the accuracy of solution should be better. By integrating numerically, the problem of differentiating the state equations can be avoided.

For either Rosen's method or this variation, the remainder of the derivation will show the state at discrete times as

$$\mathbf{x}(k+1) = \mathbf{a}_D(\mathbf{x}(k), \mathbf{u}(k)) . \tag{4.9}$$

The state equations are now linearized about a previous (ith) state-control history $(\mathbf{x}^{(i)}(0), \mathbf{x}^{(i)}(1), \ldots, \mathbf{x}^{(i)}(\mathbf{N}); \mathbf{u}^{(i)}(0), \mathbf{u}^{(i)}(1), \ldots, \mathbf{u}^{(i)}(\mathbf{N}-1))$, the ith control history being known and in particular, the 0th being supplied as the initial guess by the user. Assuming that $\mathbf{a}$ is an analytic function, the $(i+1)$st trajectory is expanded in a Taylor series about the ith trajectory, and eliminating terms higher than first order, we have

$$\mathbf{x}^{(i+1)}(k+1) = \mathbf{x}^{(i)}(k+1) + \left[\frac{\partial \mathbf{a}_D}{\partial \mathbf{x}}(\mathbf{x}^{(i)}(k), \mathbf{u}(i)(k))\right][\mathbf{x}^{(i+1)}(k) - \mathbf{x}^{(i)}(k)]$$

$$+ \left[\frac{\partial \mathbf{a}_D}{\partial \mathbf{u}}(\mathbf{x}^{(i)}(k), \mathbf{u}(i)(k))\right][\mathbf{u}^{(i+1)}(k) - \mathbf{u}^{(i)}(k)] \tag{4.10}$$

and, knowing that $\mathbf{a}_D(\mathbf{x}^{(i)}(k), \mathbf{u}^{(i)}(k))$ is equivalent to $\mathbf{x}^{(i)}(k+1)$, this equation may be rewritten as

$$\begin{aligned}\mathbf{x}^{(i+1)}(k+1) = &\left[\frac{\partial \mathbf{a}_D}{\partial \mathbf{x}}(\mathbf{x}^{(i)}(k), \mathbf{u}^{(i)}(k))\right]\mathbf{x}^{(i+1)}(k) \\ &+\left[\frac{\partial \mathbf{a}_D}{\partial \mathbf{u}}(\mathbf{x}^{(i)}(k), \mathbf{u}^{(i)}(k))\right]\mathbf{u}^{(i+1)}(k) \\ &+\mathbf{a}_D(\mathbf{x}^{(i)}(k), \mathbf{u}^{(i)}(k)) \\ &-\left[\frac{\partial \mathbf{a}_D}{\partial \mathbf{x}}(\mathbf{x}^{(i)}(k), \mathbf{u}^{(i)}(k))\right]\mathbf{x}^{(i)}(k) \\ &-\left[\frac{\partial \mathbf{a}_D}{\partial \mathbf{u}}(\mathbf{x}^{(i)}(k), \mathbf{u}^{(i)}(k))\right]\mathbf{u}^{(i)}(k)\,. \end{aligned} \tag{4.11}$$

We can further simplify this to become

$$\mathbf{x}^{(i+1)}(k+1) = \mathbf{A}(k)\mathbf{x}^{(i+1)}(k) + \mathbf{B}(k)\mathbf{u}^{(i+1)}(k) + \mathbf{c}(k) \tag{4.12}$$

where **A**, **B**, and **c** are matrices which depend upon $\mathbf{x}^{(i)}$ and $\mathbf{u}^{(i)}$ which are the previous iterations state and control histories and, hence, are known.

Equation (4.12) is now linearized about the ith state-control history. However, the state values for each step are functions of both the state value of the previous step, and the control values that were applied during that step. It is therefore possible to rewrite equation (4.12) and eliminate $\mathbf{x}^{(i+1)}(k)$ to produce the following:

$$\begin{bmatrix} \mathbf{x}^{(i+1)}(0) \\ \mathbf{x}^{(i+1)}(1) \\ \mathbf{x}^{(i+1)}(2) \\ \cdot \\ \cdot \\ \cdot \\ \mathbf{x}^{(i+1)}(N) \end{bmatrix} = \begin{bmatrix} \mathbf{D}_0^0 & \mathbf{D}_1^0 & \cdots & \mathbf{D}_{N-1}^1 \\ \mathbf{D}_0^1 & \mathbf{D}_1^1 & \cdots & \mathbf{D}_{N-1}^2 \\ \mathbf{D}_0^2 & \mathbf{D}_1^2 & \cdots & \mathbf{D}_{N-1}^2 \\ \cdot & \cdot & & \cdot \\ \cdot & \cdot & & \cdot \\ \cdot & \cdot & & \cdot \\ \mathbf{D}_0^N & \mathbf{D}_1^N & \cdots & \mathbf{D}_{N-1}^N \end{bmatrix} \begin{bmatrix} \mathbf{u}^{(i+1)}(0) \\ \mathbf{u}^{(i+1)}(1) \\ \mathbf{u}^{(i+1)}(2) \\ \cdot \\ \cdot \\ \cdot \\ \mathbf{u}^{(i+1)}(N-1) \end{bmatrix} + \begin{bmatrix} \mathbf{x}_H(0) \\ \mathbf{x}_H(1) \\ \mathbf{x}_H(2) \\ \cdot \\ \cdot \\ \cdot \\ \mathbf{x}_H(N) \end{bmatrix} \tag{4.13}$$

or

$$\overline{\mathbf{X}}^{(i+1)} = \overline{\mathbf{D}\mathbf{U}}^{(i+1)} + \overline{\mathbf{X}}_H \tag{4.14}$$

where

$$\mathbf{x}_H(k+1) = \mathbf{A}(k)\mathbf{x}_H(k) + \mathbf{c}(k), \qquad \mathbf{x}_H(0) = \mathbf{x}_0 \tag{4.15}$$

and

$$\mathbf{D}_l^{k+1} = \begin{cases} \mathbf{A(k)A(k\text{-}1)} \cdots \mathbf{A}(l+1)\mathbf{B}(l), & for\, k > l \\ \mathbf{B}(l), & for\, k = l \\ 0, & for\, k < l \end{cases}. \tag{4.16}$$

Now the cost function will be written

$$J_D = h(\overline{\mathbf{U}}^{(i+1)}) + \Delta t \sum_{k=0}^{N-1} g(\overline{\mathbf{U}}^{(i+1)}). \tag{4.17}$$

Finding the gradient of the cost function with respect to the control function values is now fairly straightforward.

Rosen's method is extremely flexible. It is a routine matter to use a third or higher order in the cost function. It is also possible to have the cost as one of the states, and its derivative with respect to the controls calculated as a matter of course in the regular calculations. The effectiveness of the method can be improved by understanding the techniques involved and liberally rearranging the basic structure.

4.3 Downhill Simplex Technique

The downhill simplex method, attributed to Nelder and Mead [20,21], is a method of finding a minimum without finding a gradient or performing any line minimizations. Its greatest advantages are that it is very robust, i.e. it does not require great accuracy in the cost function evaluations, and it is not easily 'fooled' by local minima or an irregular cost function's topology. It will often find a good or global minimum among many local minima.

The basis of the technique is creating a simplex, an N dimensional geometric figure defined by $N+1$ distinct points. Each point corresponds to a control vector $\mathbf{u}$ with an associated cost. One iteration in the simplex method requires one to:

1) take the point with the highest cost function value and reflect it through the hyperplane defined by the other points. If this is lower than the second highest cost value then this iteration is finished. If the new cost is lower than the previous lowest, go to step 2). If it is higher or equal to the second highest, then reject this point and go to step 3).

2) repeat the reflection in the previous step, but increase the distance of the reflection. This reflection and expansion causes an increase in the volume of the simplex. If this is an improvement, then accept this as the new point. Otherwise, accept the choice in 1) above as the new point. This iteration is finished.

3) (because a reflection will not reduce the cost function value:) move the high point toward the reflection hyperplane but do not pass through the hyperplane. This will reduce the volume of the simplex. If this does not reduce the cost, go to the next step.

4) (because all else has failed:) contract all of the points along their vertices toward the point with the lowest cost.

The iterations continue until an appropriate stopping criteria is satisfied. In practice, this procedure will solve problems where the cost function is fairly 'rough' much faster and more accurately than the gradient methods. This may be partly due to the step being taken relative to the other points whose value is known. If the simplex is still relatively large, then small irregularities in the surface are not likely to be noticed. Gradient methods often assume that the cost function has a smooth parabolic surface, and when this is not so, results may be unpredictable. For problems where using the gradient is not an asset, this technique is highly recommended.

4.4 Simulated Annealing and Heuristic Methods

Perhaps the simplest way of finding a minimum of a function is to randomly take control values and see what cost function values are produced. Given enough time, this method may find very good minima, but the procedure is very inefficient. It is generally referred to as an heuristic or random method. It is mentioned here because it has the advantage that it may be less susceptible to the effects of local minima. Though they are too inefficient for general work, methods such as these may occasionally be useful when a very good minimum is desired no matter what the cost in computing time.

A variation on the theme is to make a change to one variable and then determine whether or not to accept this change. If accepted, it will be used for all following cost function evaluations until it is changed again. Simulated annealing, which has recently gained popularity, employs a strategy which will accept all changes that decrease the cost but occasionally will accept changes that increase it. At the

beginning of the minimization, changes with a fairly large increase in cost will be accepted. At the end, virtually no increases will be accepted. This strategy may allow the technique to get out of local minima with a high cost and find a much better minimum.

Though the procedure works, it typically takes twice as long to run as more conventional techniques. Also, the resulting minimum is usually close to the global minimum. To overcome inefficiency, it is usually desirable to get into the vicinity of the desired minimum and then employ another, more efficient technique to finish the minimization.

4.5 Constrained Optimization

It is occasionally advantageous to utilize state and control constraint in an optimization. Dealing with vehicles, there are limitations on the control values (e.g. the steering wheel can only be turned a set angle) and often on the state values (e.g. the vehicle must not go off the road). While constraints are not considered in the vehicle simulations performed here, the topic is of sufficient importance to deserve mention.

The simplest and perhaps most often used method of employing constraints is to include them in the cost function and weight them very heavily. This has several advantages. Implementation requires that only the cost function be changed. The method of optimization may not need to be changed, regardless of constraints. If the optimization method allows for nonlinear cost functions, nonlinear constraints may be used. A primary disadvantage is that by adding the constraints to the cost function, the minimization procedure will have effects of the constrained cost thrown in unless it is done carefully. Another disadvantage is the possible extra time required to minimize these equations, in contrast to more direct methods.

An alternative method for linear equality and inequality constraints, attributable to Rosen, is known as gradient projection. The method requires that the minimization begin within an **N** dimensional hypercube for which the surfaces are made up of the

constraints. The line minimization is performed by traveling in the direction of the gradient until a constraint is encountered. If the gradient at this point indicates that the minimum is between this point and the starting point, a typical line minimization is performed. If not, the point on the surface of the constraint is taken as the beginning of the next line minimization. A projection matrix ensures that the direction of the next line minimization is along the surface of the constraints in the direction of the maximum component of the gradient. A common way of implementing this method is to linearize the equations and use these values until a minimum is found. The system equations are then relinearized about the new control history.

Rosen's method for approximating the gradient was designed for use with projected gradient minimization, which also allows easy determination of the gradient in terms of the control values. Implementing both control and state constraints is therefore straightforward. In practice, this combination of methods works well for systems that are not extremely nonlinear. In the case of the nonlinear vehicle, convergence problems have been encountered if the same linearized equations are used for an entire minimization. An alternative is to relinearize at each cost function or gradient evaluation. The problem then is that the state constraints may have moved due to the nonlinearities in the system. In general, Rosen's gradient projection is not the method of choice for complex systems, but for some problems it may be advantageous.

5 The Test Vehicle and Manoeuvres

In the past, optimal control and optimized controllers have been applied mainly as a means of performing the tracking task with little regard for what a real driver would do. Here these methods are used to model the efforts of a real driver, so their effectiveness should be graded by comparing the real driver to the model driver using a test vehicle. In order to achieve this, results produced by a real vehicle will be compared later to the numerical optimization results. In this section, descriptions are given of the tests and the test vehicle.

5.1 The Vehicle and Equations of Motion Used

The chassis of the test vehicle was a 1986 Tecno Polaris go-kart. Its dimensions and weights are listed below.

$$mass = 132\ kg$$
$$I = 15\ kg/m^2$$
$$l_f = 0.62\ m$$
$$l_r = 0.40\ m$$
$$t_f = 1.00\ m$$
$$t_r = 1.10\ m$$

The moment of inertia, I, is only an approximation, found by estimating the radius of gyration. The tires were 1988 Vega RT bias ply kart tires. Their cornering stiffnesses were estimated by the static tests described in Appendix 3. The coefficients of friction were estimated based on the maximum cornering speed of the 90° manoeuvre attempted. A maximum lateral acceleration of about 15 m/s^2 was observed for the most severe cornering manoeuvre, so a coefficient of friction of 1.5 was assumed. The tire results are listed below.

$c_f = 23{,}000$ N/*rad*

$c_r = 81{,}000$ N/*rad*

$\mu_f = 1.5$

$\mu_r = 1.5$

The engine on the kart was a 100cc two stroke direct drive (i.e. no clutch). The rear axle was solid with one disk brake attached to it. There were no brakes on the front wheels. The kart chassis contained no conventional suspension elements; therefore the front and rear wheels had essentially no vertical travel relative to the chassis.

The equations of motion are derived in Appendix 1 and are presented below.

$$\dot{X} = \dot{x}_1 = x_2 \cos x_5 - x_4 \sin x_5$$

$$\ddot{x} = \dot{x}_2 = x_6 x_4 - ((F_{fr} + F_{fl}) \sin u)/m$$

$$\dot{Y} = \dot{x}_3 = x_2 \sin x_5 + x_4 \cos x_5 \qquad (5.1)$$

$$\ddot{y} = \dot{x}_4 = -x_6 x_2 + ((F_{fr} + F_{fl}) \cos u + F_{rr} + F_{rl})/m$$

$$\dot{\theta} = \dot{x}_5 = x_6$$

$$\ddot{\theta} = \dot{x}_6 = \left((F_{fl} + F_{fl}) l_f \cos u - (F_{rr} + F_{rl}) l_r + (F_{fl} - F_{fr}) \frac{t_f}{2} \sin u \right) / I$$

where x and y are the axes of the coordinate system attached to the vehicle, X and Y the axes of the fixed coordinate system and θ is the rotational angle of the vehicle's coordinate system relative to the fixed. The tire force equations were simplified from [23] and are given by

$$F = \mu F_z \left(\bar{\alpha} - \left(\frac{\bar{\alpha}}{|\bar{\alpha}|} \right) \frac{\bar{\alpha}^2}{3} + \frac{\bar{\alpha}^3}{27} \right), \qquad |\bar{\alpha}| \leq 3.0 \qquad (5.2)$$

or

$$F = \mu F_z \left(\frac{\bar{\alpha}}{|\bar{\alpha}|} \right), \qquad |\bar{\alpha}| > 3.0 \tag{5.3}$$

with

$$\bar{\alpha} = \frac{c\alpha}{\mu F_z} \tag{5.4}$$

where the slip angles are calculated from

$$\begin{aligned}
\alpha_{fr} &= u - \tan^{-1}\left(\frac{x_4 + x_6 l_f}{x_2 + x_6 t_f/2} \right) \\
\alpha_{fl} &= u - \tan^{-1}\left(\frac{x_4 + x_6 l_f}{x_2 - x_6 t_f/2} \right) \\
\alpha_{rr} &= -\tan^{-1}\left(\frac{x_4 - x_6 l_r}{x_2 + x_6 t_r/2} \right) \\
\alpha_{rl} &= -\tan^{-1}\left(\frac{x_4 - x_6 l_r}{x_2 - x_6 t_r/2} \right).
\end{aligned} \tag{5.5}$$

Under these conditions, the front tires will saturate at 0.051 radians and the rear tires will saturate at 0.023 radians. An increase in slip angles above these values will not change the lateral tire forces. The lateral force versus slip angle curves are shown in Figure 5.1.

The only control input is considered to be steering as the throttle was only used to maintain the vehicle's speed and was not varied.

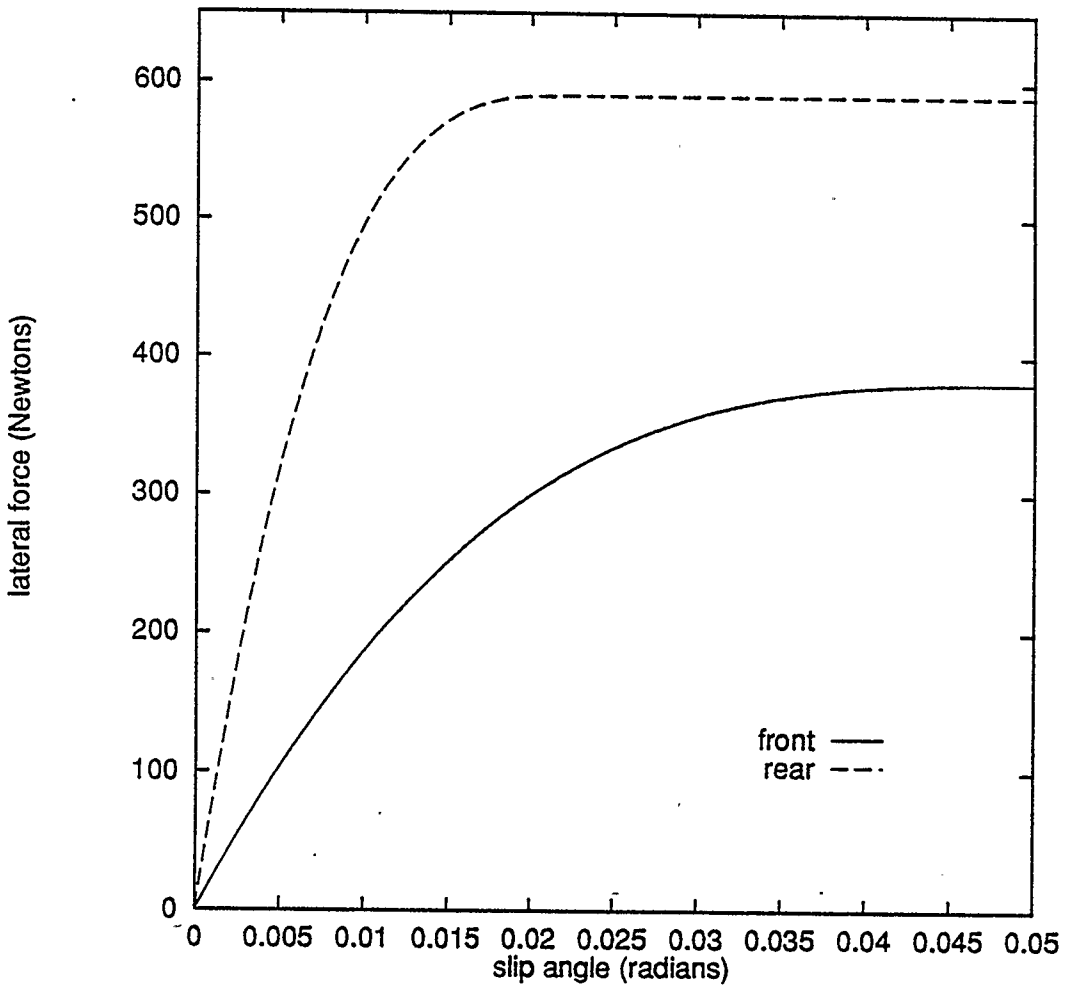

Figure 5.1: Lateral Force versus Slip Angle for the Tire Model

5.2 The Manoeuvres and Conditions

Two manoeuvres were attempted, the obstacle avoidance manoeuvre and the 90° corner, chosen because of their differences. In the first, the amount of yaw and steering necessary to complete it is very small; this tends to be a straight manoeuvre. In contrast, the second manoeuvre requires large amounts of yaw and larger steering inputs.

The obstacle avoidance manoeuvre, more generally called the lane change manoeuvre, involves following a path defined by the error function

$$x_{3\ desired} = \frac{2c_1}{\sqrt{\pi}} \int_0^{x_1/c_2} e^{-\zeta^2} d\zeta . \qquad (5.6)$$

where x_1 and x_3 are, respectively, the X and Y of the fixed coordinate system. This manoeuvre has been discussed extensively in past optimal control papers [18,19]. For the tests, $c_1 = 1.00$ and $c_2 = 4.50$. The lane change started at $x_1(t_o) = -15.0\ m$ and $x_3(t_o) = 1.0\ m$ and ended at $x_1(t_f) = 10.0\ m$ where $x_3(t_f) = -1.0\ m$.

The corner manoeuvre consisted of three parts: a 10 m straight entrance, a 90° arc of 10 m radius, and a 10 m straight exit. The 10 m straight entrance was present to allow the driver or optimal control to 'set up' for the corner.

All tests were done on a relatively smooth and dusty asphalt surface. The lines of the desired trajectory were marked in chalk on the pavement. Markers were set up at the beginning and end of the manoeuvre and used as a reference for initiating instrument recording by an observer, who recorded the duration of the manoeuvre with a stopwatch. Each test run began by 'scrubbing' the tires to warm them up, although full operating temperature for the type of tire was never achieved. The

manoeuvre was run, the kart stopped, and the data downloaded to a computer for processing. Comments of the driver and observer about tracking quality and driving irregularities were recorded. All driving was done by the author.

The two desired quantities were the vehicle speed, measured by an optical switch reading from a slotted disk attached to the rear axle, and the steer angle, measured using a shaft encoder attached to the steering shaft. The data was recorded using a microprocessor-based data acquisition system, designed and built as a part of this project, and attached to the kart frame. A button on the steering wheel initiated data collection. The data was sampled at roughly 100 Hz. (For a more complete description of the instrumentation system, see Appendix 2.)

6 Results of Simulations

Below are the computed optimization results using the optimal control and optimal controllers described in chapters 3 and 4. Four manoeuvres were performed in all, two approximating slow and fast lane changes, and two approximating slow and fast corners. The graphs associated with these manoeuvres are presented in more detail in the next section.

6.1 Optimal Control

The dimensionless cost function **J** to be minimized was

$$J = \int_{t_o}^{t_f} [R_e(error_{tracking})^2 + R_u(u)^2] dt \qquad (6.1)$$

where $error_{tracking}$ is the minimum distance from the vehicle's center of gravity to the desired trajectory, u is the steer angle, and coefficients R_e and R_s are 1 $m^{-2}s^{-1}$ and 1 $rad^{-2}s^{-1}$, respectively. The optimal control is represented by a 100 pulse evenly segmented control. The gradient was calculated using the modified Rosen's technique. The minimization was done using the Fletcher-Reeves-Polak-Ribiere minimization as implemented in Press [20] with only the line minimization calling routine modified. The accuracy tolerance is 1.0×10^{-4}. The cost associated with each manoeuvre is

slow lane change	0.002645
fast lane change	0.001746
slow corner	0.023482
fast corner	0.093202

The value of the fast lane change is lower than that of the slower manoeuvre because less time is required to complete it, though the tracking and steering are similar. The tracking error and steering for the fast corner are significantly higher than for the slow corner.

The initial control history was set to a small constant value (0.001 to 0.0001 radians) for all manoeuvres except the fast corner manoeuvre, in which the initial control history was 0.045 radians. Although the smaller initial values were not absolutely necessary, they did seem to reduce the optimization time. The larger value for the fast corner was necessary because the cost function for this manoeuvre appears to have many local minima. In one case where a small initial control was given, the minimum consisted of turning the front wheels perpendicular to the direction of travel (1.57 radians) and maintaining this value until the vehicle had almost come to a stop. One of the chief drawbacks of this method is its tendency to find very undesirable minima.

6.2 Optimal Controller

Decisions as to the form and degree of complexity of the optimal controller were fairly arbitrarily made in order to represent a reasonably realistic and typical situation, balanced between extremes. The cost function was the same as the one used for the optimal control. The controller consisted of six parts, each of which took an anticipated future error (as shown in Figure 6.1) and multiplied it by a parameter to be changed by the optimization algorithm. These values were summed to produce the steering, hence

$$u = c_1 error(0.10) + c_2 error(0.25) + c_3 error(0.50) + c_4 error(0.75) + c_5 error(1.00) + c_6(1.50) \qquad (6.2)$$

where $error(t)$ is the anticipated error at time t in the future. This anticipated error, also shown in Figure 6.1, is calculated by first determining the vehicle's position traveling in a straight line at the present speed and direction for t seconds. The error is then the distance between this future position and the desired trajectory at this point.

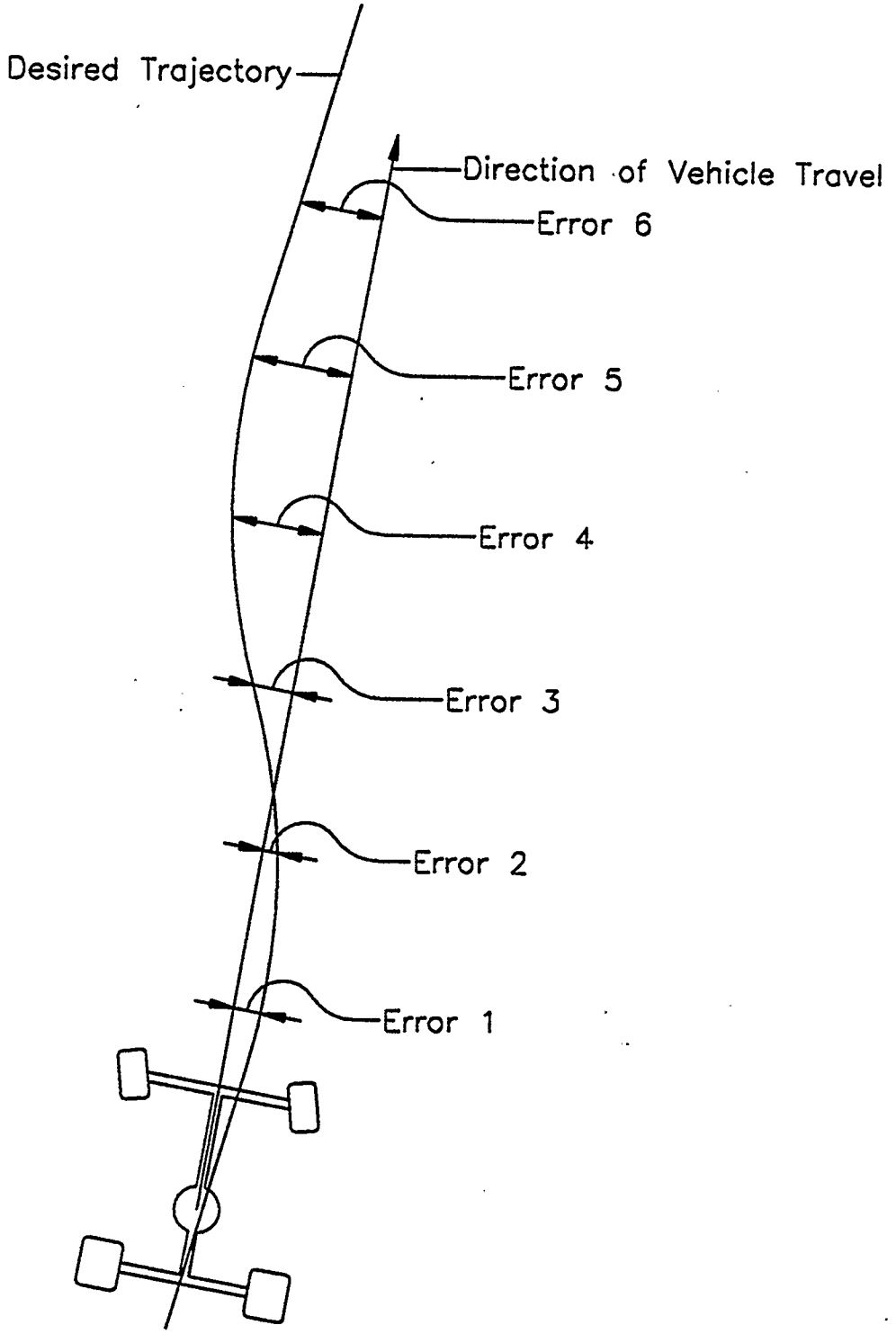

Figure 6.1: Error Inputs to the Optimal Controller

The downhill simplex technique was used to optimize. The initial values of the controller parameters were chosen by a random number generator which produced uniform random deviates between -1.0 and 1.0. This proved to be an easy method of getting a wide range of control parameter sets. The final values are shown in Table 6.1, and the costs are shown below.

slow lane change	0.003088
fast lane change	0.001911
slow corner	0.030574
fast corner	0.102688

	slow lane	fast lane	slow corner	fast corner
c_1	-0.1671796	-0.8303345	0.0209960	-0.0863910
c_2	-0.1169495	0.7073845	-0.0258471	-0.0784005
c_3	0.4070435	-0.0806202	0.0608595	0.1852392
c_4	0.0998517	-0.0429414	0.1970839	0.1605817
c_5	-0.1593351	0.0351648	-0.1041405	-0.1579004
c_6	0.0211886	-0.0077323	0.0002157	0.0198238

Table 6.1. The Controller Parameter Values for the Optimal Controller.

6.3 The Optimal Driver: Optimization Based upon the Driver's Results

With the two preceding optimal methods, no regard was taken for the results of the test driver. In particular, the effect of steering on the cost function was given purely by the steering variance from zero steer angle. An alternative to this is to measure the effect of the steering on the cost relative to the steering produced by the test

driver, so the control produced by the optimization might display a steering form closer to the driver's. This may give an indication of the resultant movements of the vehicle if they are not available.

The third set of results computed is identical to the optimal control program used above, except for a change to the cost function, now

$$J = \int_{t_o}^{t_f} [R_e(error_{tracking})^2 + R_s(u - u_{driver})^2] dt \qquad (6.3)$$

where u_{driver} is the control produced by the driver of the test vehicle. The coefficient R_e is 1 $m^{-2}s^{-1}$ and R_s is 10 $rad^{-2}s^{-1}$. The method will be referred to as the "optimal driver", an appropriate name, if not entirely accurate.

7 Comparison of Results

This section compares and comments on the numerical results produced by optimal control techniques with the experimental ones produced by a driver, for four different manoeuvres. Steering, which is the control, is the main source of comparison, to determine if the steering results are generally similar, and if the optimal control exceeds the driver's capabilities. Movement resulting from the control is also examined; the vehicle must accurately perform the manoeuvre, and in a manner which is physically possible and probable for the driver.

The complete presentation shows that for all the results it is generally the case that

1) the calculated results are realistic for the manoeuvres and similar to what might be expected of the driver and, in the case of the steering controls, are close to the measured control inputs.

2) the state values produced by the numerical methods are similar, but not identical. The path-tracking through the manoeuvres was very good in each case, so it is apparent that different control and state histories can be used for the same path.

Variations in the numerically produced controls are due not only to differences in optimization techniques; different initial control histories used for starting the optimization will often produce different final control histories. This suggests that either the cost function has many local minima, or that the global minimum is so indistinct that the numerical techniques are not capable of locating exactly the point of the minimum.

7.1 The Slow Lane Change Manoeuvre

The slow lane change manoeuvre was performed at about 7 m/s, at which speed the driver could comfortably follow the prescribed path. The numerical and experimental results are presented in Figures 7.1.1 to 7.1.10. The results from the optimal control, optimal controller and optimal driver are presented in each plot. The

experimental results are included in Figures 7.1.1 and 7.1.4, which represent the steering and forward speed. All of the figures show that the state values are realistic for a driver. Figure 7.1.2 reveals that the computed tracking is excellent.

The simplest way of following the prescribed path in a lane change is to steer in the direction of the lane, then in the opposite direction from the half-way point until the manoeuvre is complete. The driver's results, and all three sets of numerical results generally conform to this pattern.

A notable feature is that the peak values of steering inputs of the test results are larger than those of all of the optimization techniques. The experimental steering inputs (see Figure 7.1.1) are about -0.067 radians at the first peak and 0.081 radians at the second peak, while the optimal control has maxima of about -0.046 and 0.042 radians. However, both steering inputs are of the same form with the peaks and zero value crossovers occurring at similar times. There are some small oscillations at the beginning of the manoeuvre for the driver inputs, but these could be attributed to roughness on the road surface or disturbances from the driver. These oscillations of steer angle are small in magnitude and include the effect of the driver pushing the 'start record' button which was located on the steering wheel.

The difference in steering input magnitudes between the experimental and computer simulations is evident in all of the manoeuvres. This should not occur in slow manoeuvres, where the steering angles should be the same for a vehicle regardless of the tire characteristics. Optimal control results were obtained for several different combinations of tire characteristics, revealing that large changes in the tires appear to have minimal effects on the steering for this manoeuvre. The discrepancies are most likely due to effects caused by the front steering geometry not considered in the numerical vehicle model.

The path-following accuracy can be seen in Figures 7.1.2 and 7.1.3. The largest tracking error is about 0.045 meters, which represents 2.3% of the 2.0 meters of lateral travel, accurate enough to be acceptable as an approximation of the driver's efforts to follow the path. The oscillations in tracking accuracy in Figure 7.1.3 are positional

errors created by 'cutting the corners' on the manoeuvre, and do not reflect a rotational oscillation, which would signal the onset of an instability. In Figure 7.1.4, the numerical optimization techniques maintain a steady speed, while the driver's speed varies by 1.0 m/s.

The front and rear slip angles are shown in Figures 7.1.5 and 7.1.6. Values plotted are the average of both the right and left slip angles. The variance in the slip angles among the three types of optimization suggests that various slip angle histories can produce very similar tracking characteristics, a result not originally anticipated.

Figures 7.1.8 and 7.1.9 show the lateral and rotational velocities of the vehicle, which share the general form of the steering inputs shown in Figure 7.1.1. In past optimal control study [18,19], this was found to be the case for all vehicles, provided the manoeuvre is not too aggressive relative to their capabilities. The rotational positions (Figure 7.1.7) are the integration of the rotational velocity. The rough contours of the rotational velocity are smoothed by the integration.

Figure 7.1.10 is a plot indicating the understeer/oversteer coefficient. The coefficient roughly indicates the effects of nonlinearities in the side force characteristics of tires as a function of slip angle; the understeer or oversteer will change as the vehicle's state changes. For a more detailed description of this coefficient, see Appendix 4. A coefficient of zero indicates a neutral steering vehicle. A +1.0 indicates a vehicle with the front cornering stiffness of zero and a non-zero rear cornering stiffness, the extreme of an understeering vehicle. A value of -1.0 is given to a vehicle with a rear cornering stiffness of zero and a non-zero front cornering stiffness, the extreme oversteering vehicle. The vehicle model used has a 'base' coefficient (based on the cornering stiffness when the slip angles are all zero) of about +0.55, indicating understeer.

The coefficient remains near its base value. Generally, a tire can be considered to have linear characteristics up to 1/3 of the slip angle at which the tire saturates (i.e. the side-force reaches its maximum value). Hence, the linear range for the test vehicle's tires can be expected to be up to about 0.017 radians for the front tires and

0.008 radians for the rear. For this manoeuvre, the slip angles are within this range. This and the lack of change in the understeer/oversteer coefficient suggests that this manoeuvre is not a good indicator of the vehicle's handling characteristics in any other than the linear range of the tires.

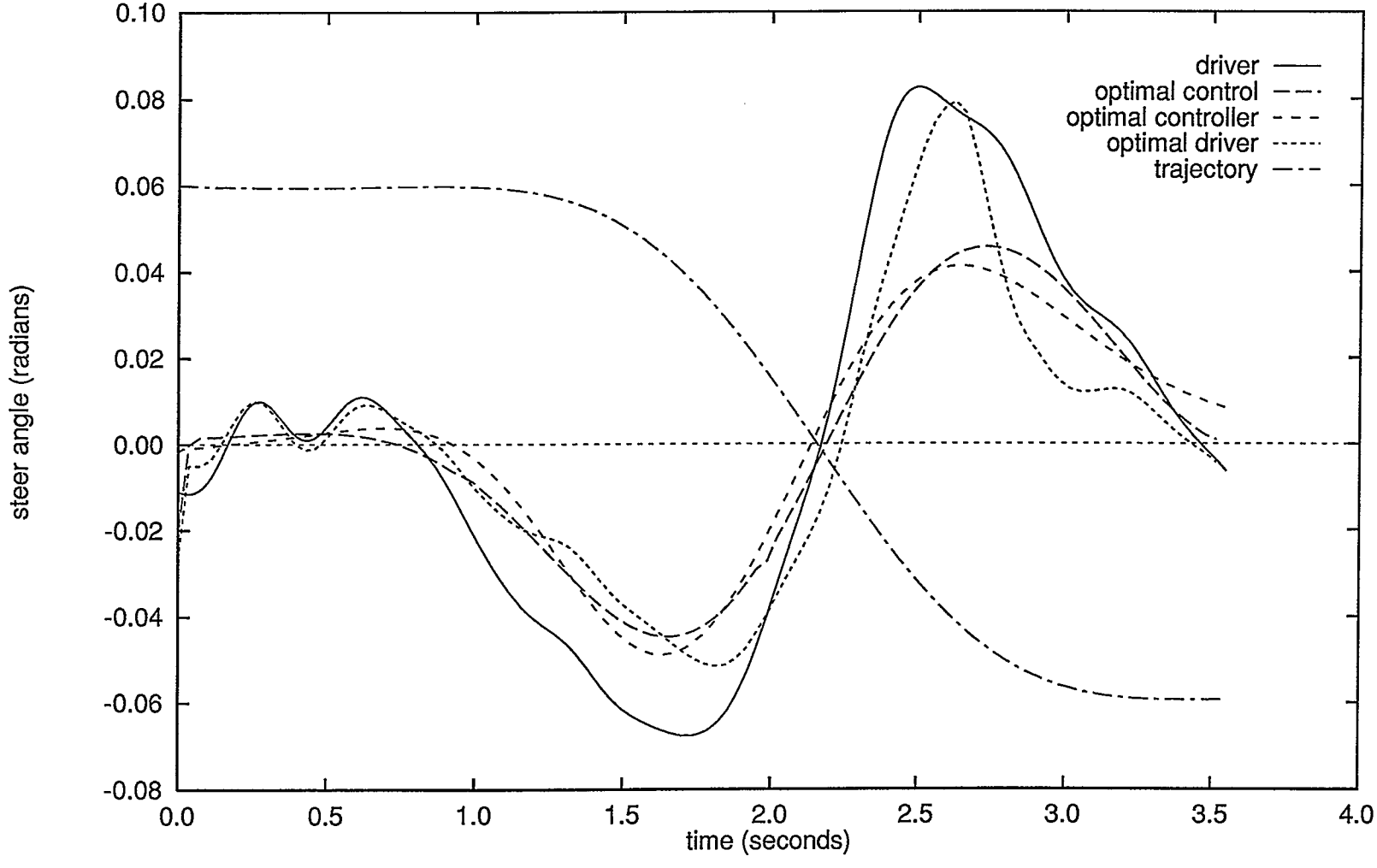

Figure 7.1.1: Steering for Slow Lane Change Manoeuvre

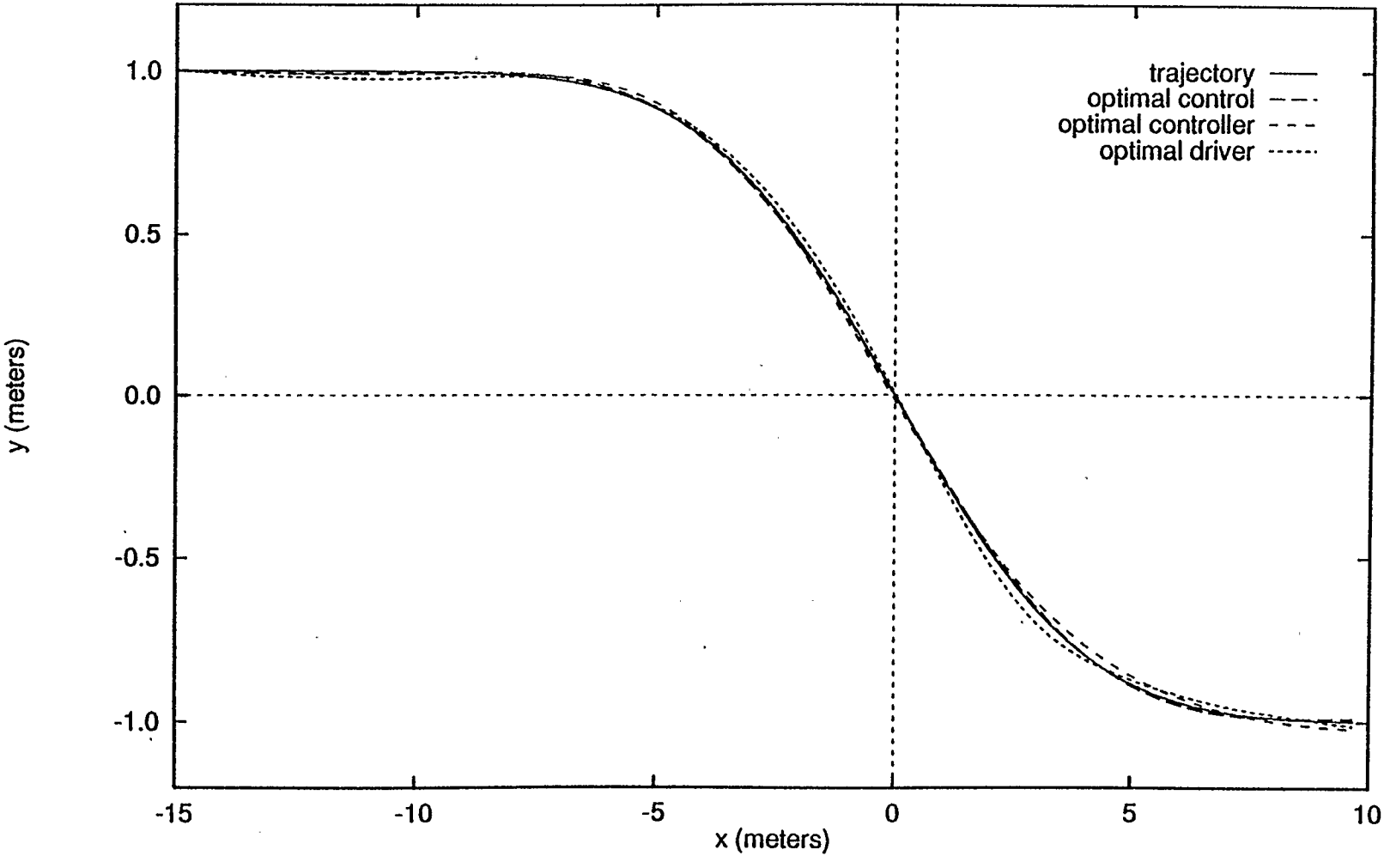

Figure 7.1.2: Trajectories for Slow Lane Change Manoeuvre

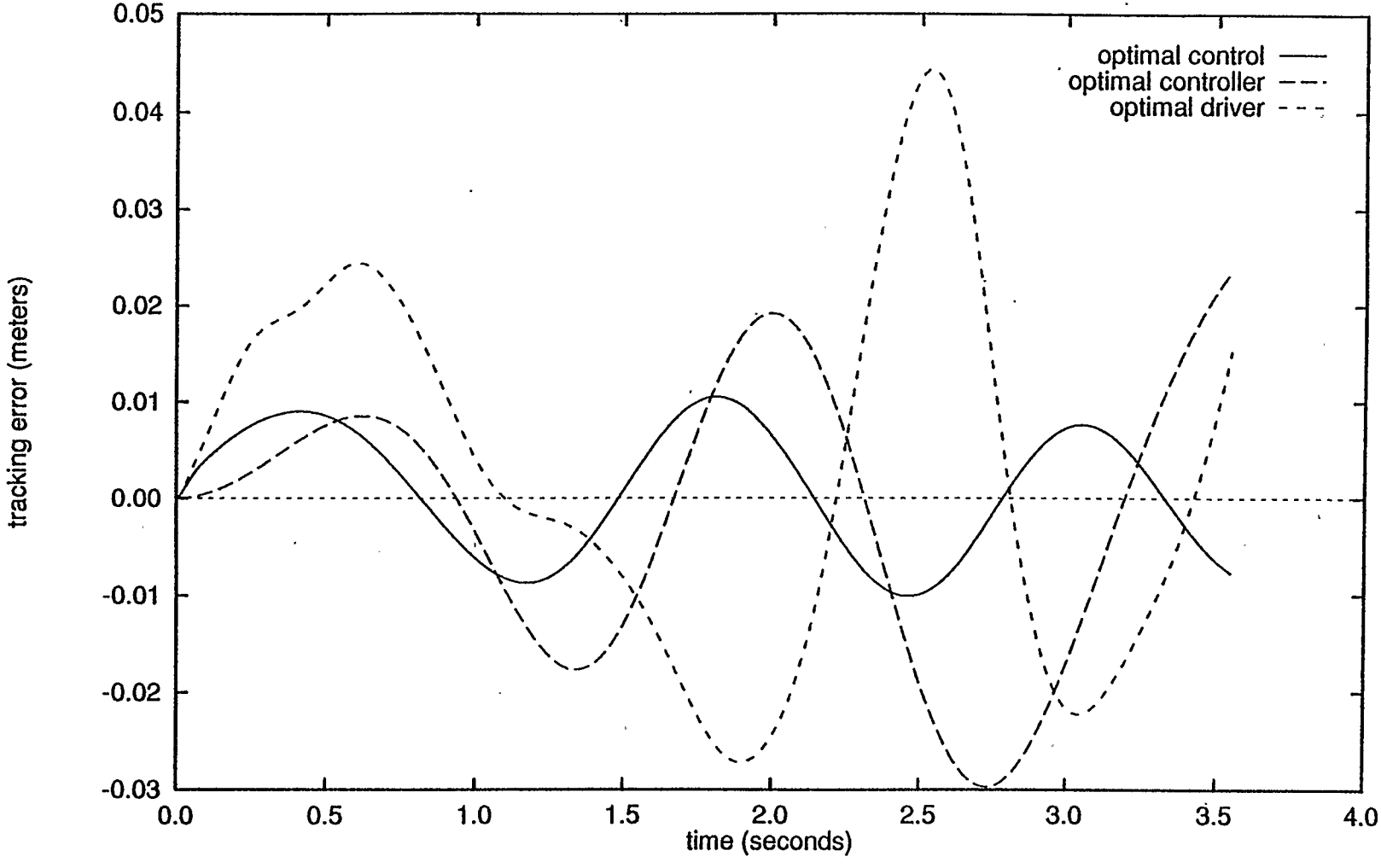

Figure 7.1.3: Tracking Error for Slow Lane Change Manoeuvre

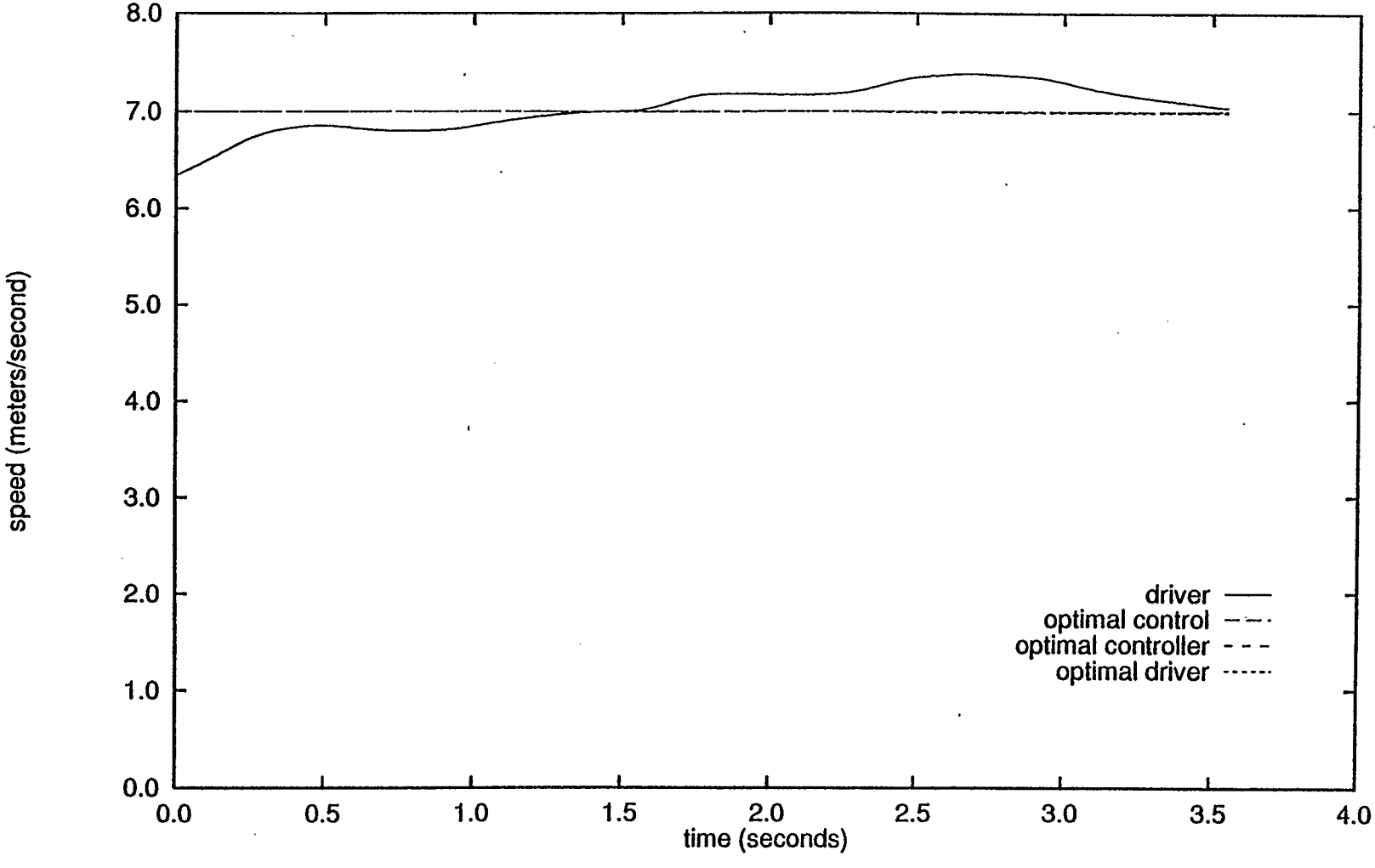

Figure 7.1.4: Speeds for Slow Lane Change Manoeuvre

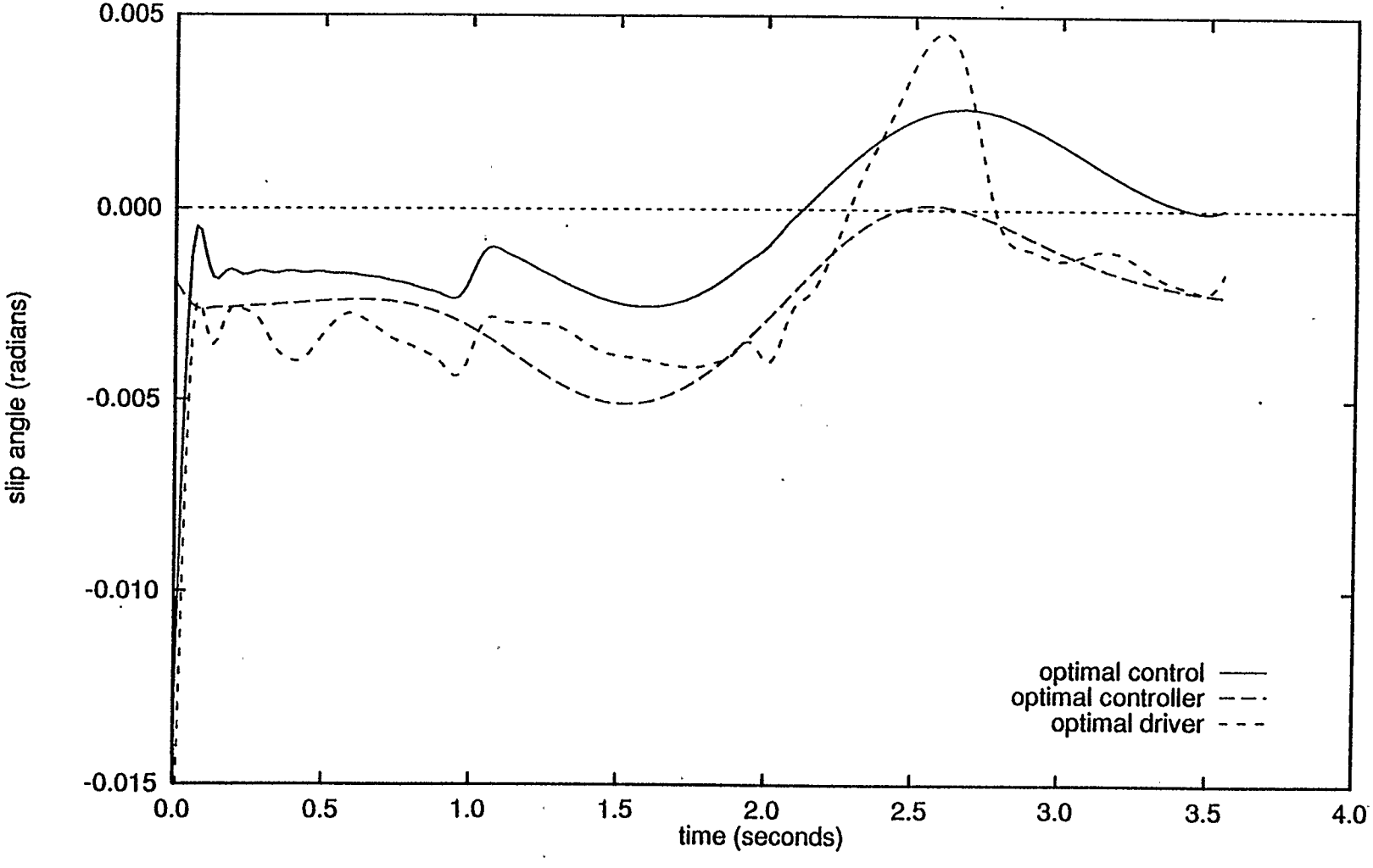

Figure 7.1.5: Front Slip Angles for Slow Lane Change Manoeuvre

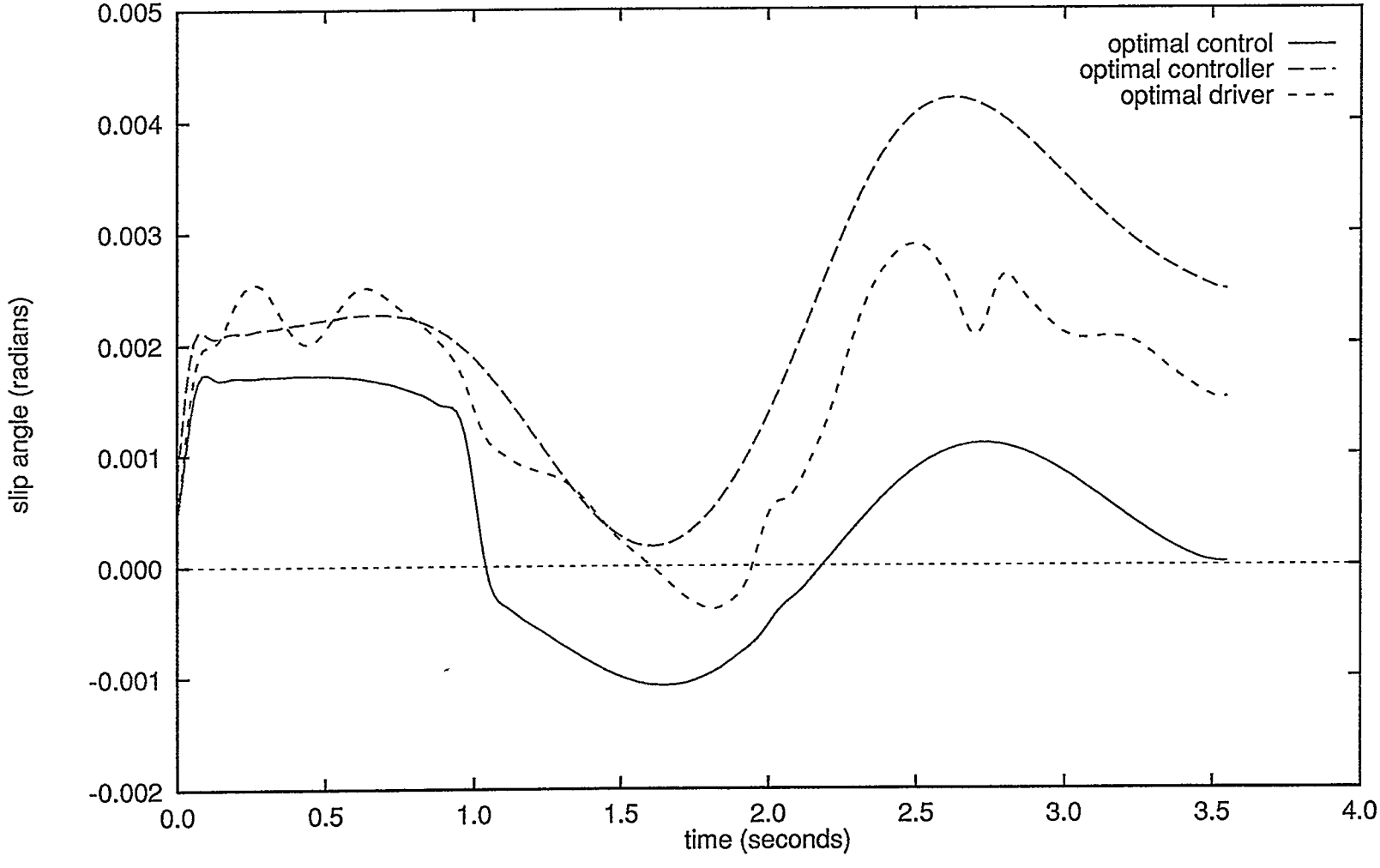

Figure 7.1.6: Rear Slip Angles for Slow Lane Change Manoeuvre

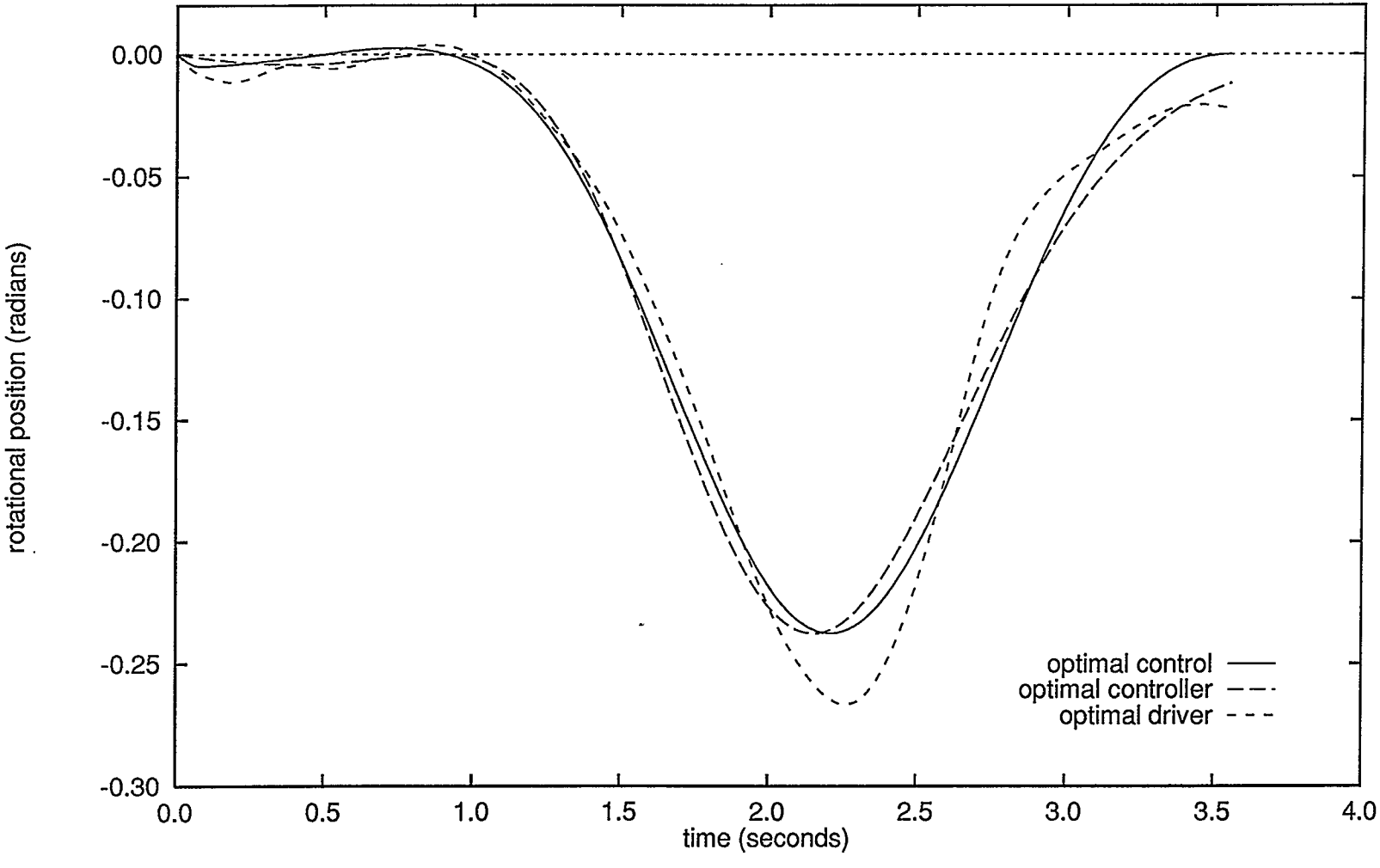

Figure 7.1.7: Rotational Positions for Slow Lane Change Manoeuvre

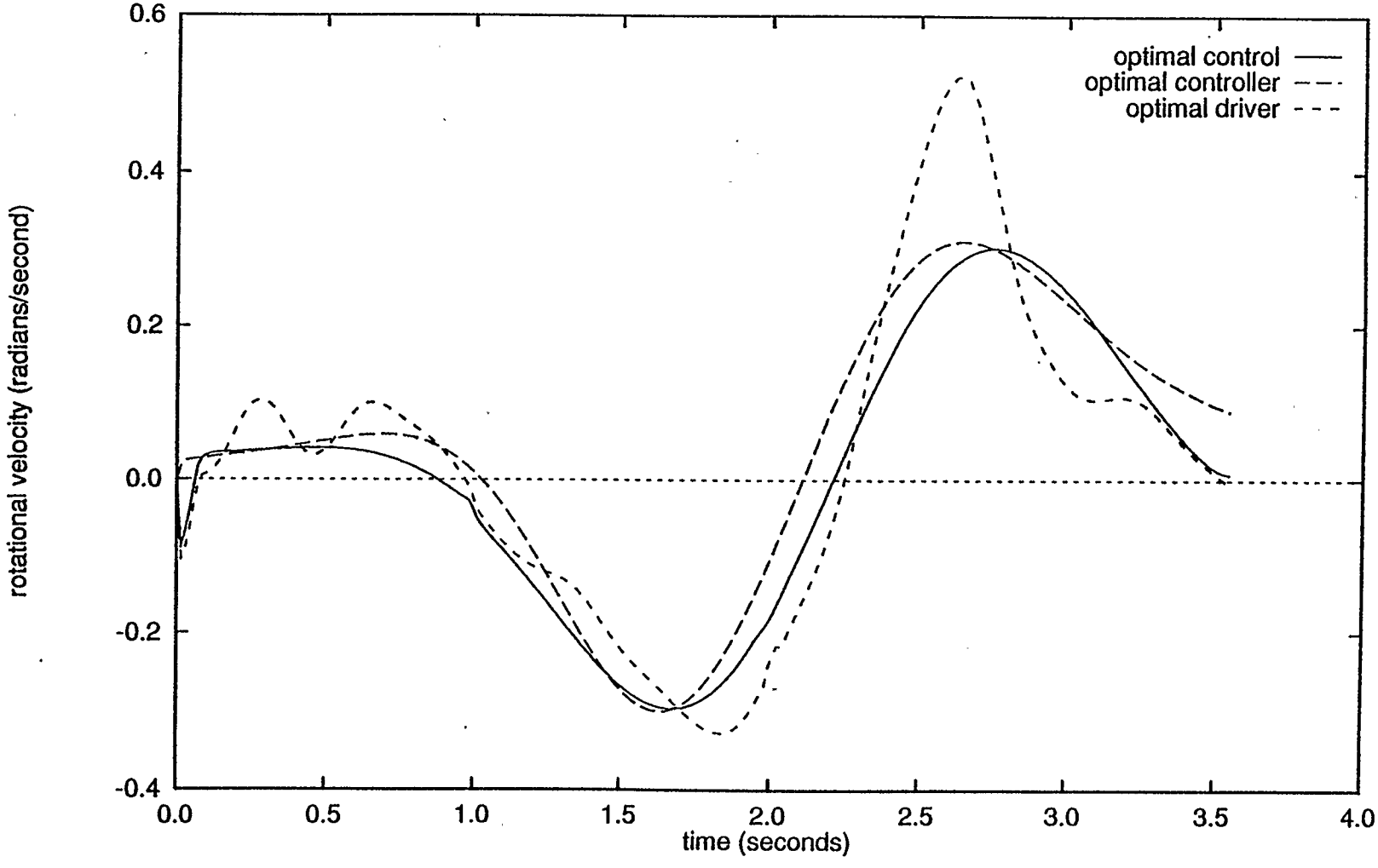

Figure 7.1.8: Rotational Velocity for Slow Lane Change Manoeuvre

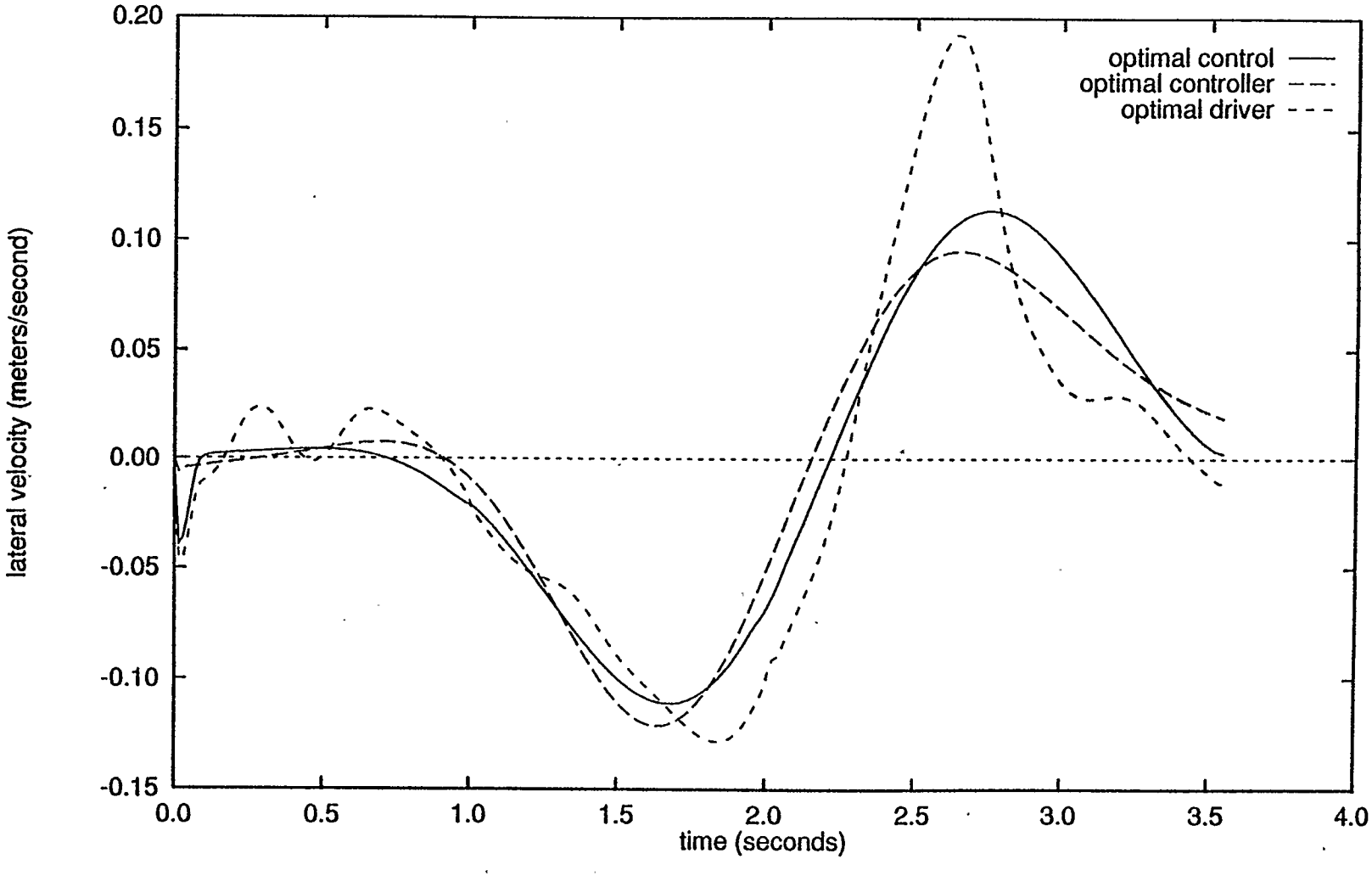

Figure 7.1.9: Lateral Velocity for Slow Lane Change Manoeuvre

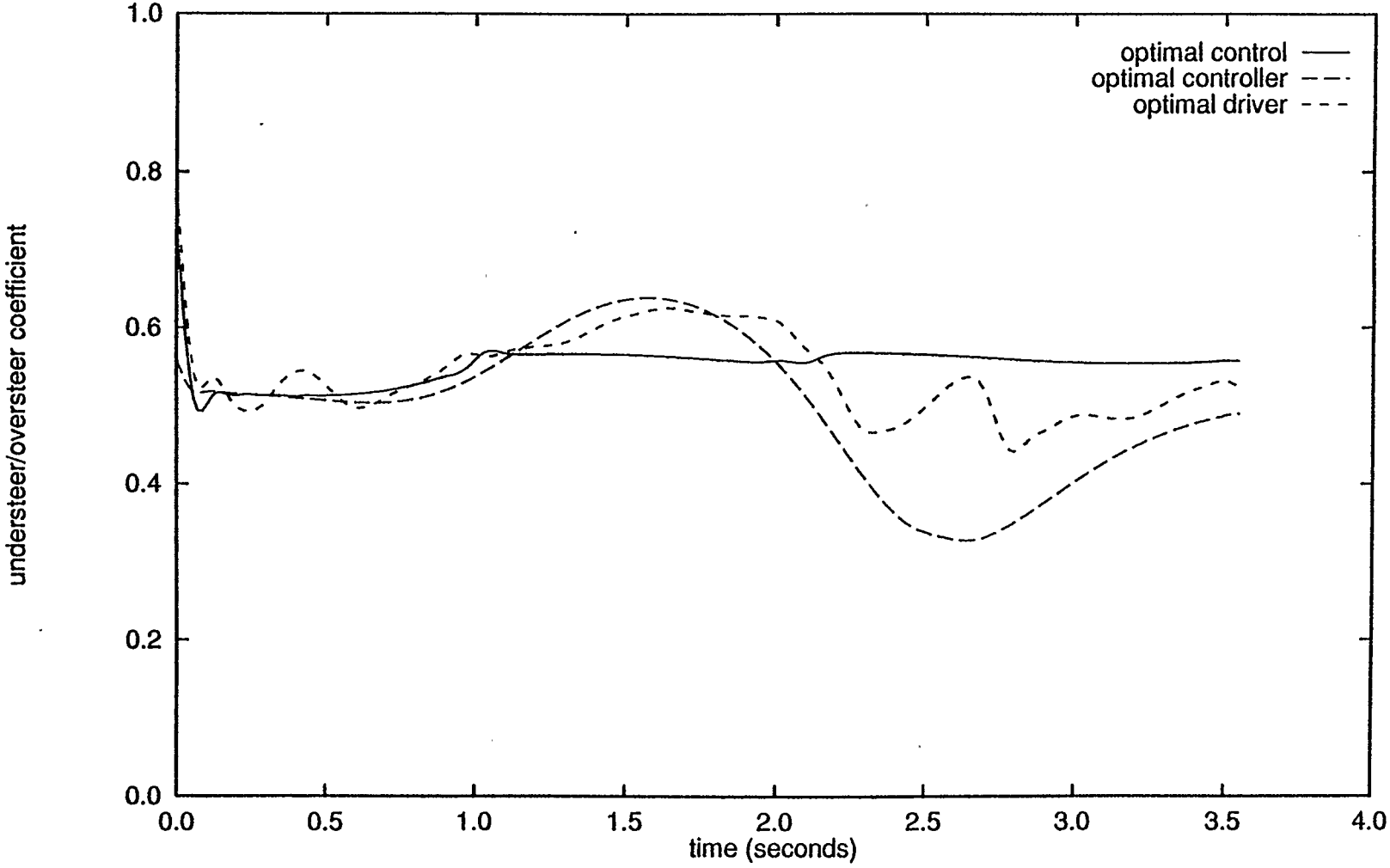

Figure 7.1.10: Understeer/Oversteer Coefficient for Slow Lane Change Manoeuvre

7.2 The Fast Lane Change Manoeuvre

The fast lane change manoeuvre was performed at about 12 *m/s* and represents the highest speed at which the driver was able to drive through the lane change and still maintain adequate tracking accuracy. The plotted results from the fast lane change manoeuvre are shown in Figures 7.2.1 to 7.2.10. Although the velocity is higher here (12 m/s as opposed to 7 m/s,) most of the results produced by the optimal control and controller are similar to those for the slower manoeuvre. The tracking shown in Figure 7.1.2 is excellent.

The steering input by the driver has first and second peak values of about -0.06 radians and 0.09 radians, while the optimal control has values of -0.047 and 0.05 radians. These values are only slightly higher than those of the slow lane change.

The accuracy of the path following is very good, with the exception of the optimal driver. Because the optimal driver attempts to mimic the inputs of the driver, it will try to reproduce the large steer angles of the driver. The tracking error for the optimal driver is large by the end of the manoeuvre (0.15 meters) and the vehicle is rotated 0.05 radians away from the rotational position of the trajectory. This indicates that the vehicle may be in the process of going out of control, although the driver experienced no such difficulties.

Despite the increase in speed from 7 m/s to 12 m/s, the slip angles stay in the linear range and the understeer/oversteer coefficient remains at about the base value, +0.55. Though this is the fastest the driver was capable of travelling through the experimental manoeuvre, the vehicle seems to have roughly the same control characteristics as in the slower manoeuvre. Also similar is that the tires remain in the linear range; the coefficient therefore provides no indication of the vehicle's handling characteristics at the limits of the tires' adhesion. It actually shows more about the limits of the driver's abilities.

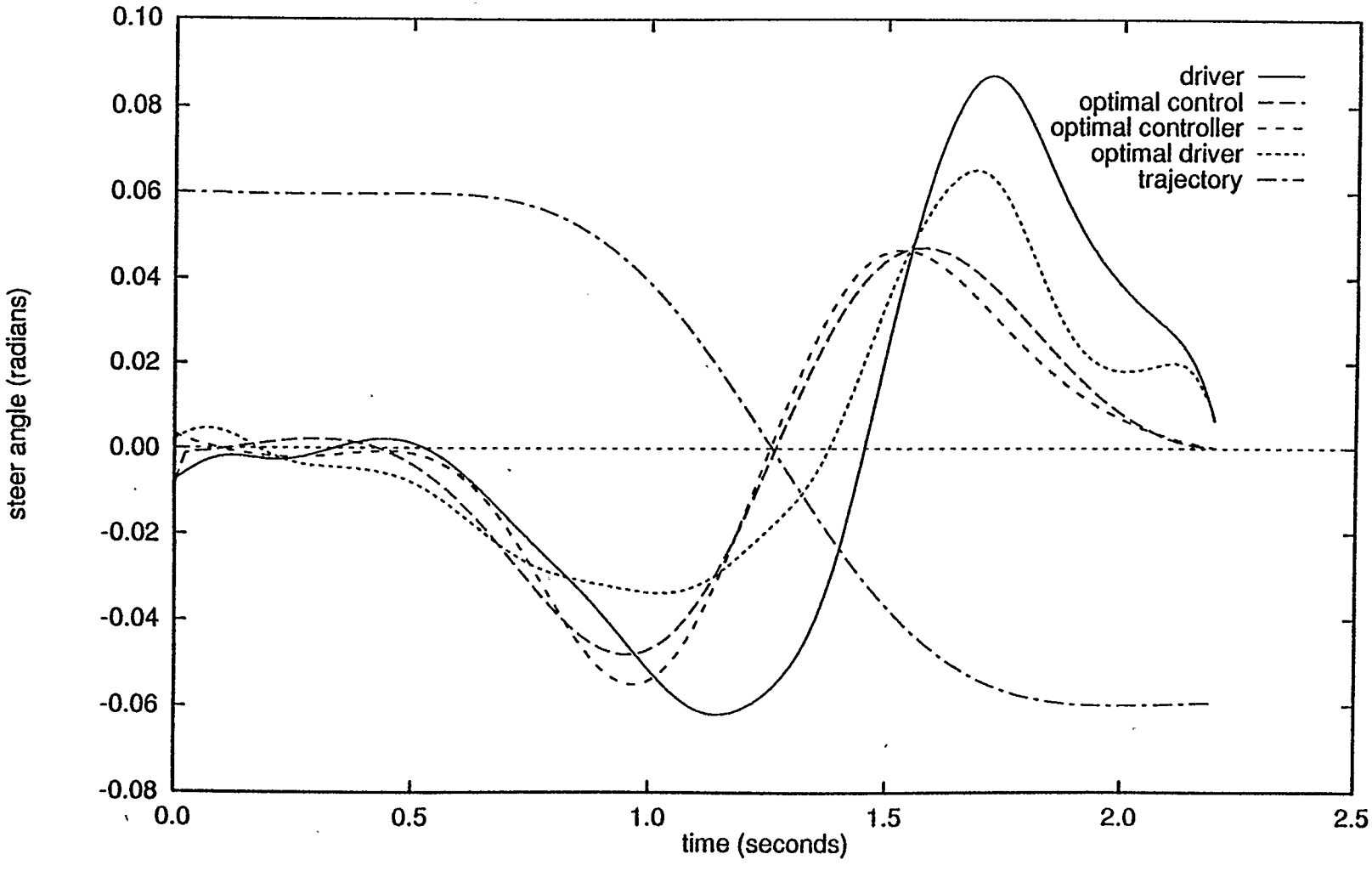

Figure 7.2.1: Steering for Fast Lane Change Manoeuvre

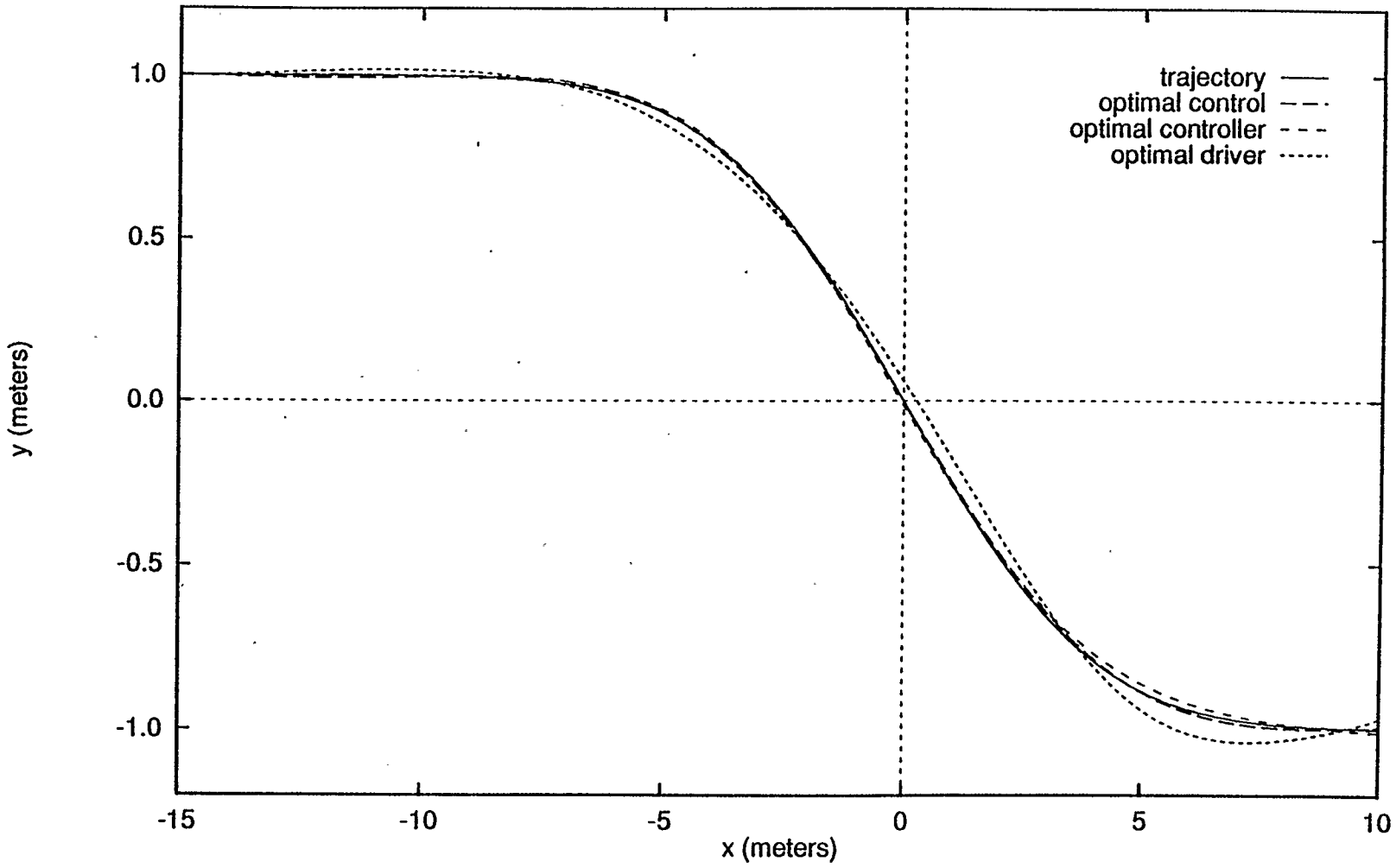

Figure 7.2.2: Trajectories for Fast Lane Change Manoeuvre

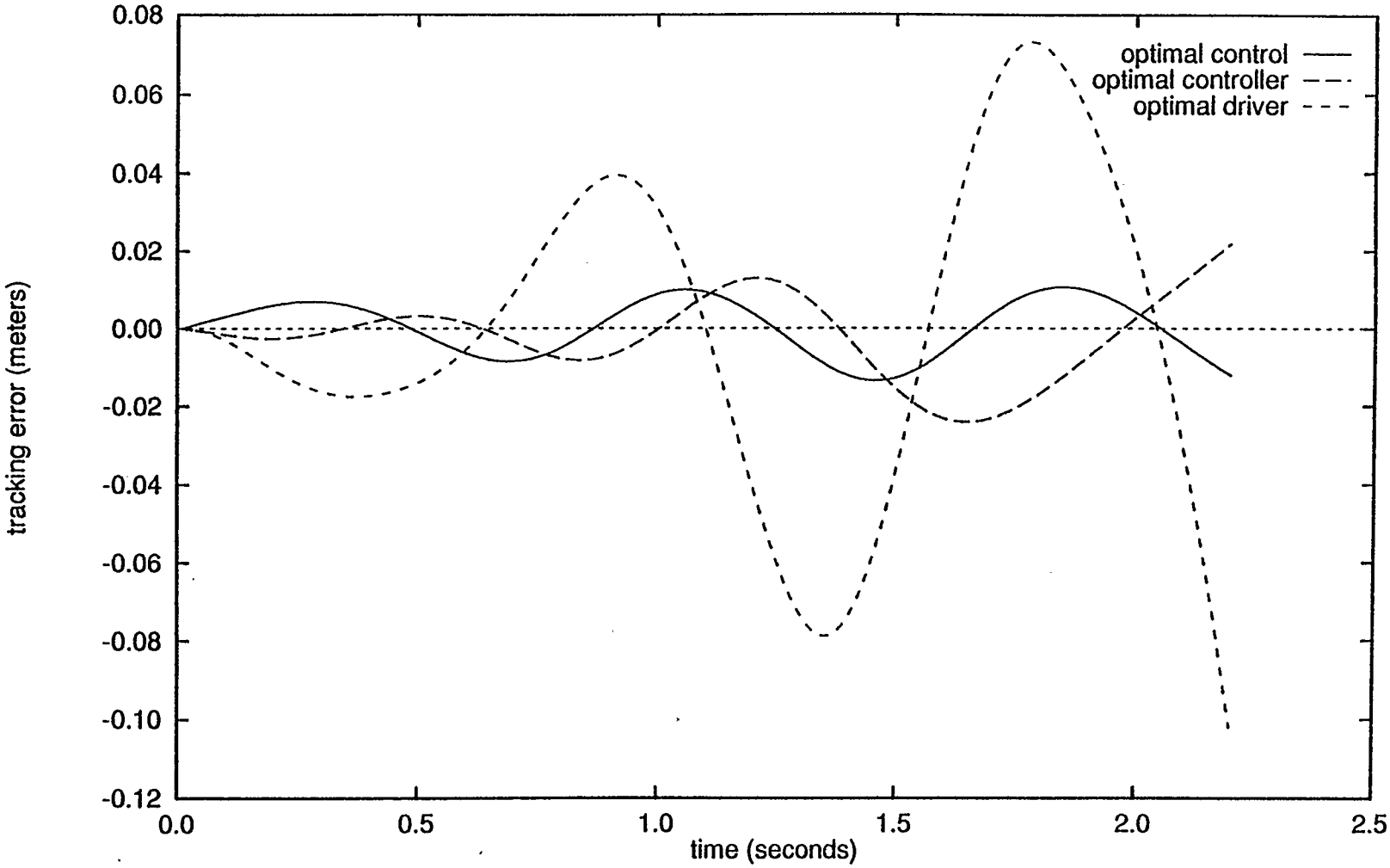

Figure 7.2.3: Tracking Error for Fast Lane Change Manoeuvre

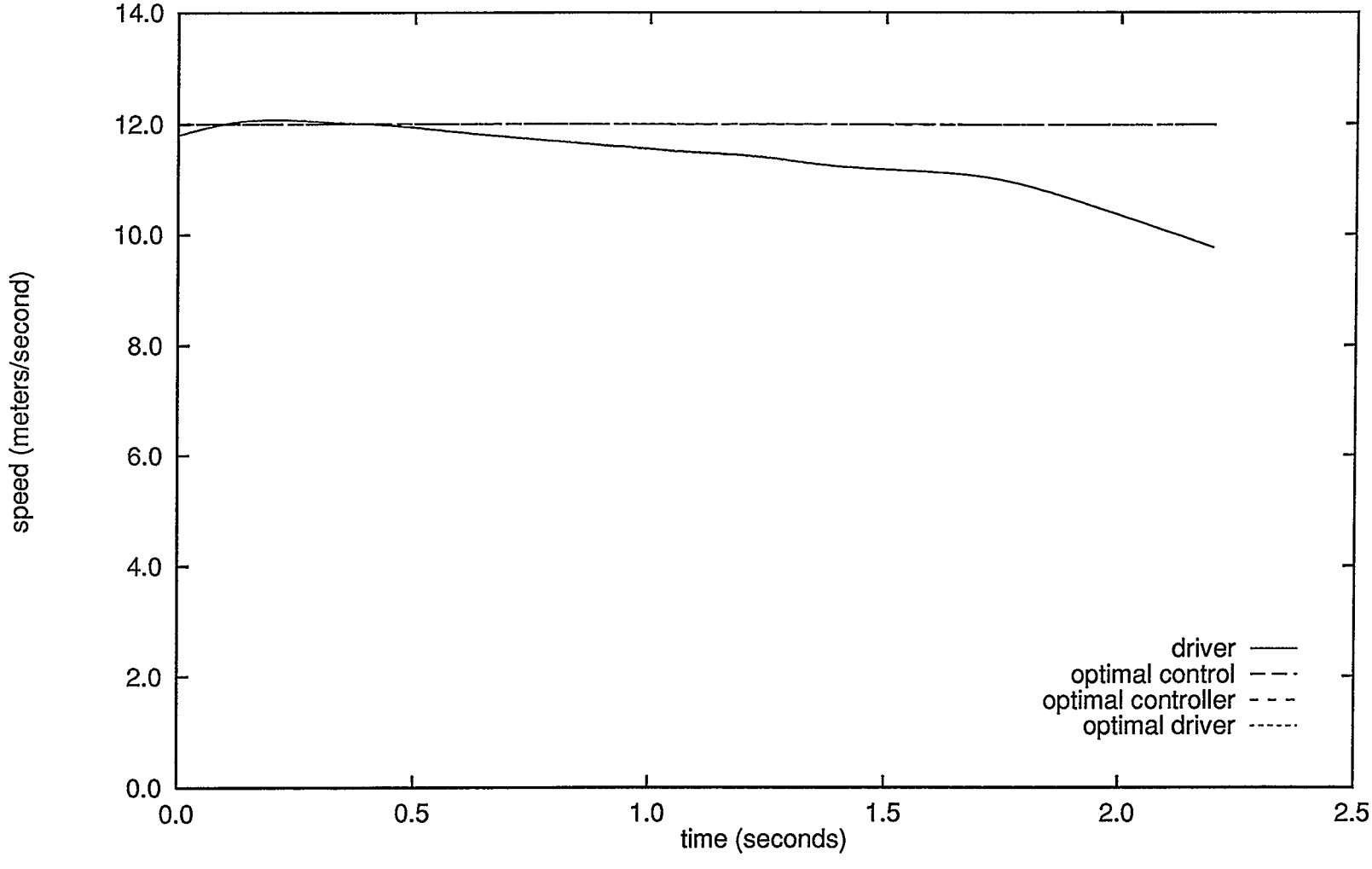

Figure 7.2.4: Speeds for Fast Lane Change Manoeuvre

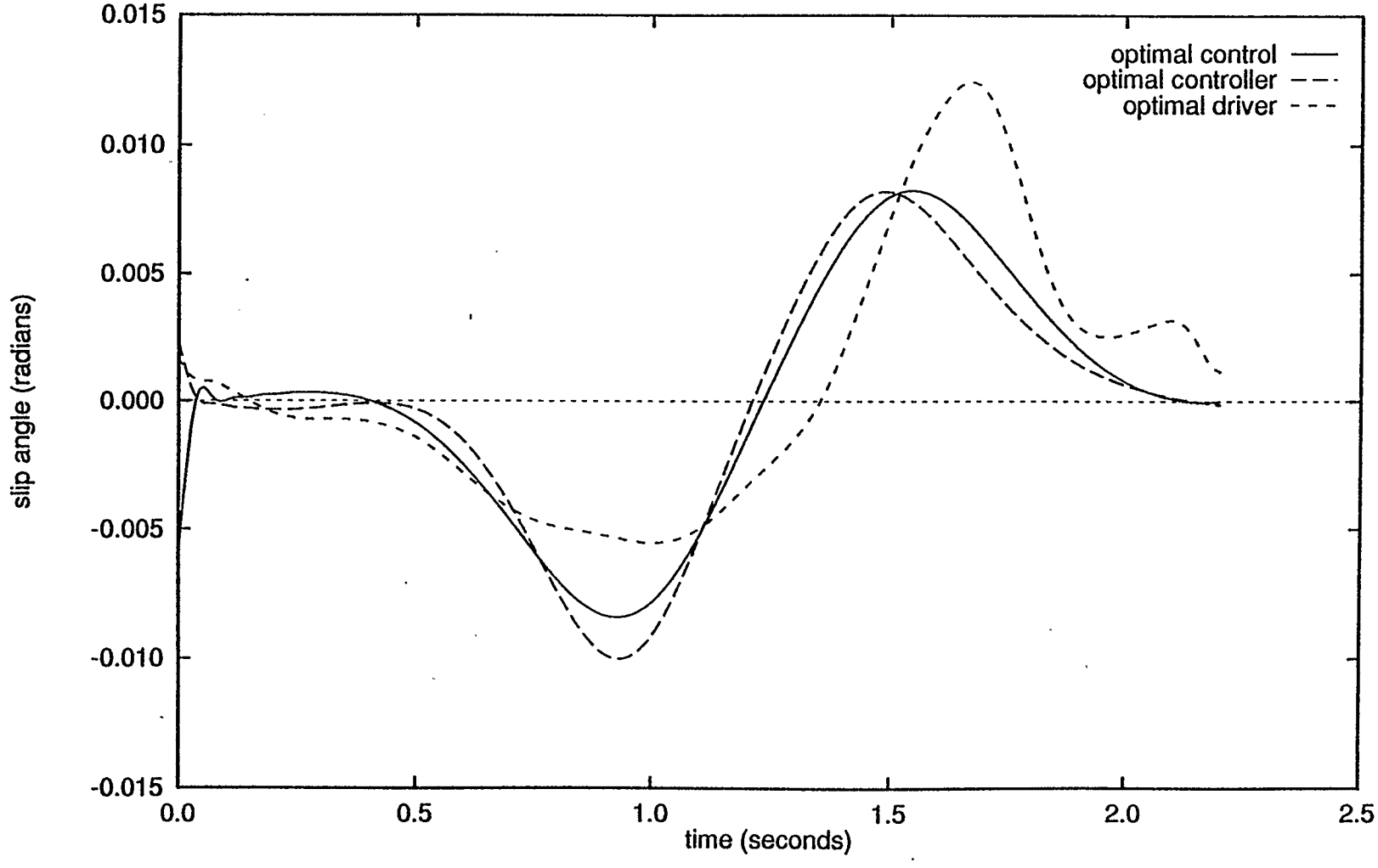

Figure 7.2.5: Front Slip Angles for Fast Lane Change Manoeuvre

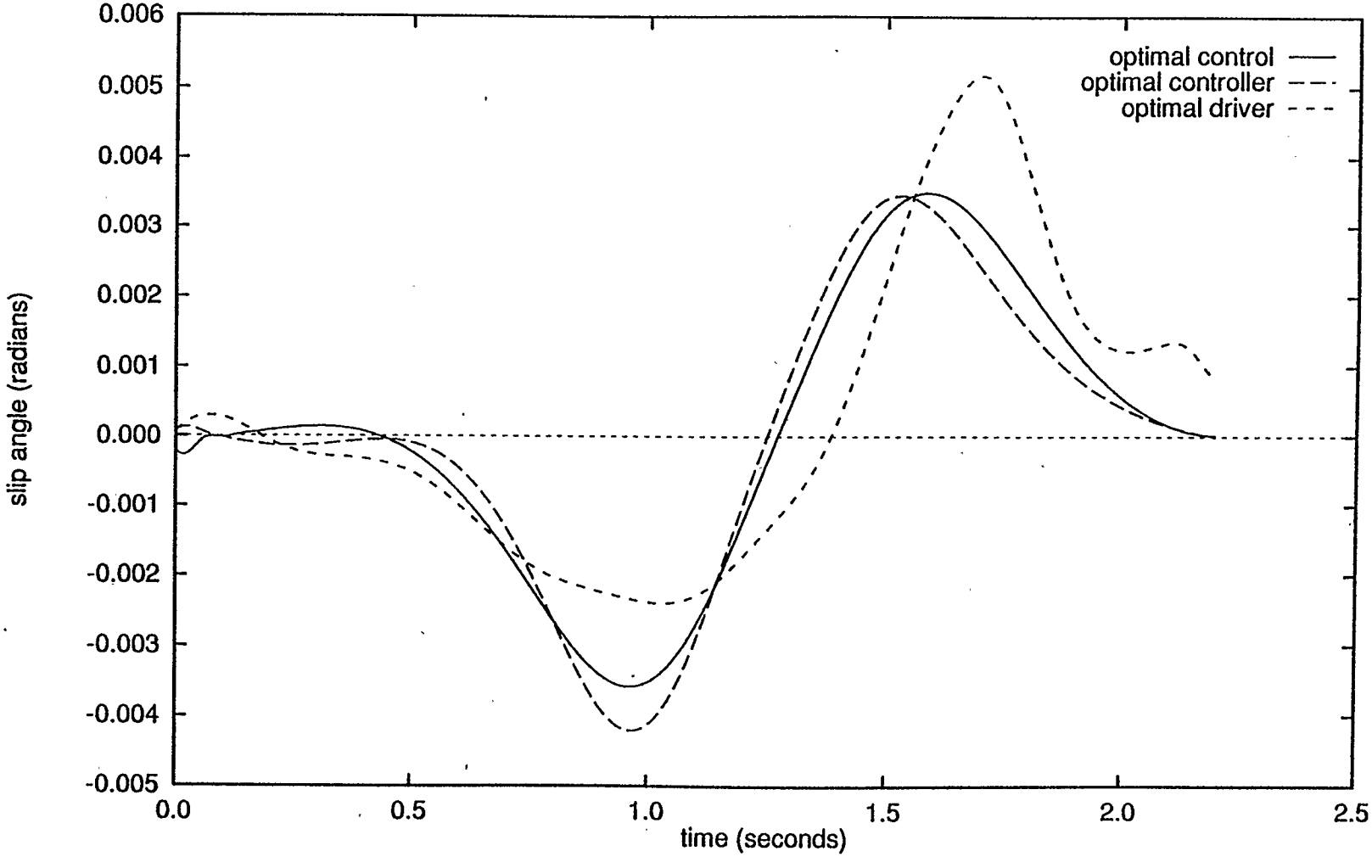

Figure 7.2.6: Rear Slip Angles for Fast Lane Change Manoeuvre

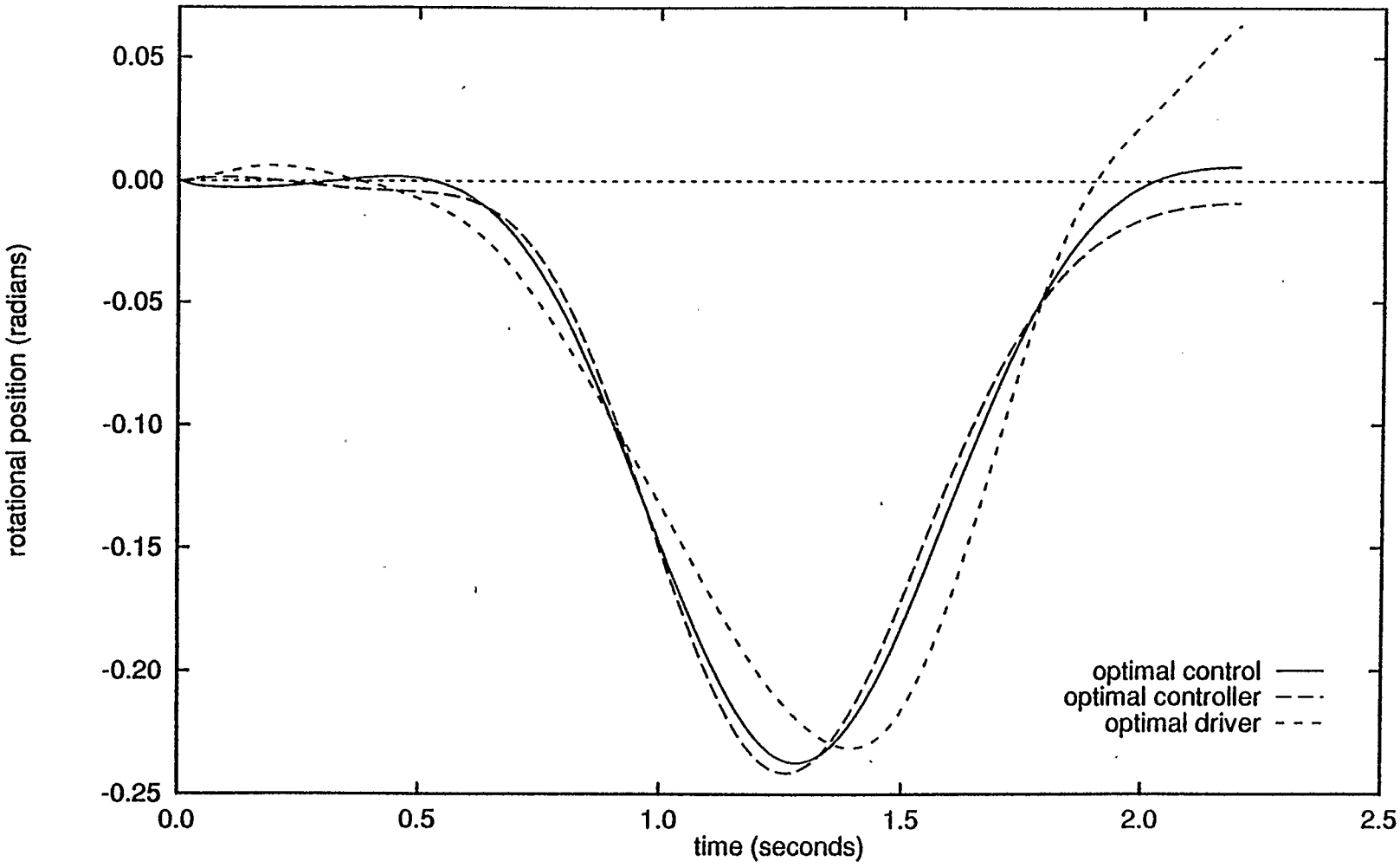

Figure 7.2.7: Rotational Positions for Fast Lane Change Manoeuvre

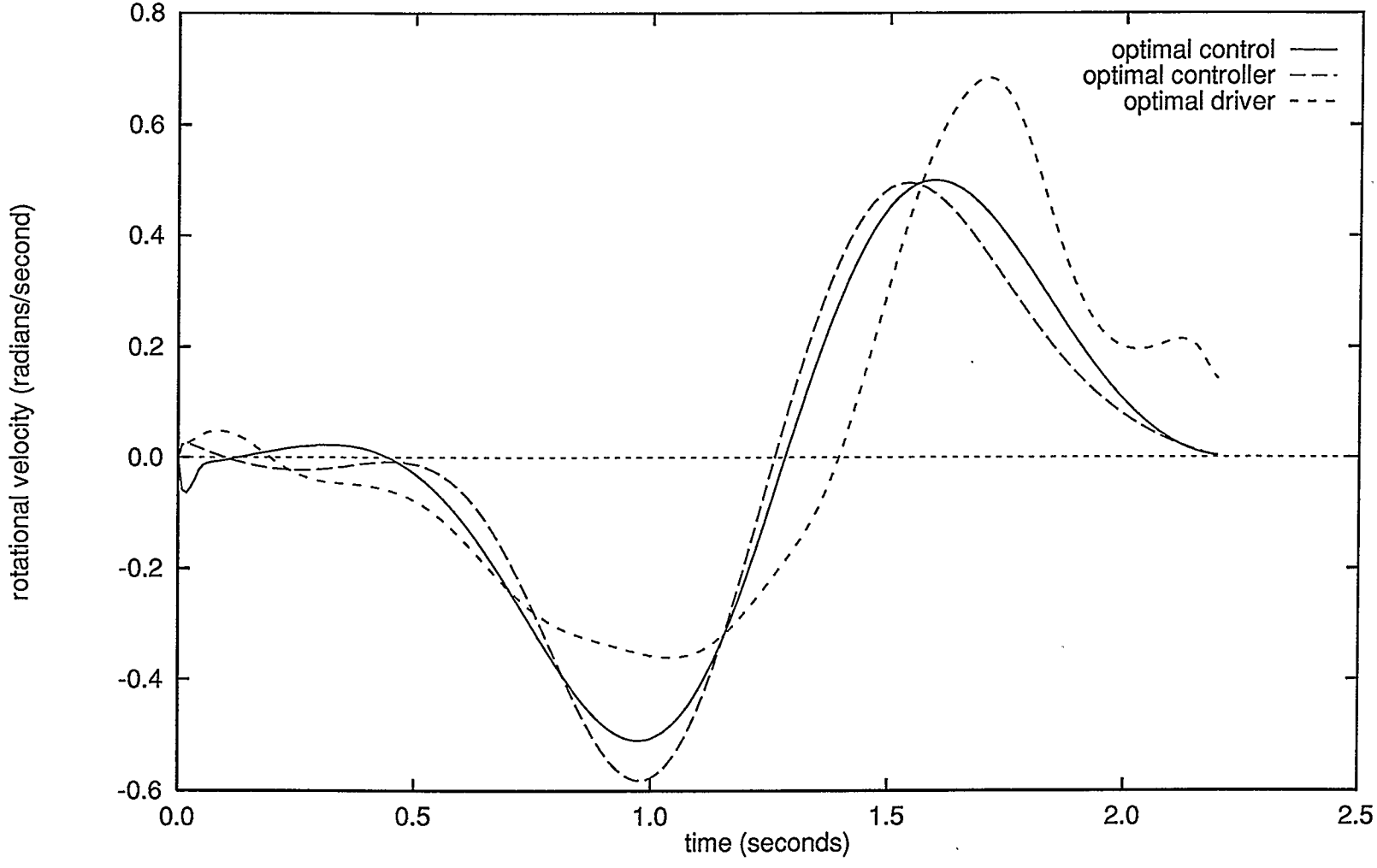

Figure 7.2.8: Rotational Velocity for Fast Lane Change Manoeuvre

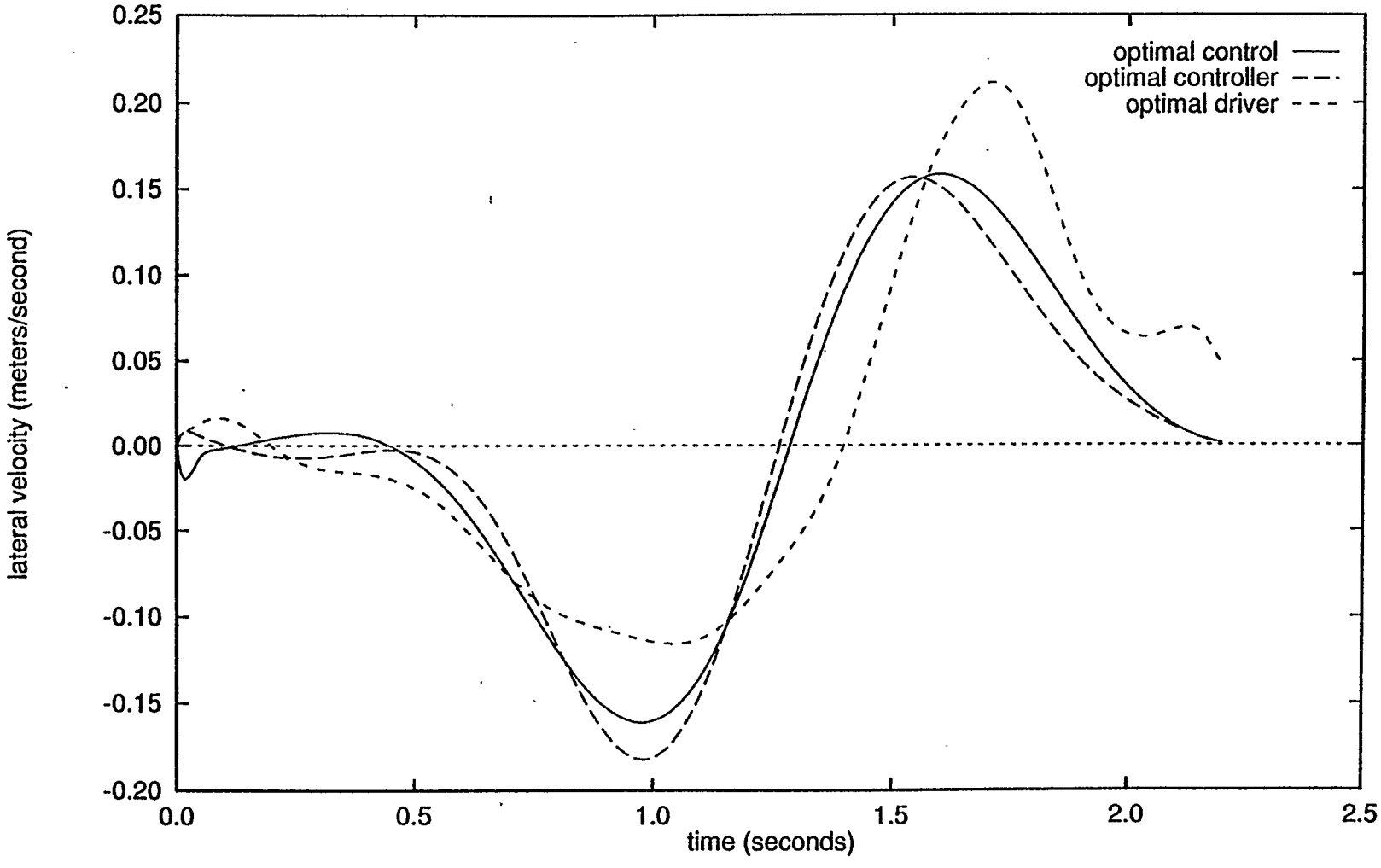

Figure 7.2.9: Lateral Velocity for Fast Lane Change Manoeuvre

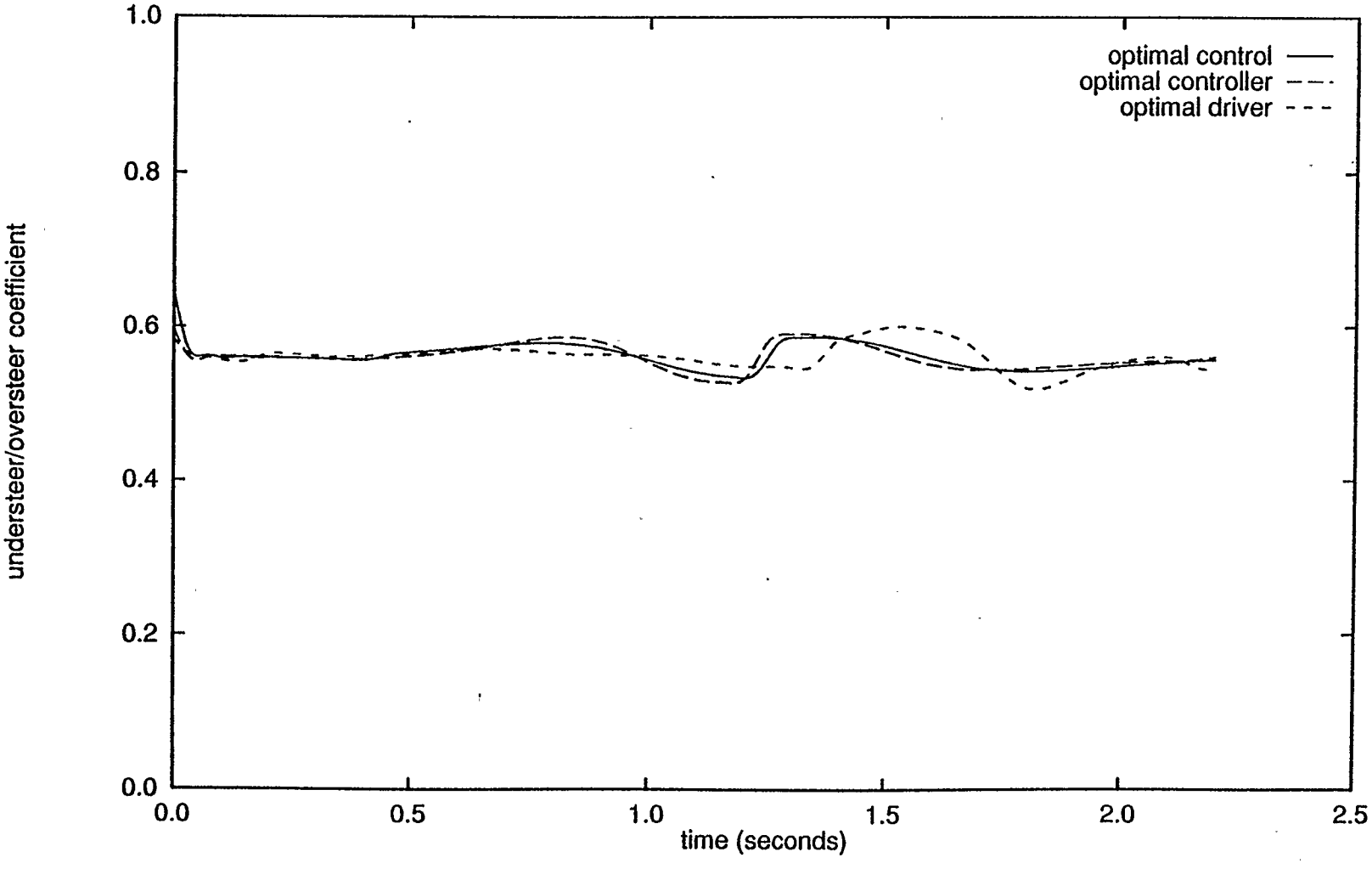

Figure 7.2.10: Understeer/Oversteer Coefficient for Fast Lane Change Manoeuvre

7.3 The Slow Corner Manoeuvre

The slow 90° corner manoeuvre was performed at about 9 m/s. At this speed the driver could comfortably follow the prescribed path. The results from the slow manoeuvre are plotted in Figures 7.3.1 to 7.3.10 and reflect realistic values. A frequent tendency of the steering input is a gradual rise in steering value until the corner is entered. At this point, the steering input reaches a plateau lasting until the end of the corner. The input then gradually declines to a zero steer angle as the vehicle straightens out. The actual steering is often somewhat rough, with numerous local oscillations, which are sometimes driver corrections applied to minimize the error.

The steering values are shown in Figure 7.3.1. As with the lane change manoeuvres, the steering values produced by the driver are larger than the numerical simulation results: 0.23 radians peak for the driver, while the largest value for the optimal control is 0.12 radians. The ratio of these values is generally consistent with those of the lane change manoeuvre. For the optimized driver, the front slip angles (Figure 7.3.5) of the front tire peak briefly at 0.086 radians. This seems to be an attempt to improve the cost function value by conforming to the driver's steering input at the expense of tracking accuracy. The front tires saturate at a slip angle of about 0.05 radians. Because the lateral forces remain the same at slip angles higher than this, any steering which keeps the slip angles above this value has no additional effect on the vehicle's movement.

The effect of this brief period of operation in a saturated state is shown in Figure 7.3.10. At this time, the understeer/oversteer coefficient goes to +1.0, indicating that the vehicle is understeering to an extreme. This also happens at the beginning of the manoeuvre. At all other times the coefficient for the optimized driver remains very close to the base value of +0.55 and the tires remain in the linear operating zone. For the other two optimization techniques, the tires remain in the linear zone for the entire manoeuvre, so the coefficients remain at the base value.

The vehicle's speed is about 9 m/s on a 10.0 m radius curve. A lateral acceleration of about 8.1 m/s^2 would be required to follow the corner exactly. Based on the tire coefficient of friction of 1.5, a maximum lateral acceleration of about 15 m/s^2 is possible. This indicates that the vehicle is not close to the limits of its performance.

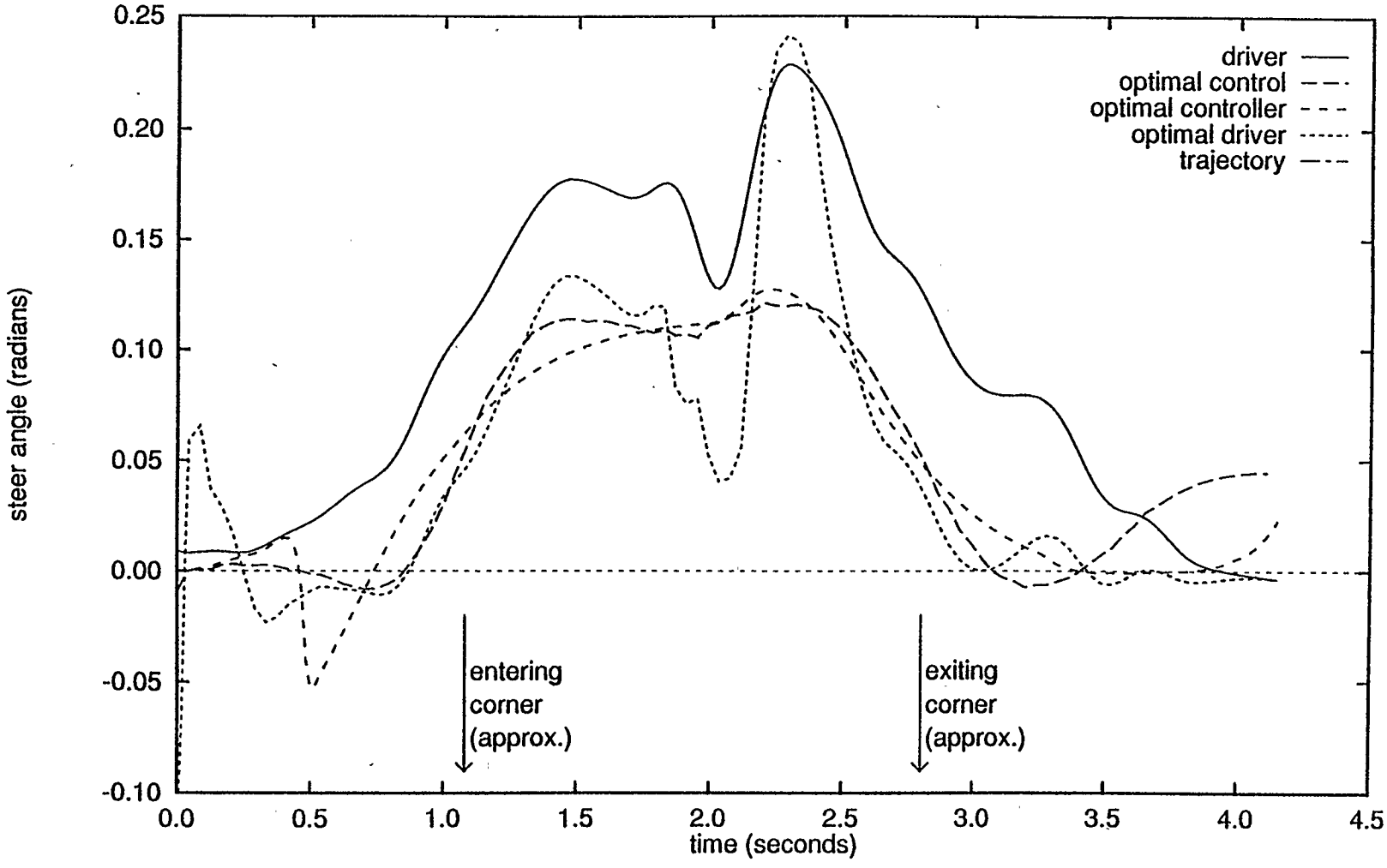

Figure 7.3.1: Steering for Slow Corner Manoeuvre

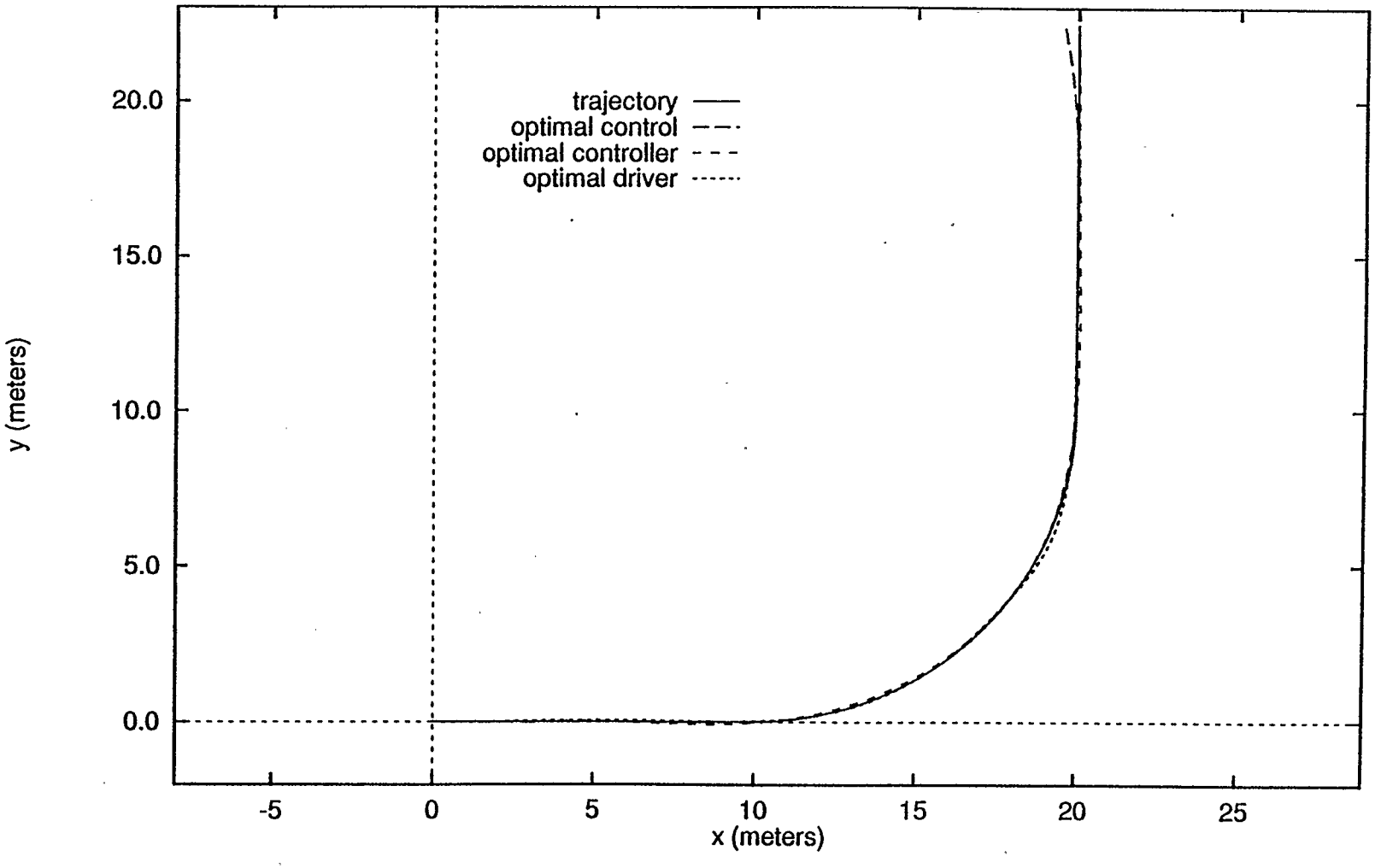

Figure 7.3.2: Trajectories for Slow Corner Manoeuvre

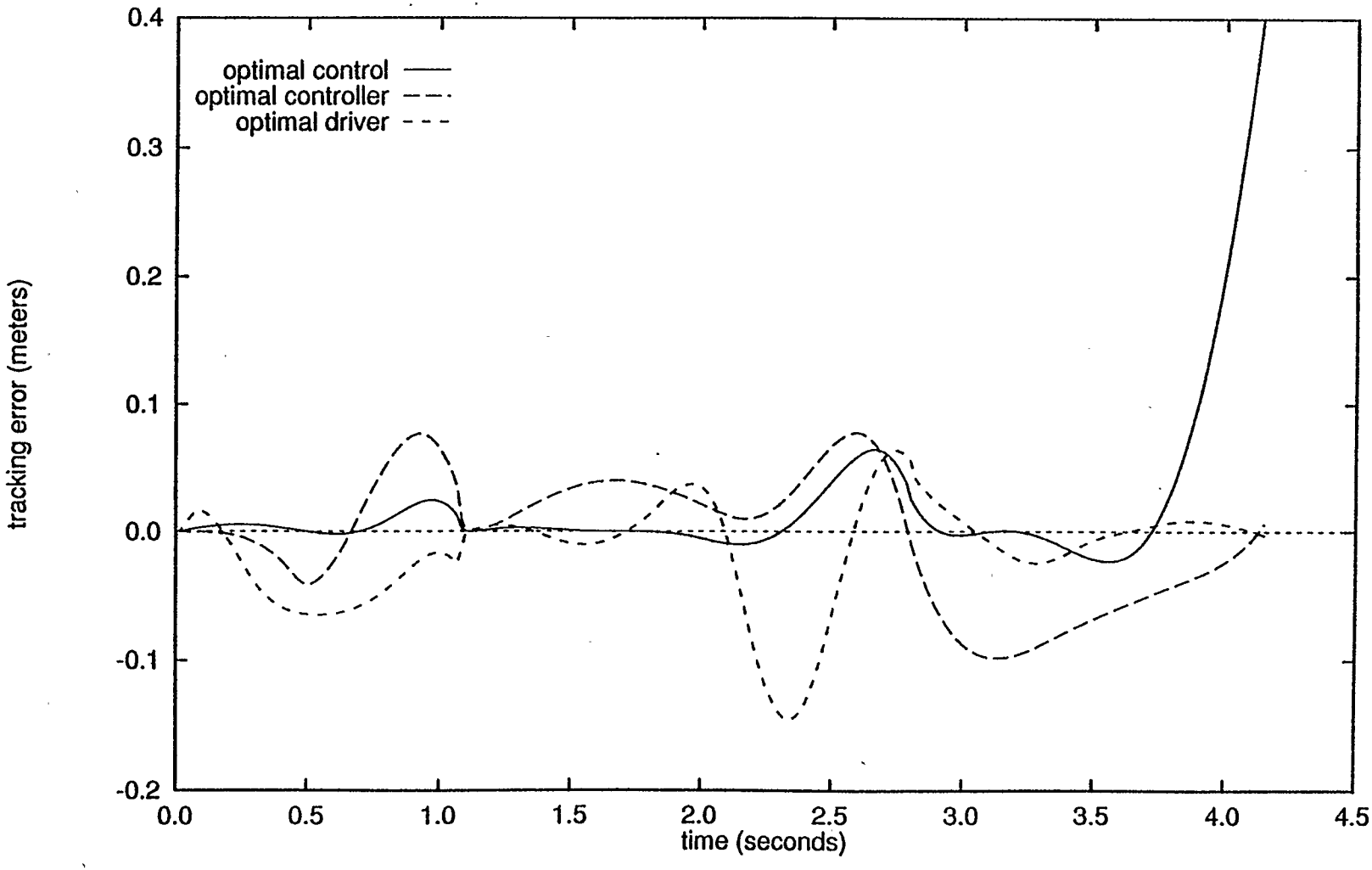

Figure 7.3.3: Tracking Error for Slow Corner Manoeuvre

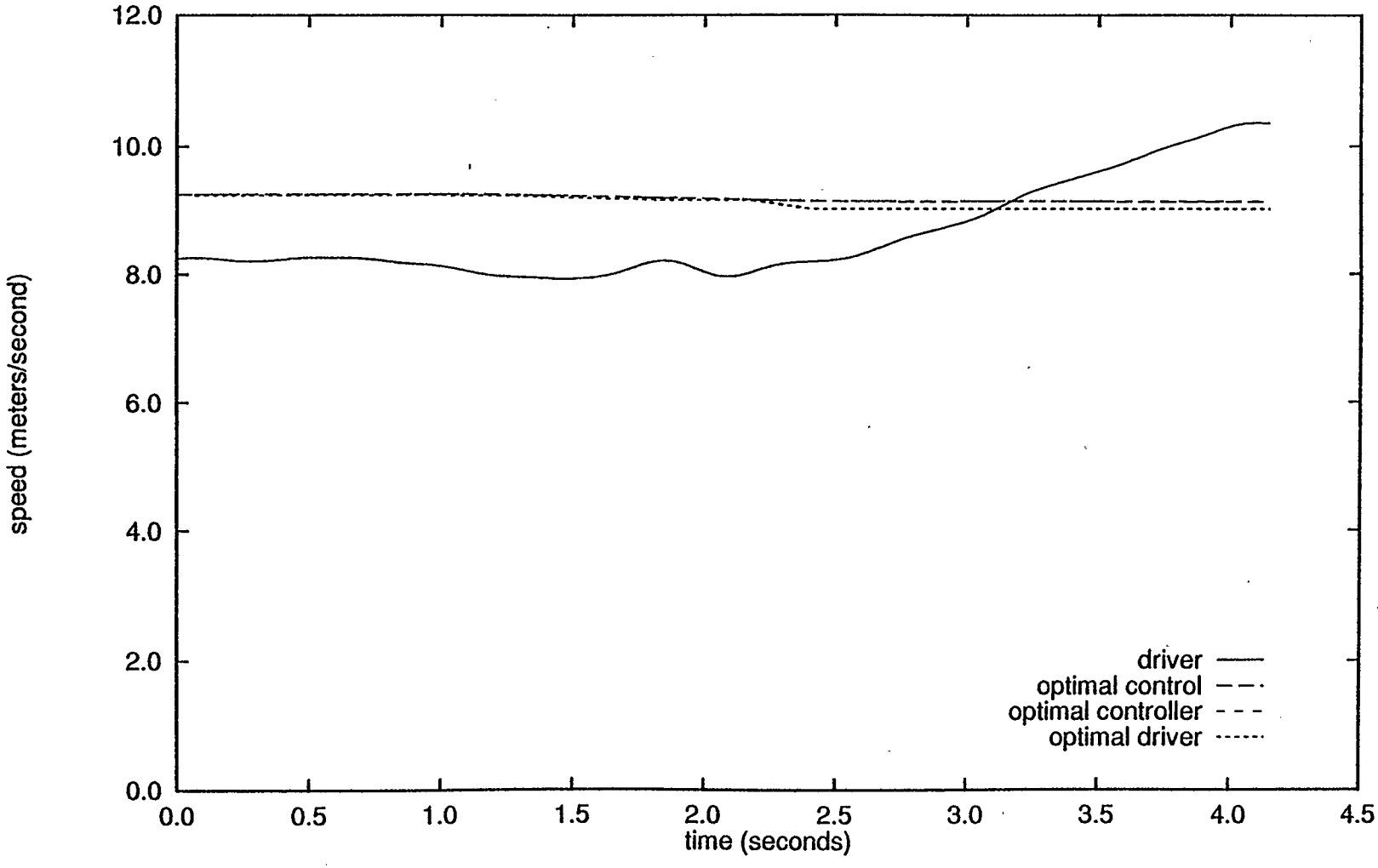

Figure 7.3.4: Speeds for Slow Corner Manoeuvre

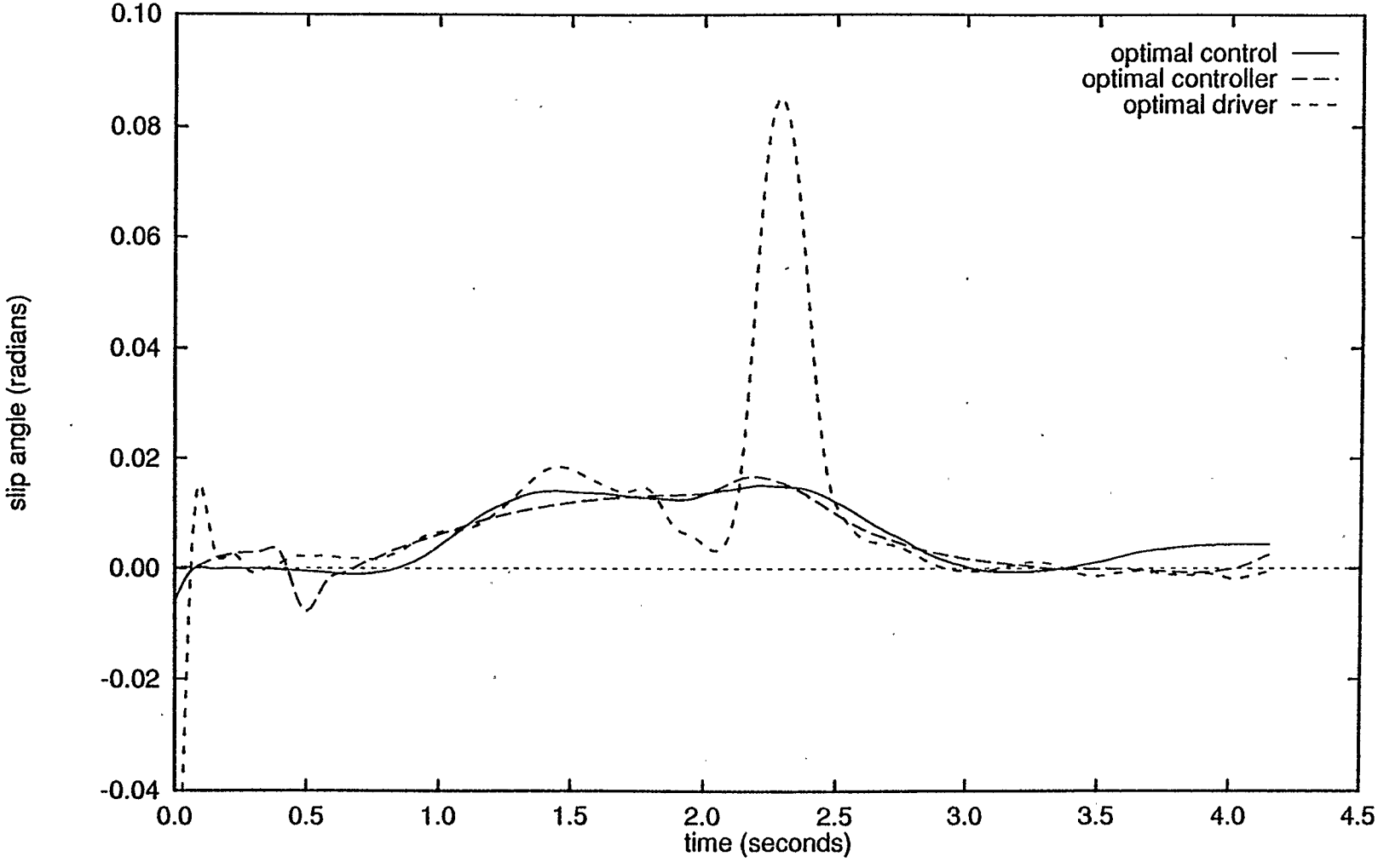

Figure 7.3.5: Front Slip Angles for Slow Corner Manoeuvre

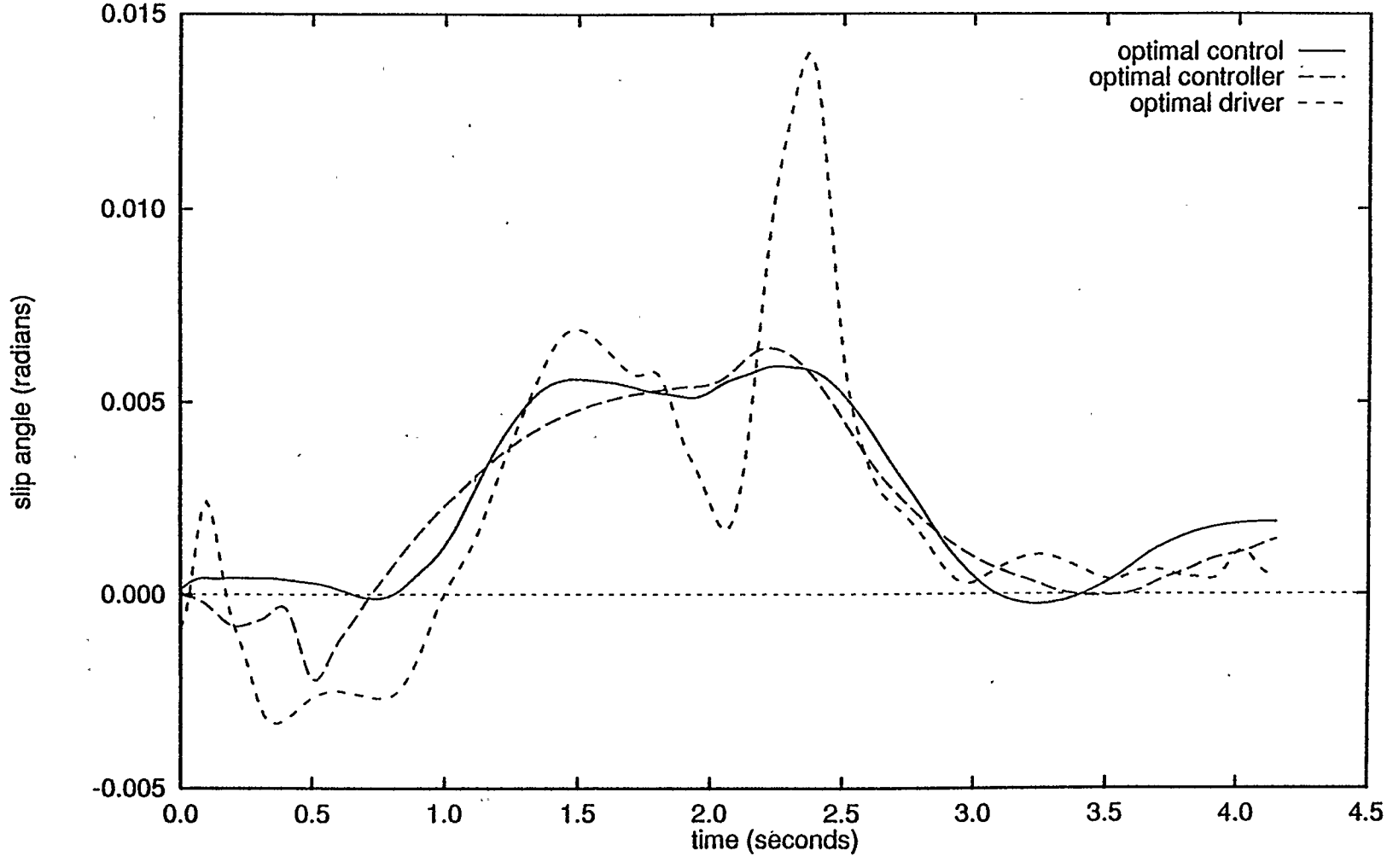

Figure 7.3.6: Rear Slip Angles for Slow Corner Manoeuvre

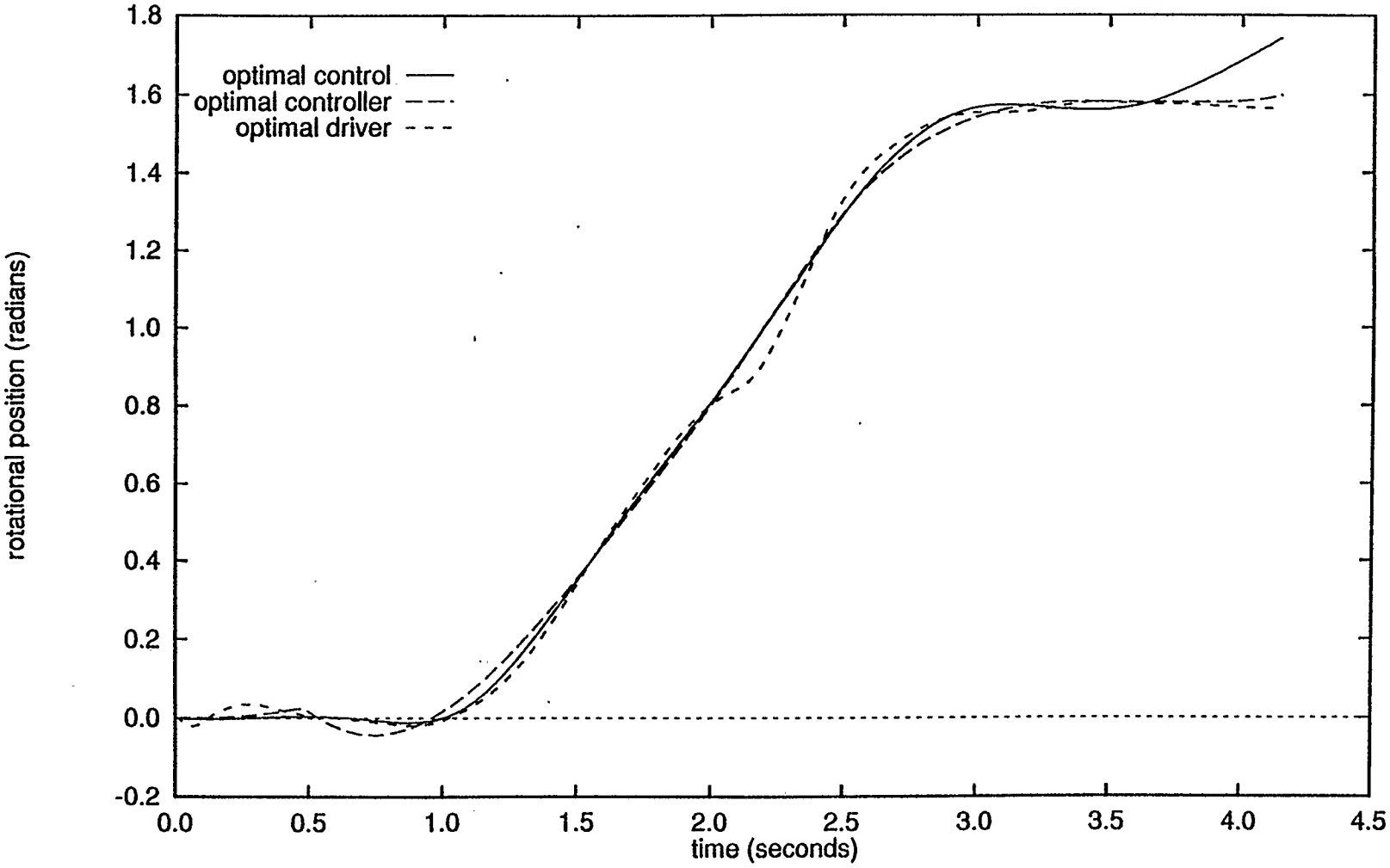

Figure 7.3.7: Rotational Positions for Slow Corner Manoeuvre

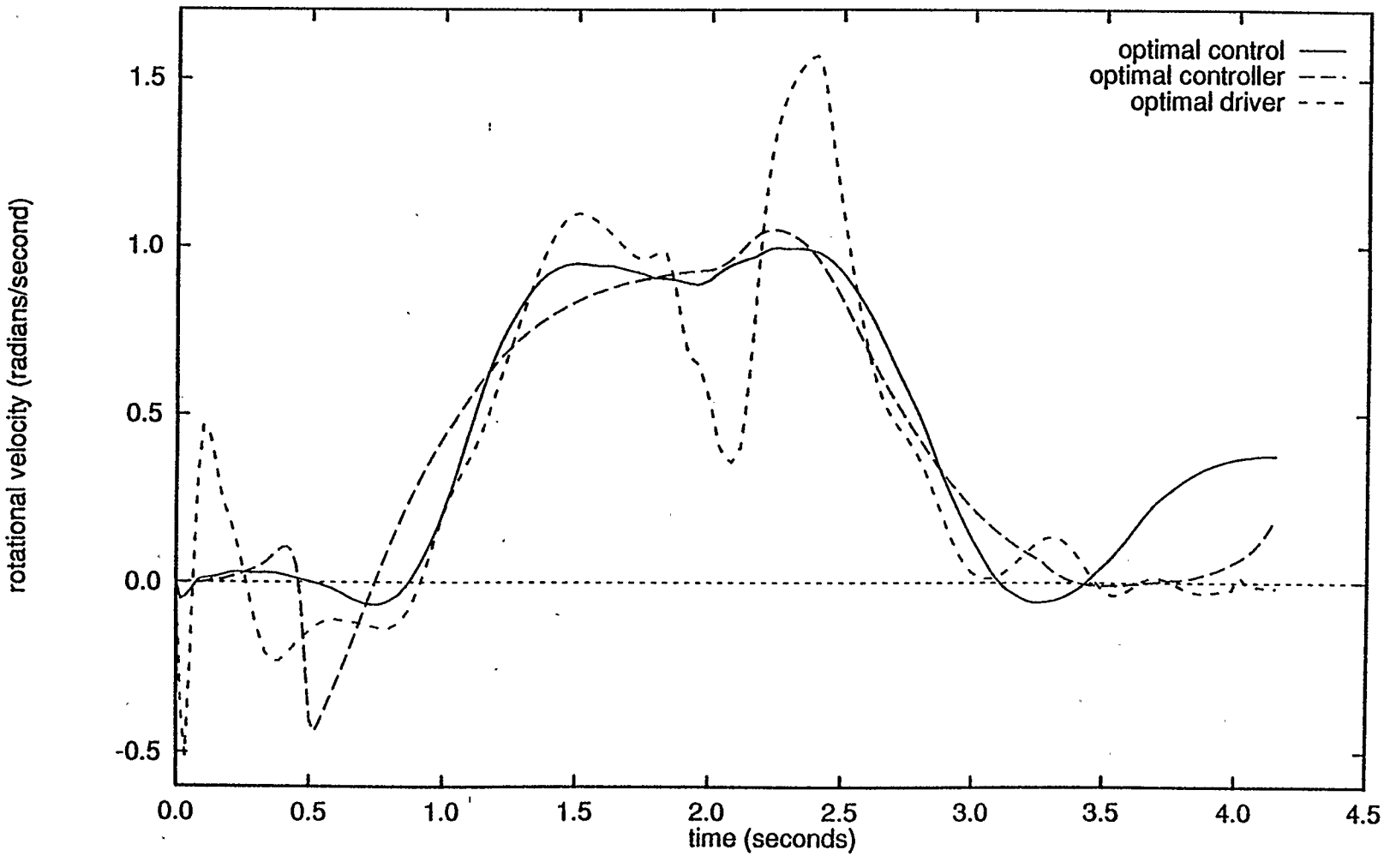

Figure 7.3.8: Rotational Velocity for Slow Corner Manoeuvre

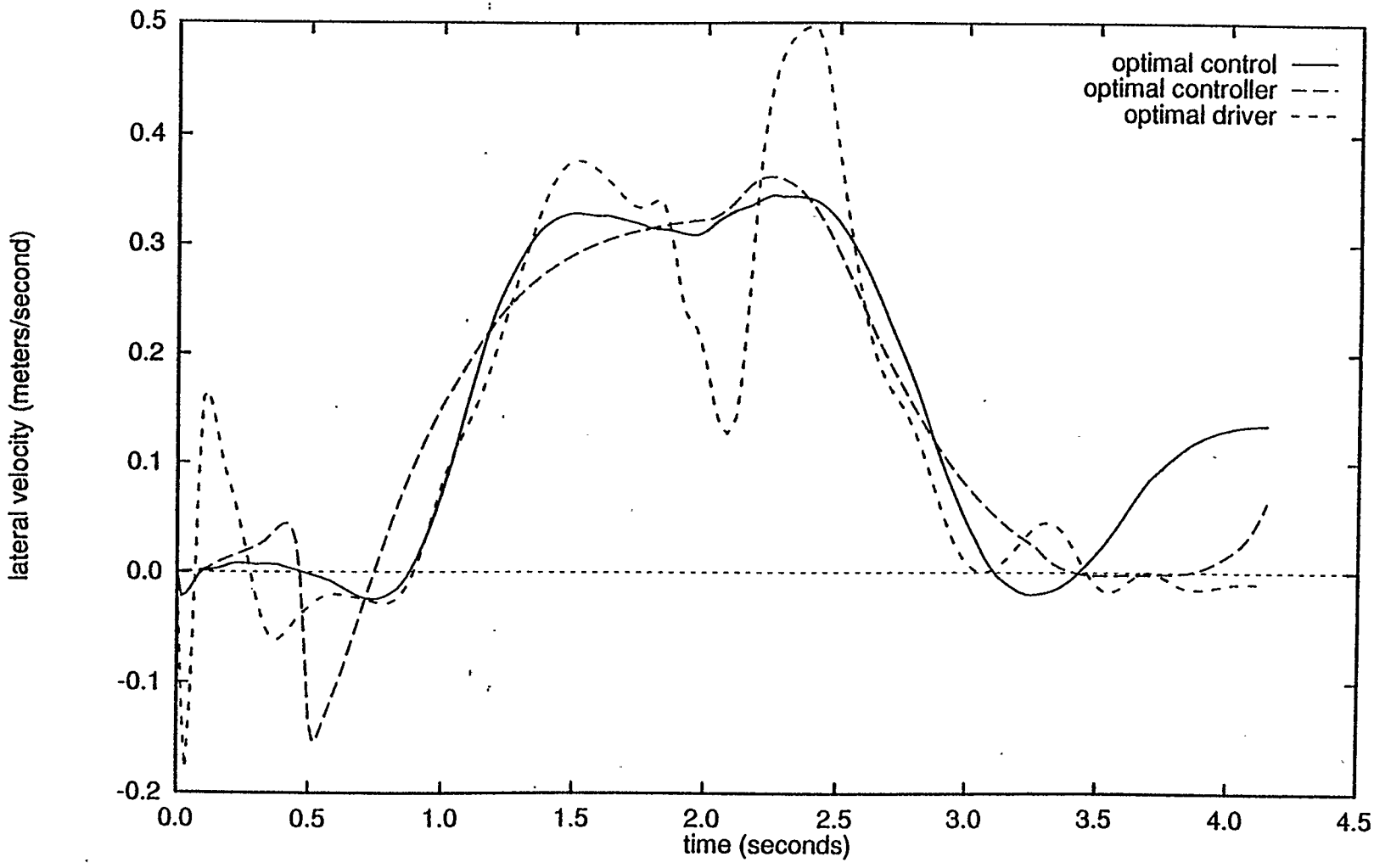

Figure 7.3.9: Lateral Velocity for Slow Corner Manoeuvre

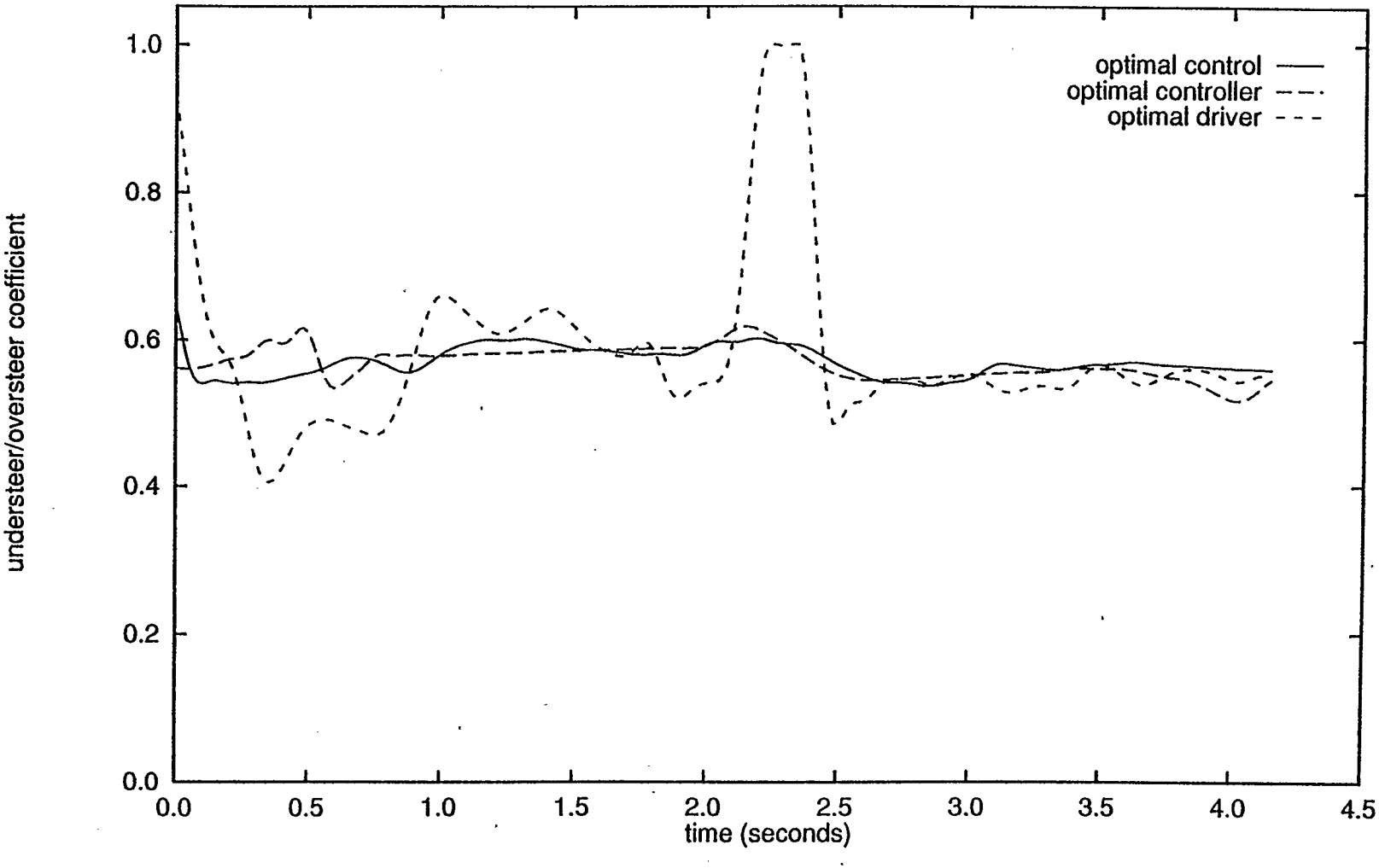

Figure 7.3.10: Understeer/Oversteer Coefficient for Slow Corner Manoeuvre

7.4 The Fast Corner Manoeuvre

The graphs associated with the fast 90° manoeuvre are presented in Figures 7.4.1 to 7.4.10. This is the fastest that the driver could enter the corner and still manage to exit the manoeuvre with little tracking error. The steering is still of the basic form seen in the slow corner except here there are large oscillations at the beginning and end of the manoeuvre.

Generally, the extremes of behavior found in the computed results coincide well with observations of experimental results. The computed path following shown in Figures 7.4.2 and 7.4.3 indicates that the path following is not as good as with the slower manoeuvre. Further, the slip angle results shown in Figures 7.4.5 and 7.4.6 indicate that at times during the manoeuvres the front tires saturate, and therefore the vehicle has reached a performance limit.

Unlike the lane change manoeuvres, where the speed was limited by the driver's abilities, these results indicate a manoeuvre where the speed is limited by the vehicle's limits of adhesion. The vehicle enters the corner at 13 m/s and leaves at around 12 m/s which, if the vehicle were to follow the curve exactly, would represent lateral accelerations from 16.9 m/s^2 down to 14.4 m/s^2 so the vehicle is near or at the limits of adhesion laterally. This is consistent with the driver's feeling that the limits of the tires' adhesion had been reached. With a tire coefficient of friction of 1.5 and a maximum lateral acceleration of about 15 m/s^2, 16.9 m/s^2 is above the vehicle's maximum of 15.0 m/s^2. The vehicle does not follow the curve exactly, but instead follows a path that has a larger radius of curvature.

The intensity of this manoeuvre is visible on most graphs at the beginning and end of the manoeuvres, while the steering itself has fewer fluctuations. For the steering angles in Figure 7.4.1, all of the numerical techniques show oscillations at the beginning of the manoeuvre, very large with the optimal control. The driver, on the other hand, shows no oscillations at the beginning, but large, probably corrective, oscillations at the end.

The slip angle plots in Figures 7.4.5 and 7.4.6 reveal the reason for the strong setup at the beginning of the manoeuvre. The front slip angle values are past the 0.051 radian value at which the front tires saturate. Once the vehicle has entered the corner, its ability to be controlled by steering input is limited. It must therefore enter the corner in a state which allows it to exit properly without much assistance in the way of steering input.

The effects on the handling of the vehicle are shown in the understeer/oversteer graph, Figure 7.4.10. After some initial oscillations in the front steering angle, the vehicle briefly has an understeer/oversteer coefficient of +1.0, indicating the extreme case of understeer. When the corner is past, in order for the vehicle to initiate a straight line of travel and stop all rotation, the front steer angle is reduced, which in turn reduces the front tire slip angle. This has the effect of increasing the cornering stiffness of the front tires; for a brief period, the rear tires are at the very low cornering stiffnesses corresponding to high slip angles. At this point the vehicle temporarily becomes almost a neutral steering vehicle, but soon returns to its base operating coefficient.

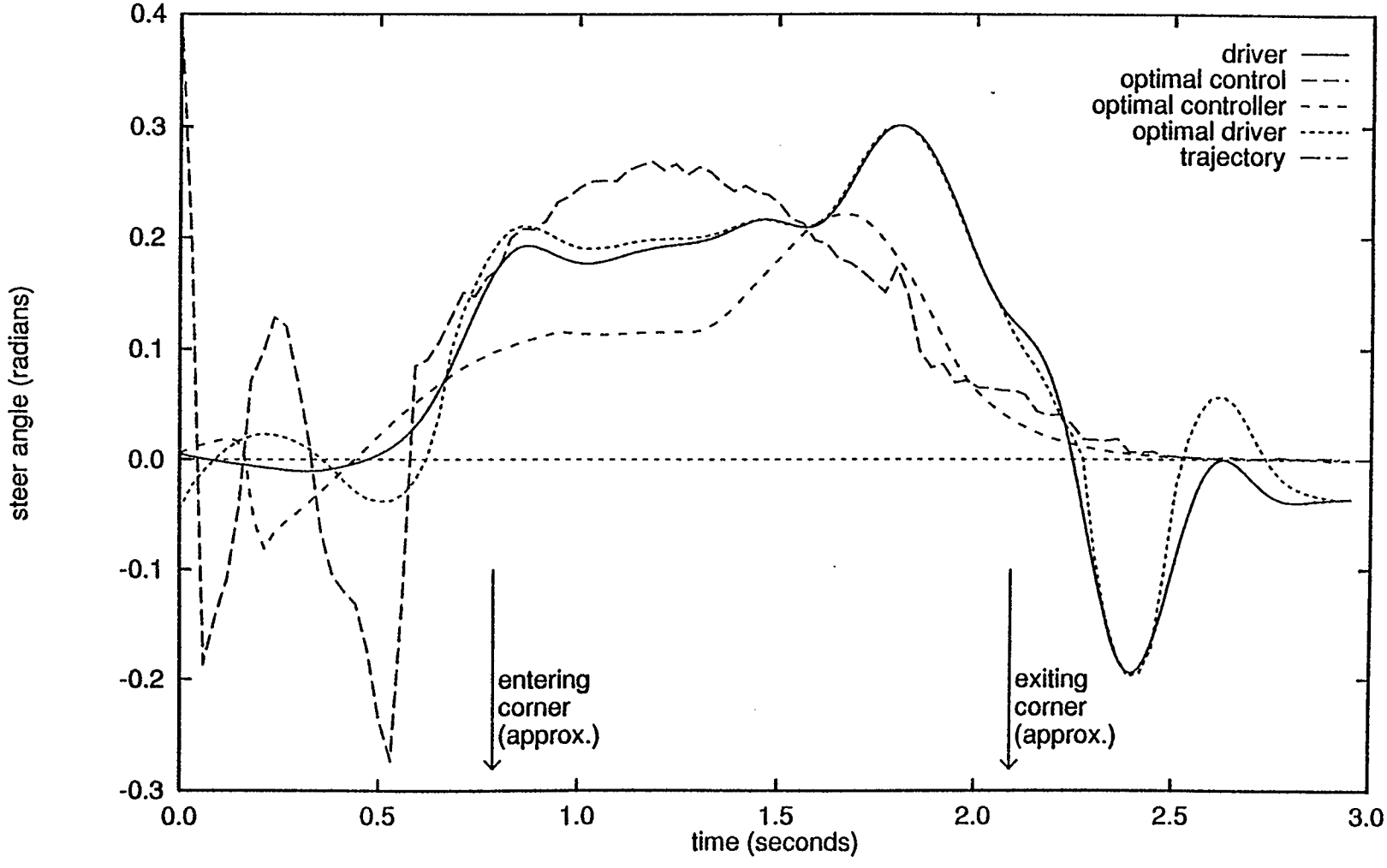

Figure 7.4.1: Steering for Fast Corner Manoeuvre

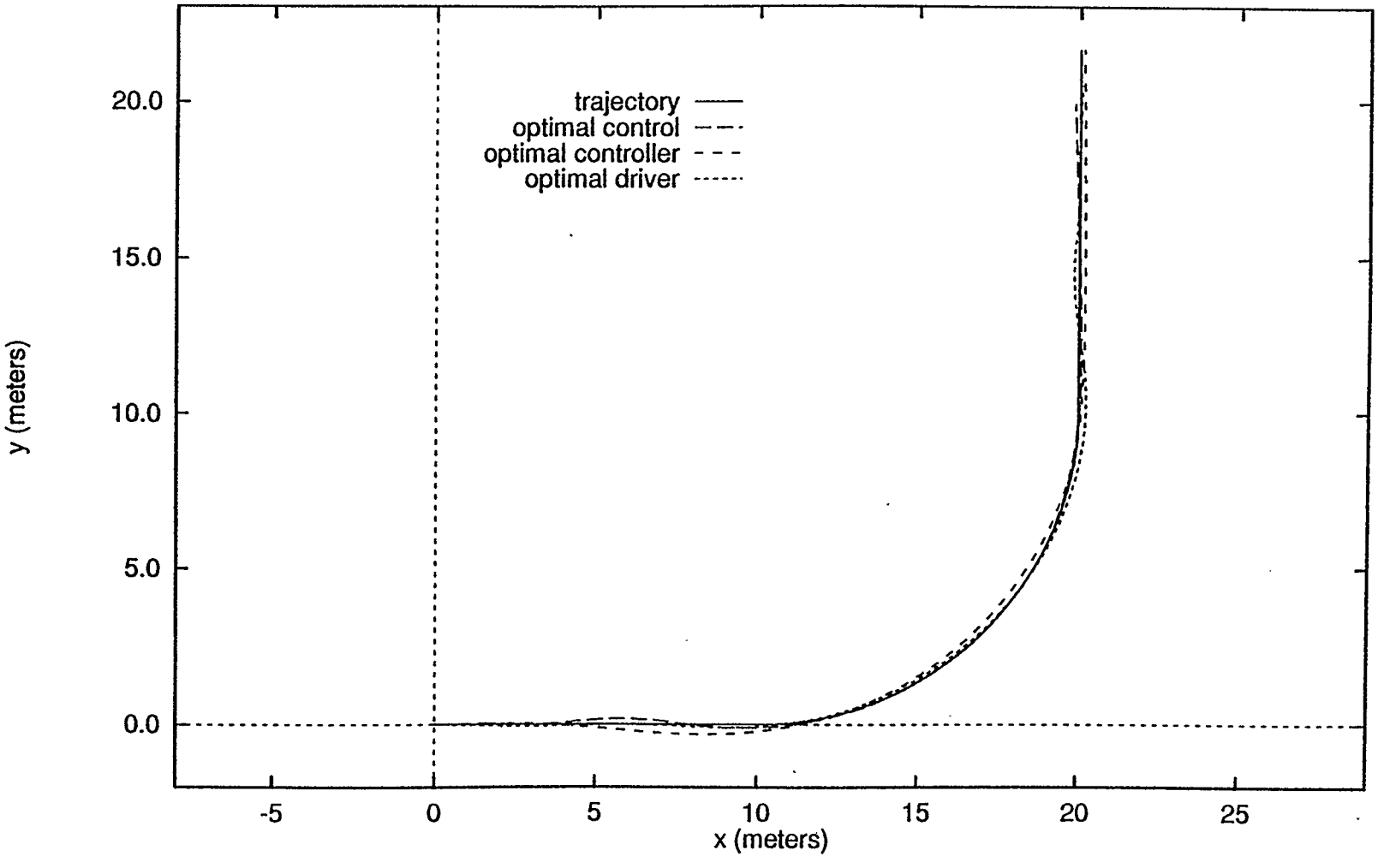

Figure 7.4.2: Trajectories for Fast Corner Manoeuvre

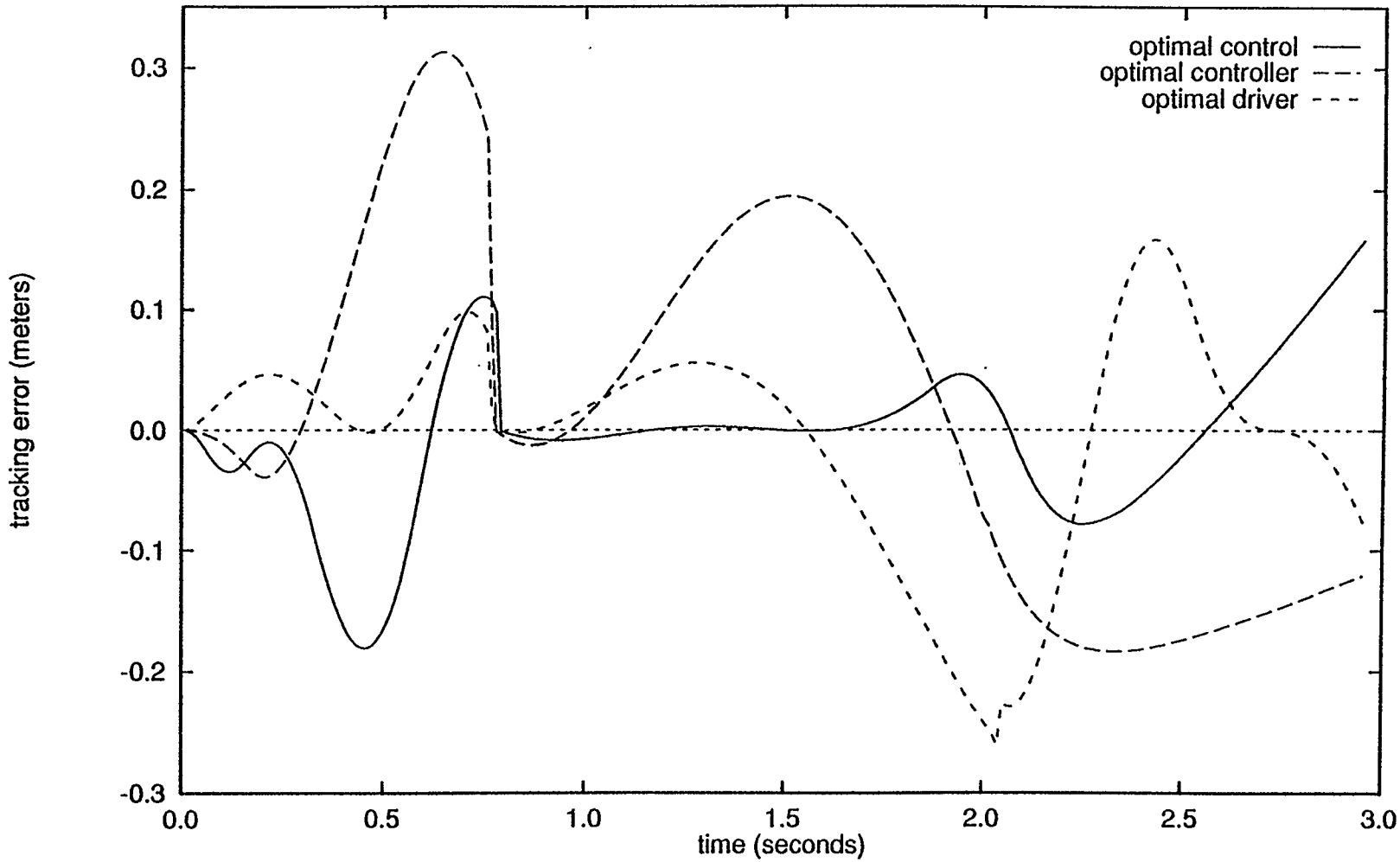

Figure 7.4.3: Tracking Error for Fast Corner Manoeuvre

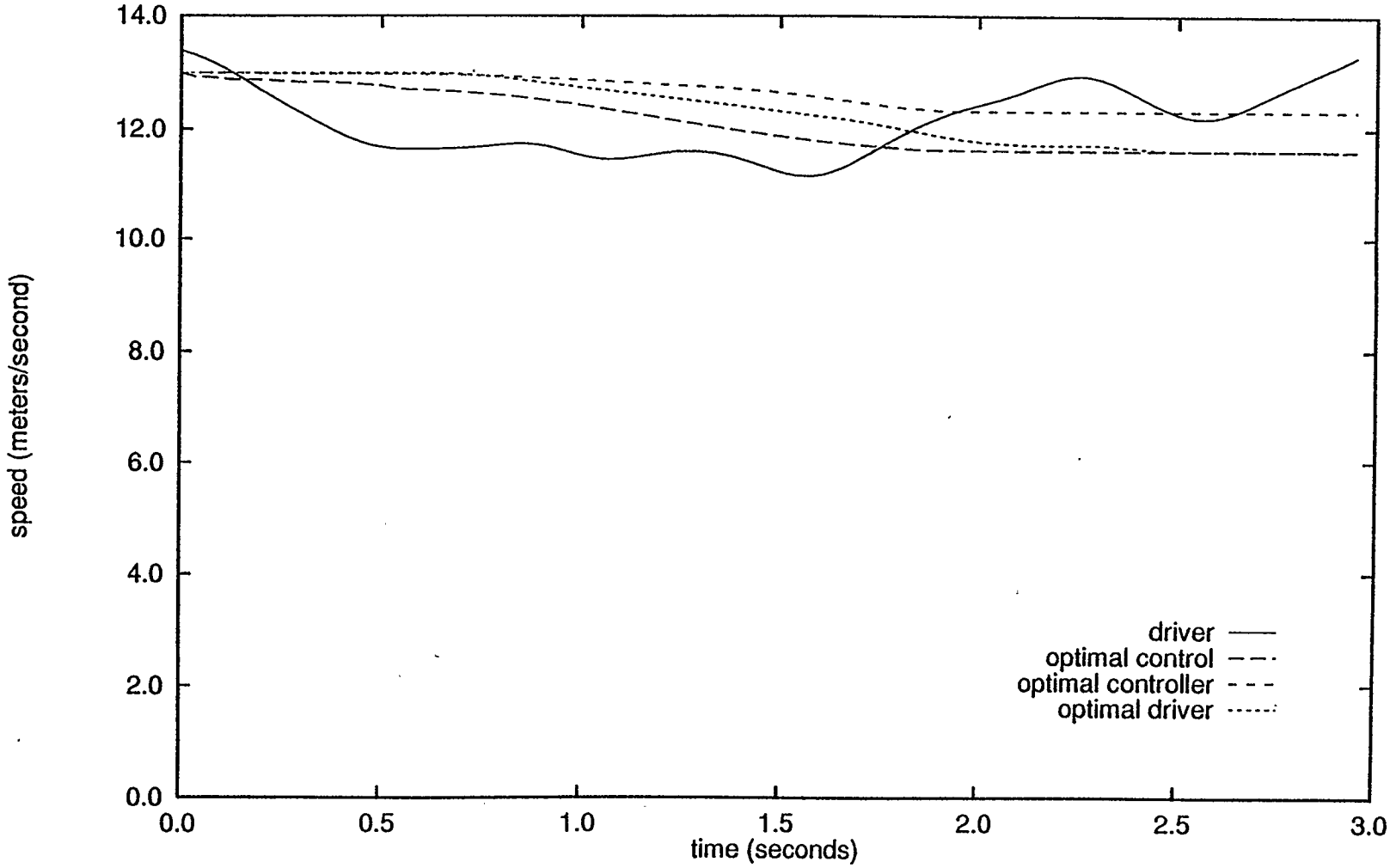

Figure 7.4.4: Speeds for Fast Corner Manoeuvre

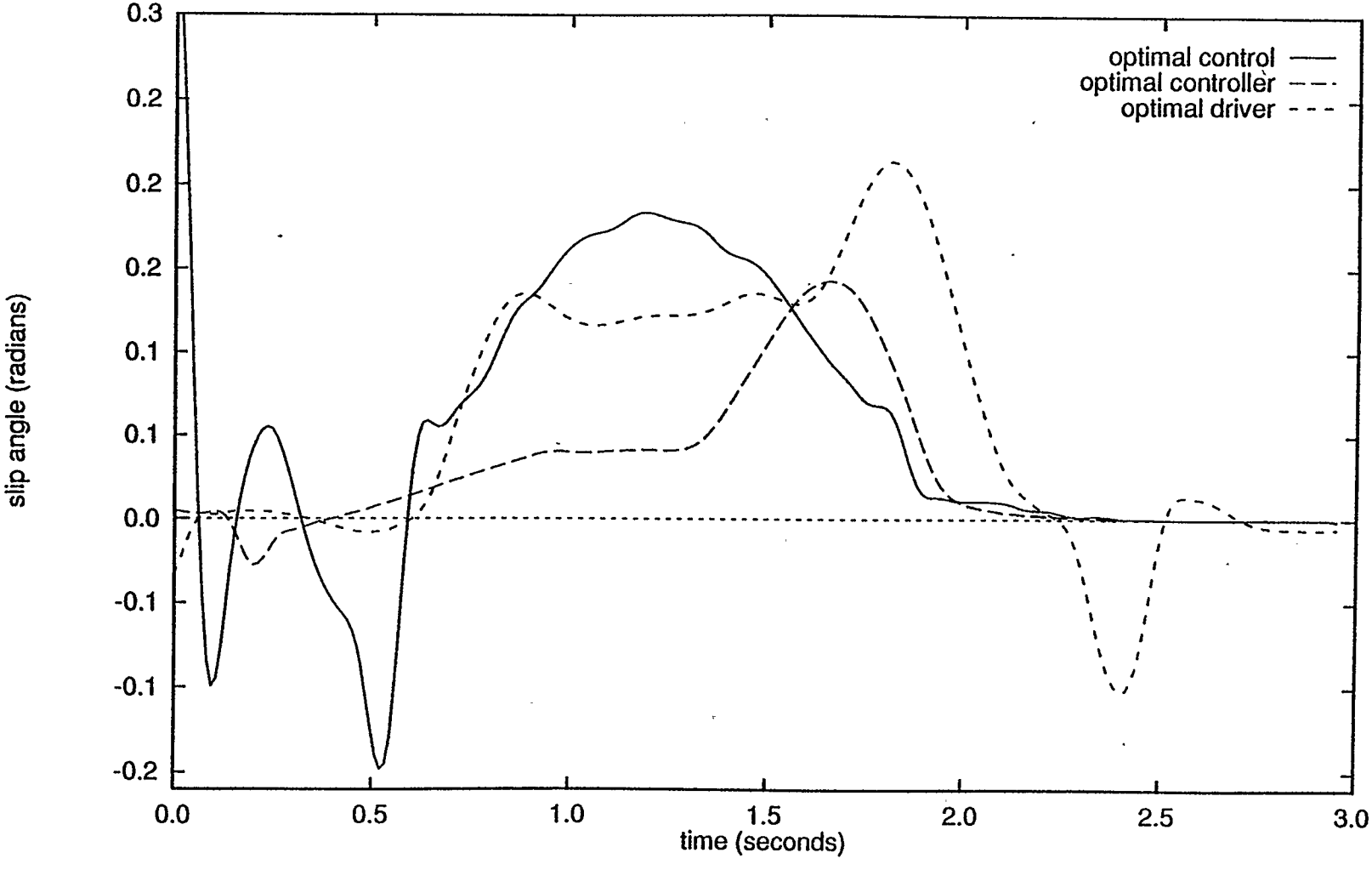

Figure 7.4.5: Front Slip Angles for Fast Corner Manoeuvre

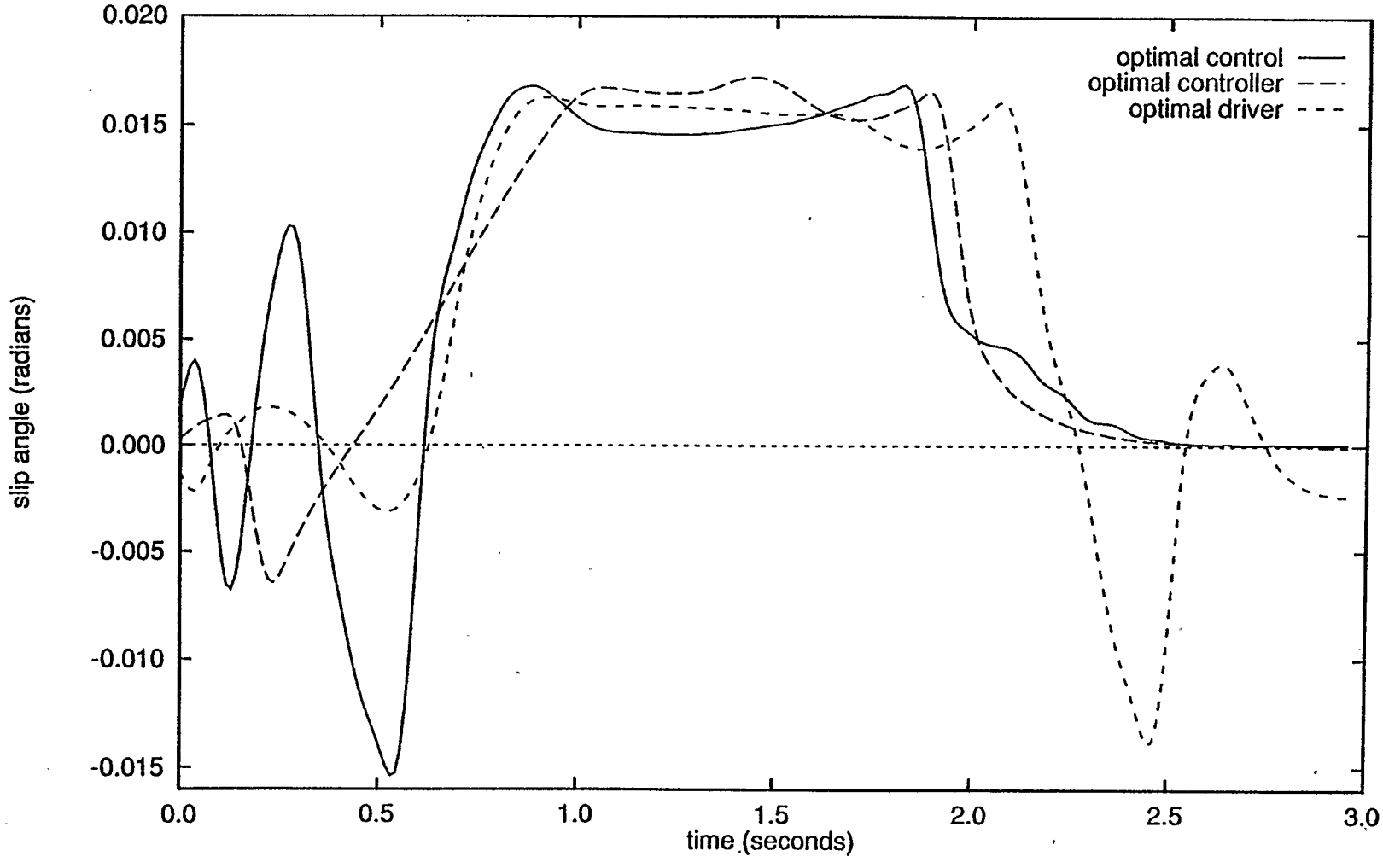

Figure 7.4.6: Rear Slip Angles for Fast Corner Manoeuvre

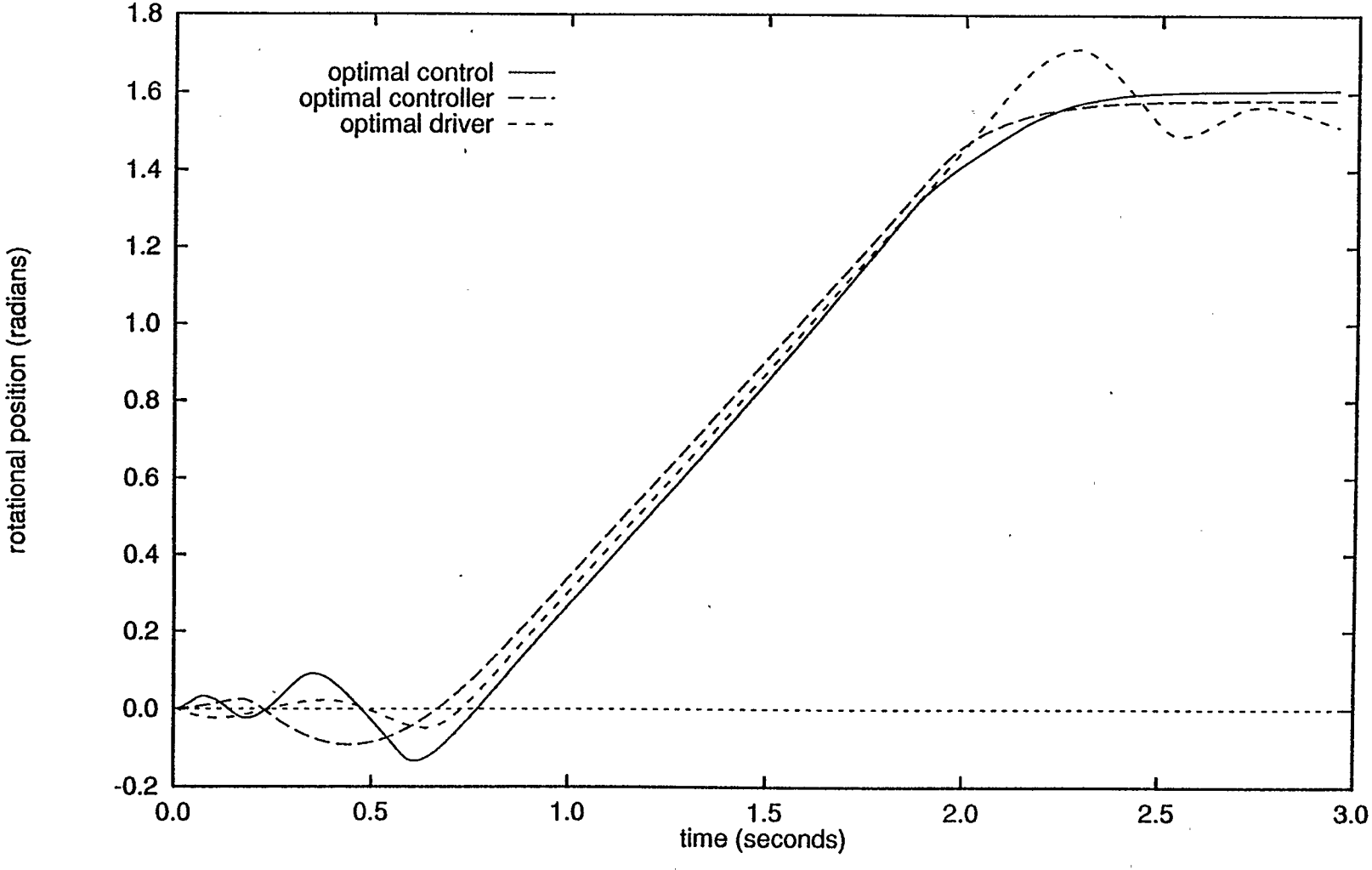

Figure 7.4.7: Rotational Positions for Fast Corner Manoeuvre

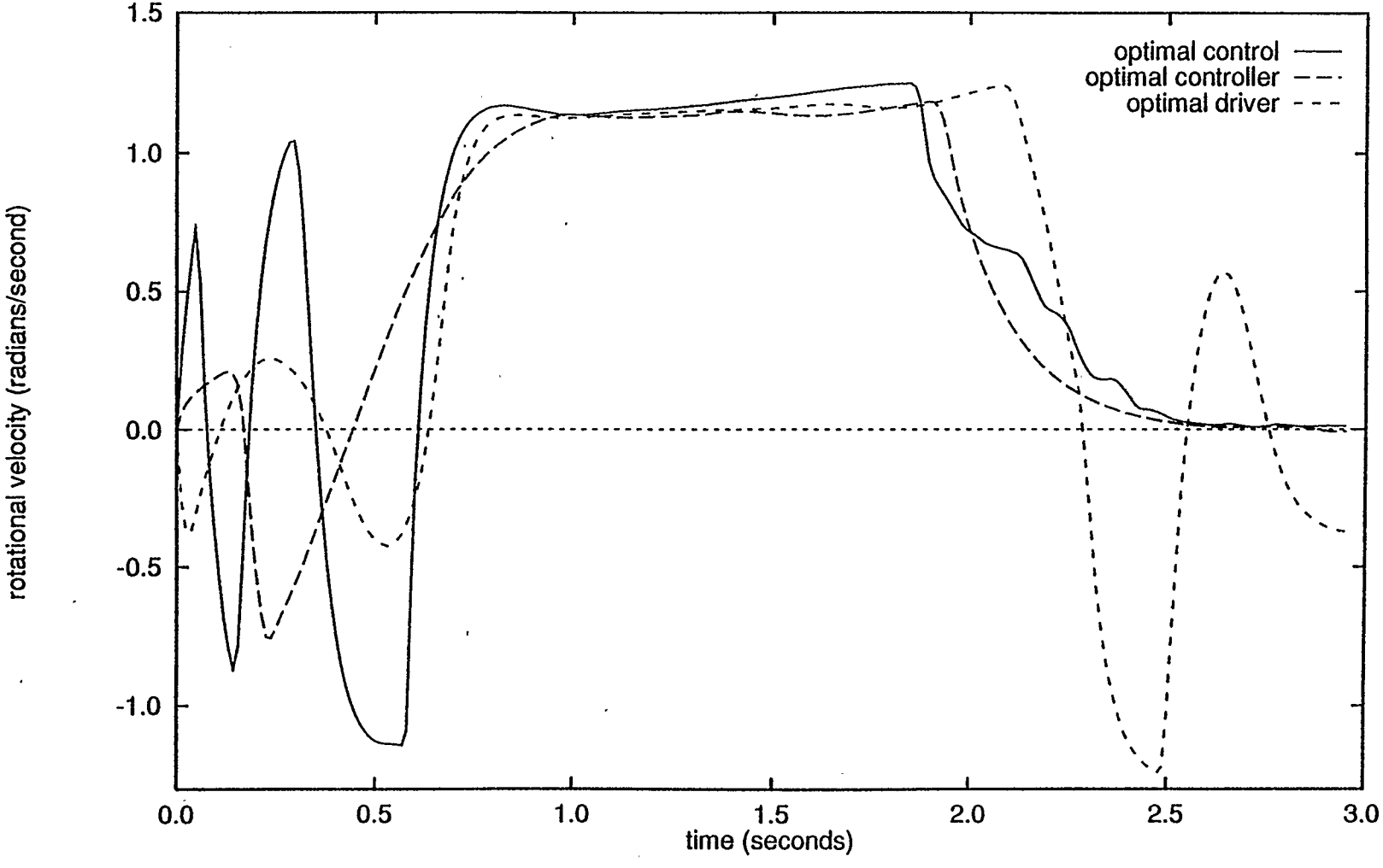

Figure 7.4.8: Rotational Velocity for Fast Corner Manoeuvre

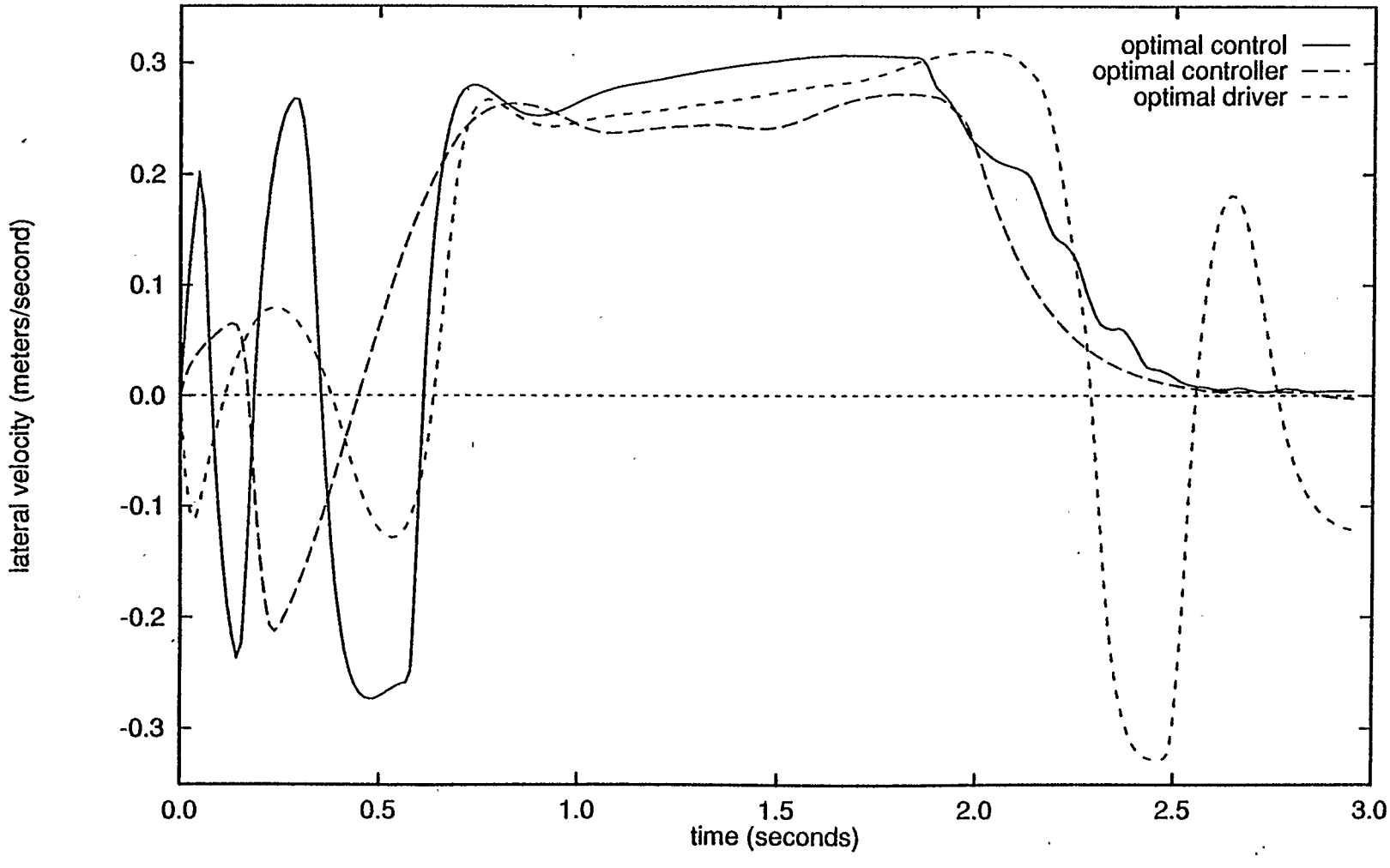

Figure 7.4.9: Lateral Velocity for Fast Corner Manoeuvre

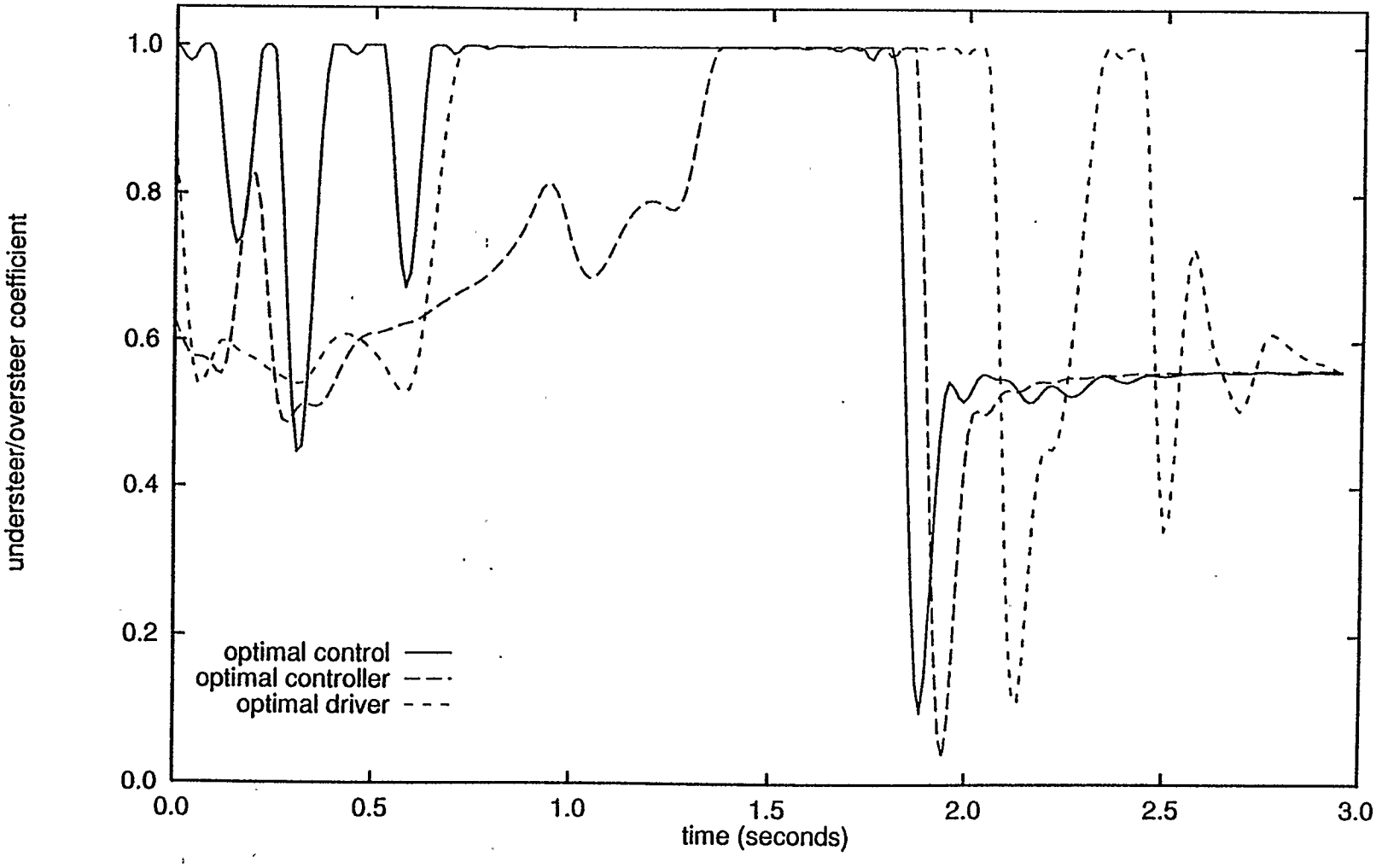

Figure 7.4.10: Understeer/Oversteer Coefficient for Fast Corner Manoeuvre

8 Conclusions Regarding the Use of Optimization Techniques in Vehicle Dynamics

The goal of this thesis is to improve upon the formulation and solution techniques for optimal control methods in simulating the control of a human driver. Success is measured by the degree of similarity between the optimal control results and the experimental test results, in terms of the form of the control and the accuracy of the vehicle's motion. In general, the form of the driver's inputs and those computed using the optimization methods agree, the motion which results from the numerically produced control values is suitable for the manoeuvre, and it is physically possible and probable for the driver.

While the numerical results show many similarities to the driver's results, there remains much research to be done to confirm the nature and extent of the similarities. This thesis reveals a general agreement between numerical and experimental results. Future research in this area must take into account:

1) Variations among drivers, and the effect of different vehicles and road conditions on them. For these tests, only one driver was used and relatively few tests were performed.

2) The vehicle model, which is only a crude approximation of the actual test vehicle and road conditions. In this case, the tire characteristics were largely approximated. These characteristics also change with road conditions and tire temperatures. The magnitude of the errors is difficult to estimate.

Even when these points are not taken into account, a reasonable correlation between the optimal control results and the driver's results can be achieved, all the more impressive in light of the simple cost function used.

Two forms of optimal techniques have been outlined here; optimal control and optimal controllers. For the type of path following problem examined in this thesis, both techniques can be recommended. For other situations, the deciding factor that distinguishes these techniques is the complexity of the problem. For example, the path

may be defined by the wide outer limits of a track, or by a set of pylons to be avoided. To find a good solution to this problem using a controller would require a much higher degree of complexity than that of the controller used in this thesis. Optimal control would likely be preferred, as it is more adaptable to constraints or non-uniform problems. However, an important advantage to using an optimal controller is that if it is powerful enough, the controller needs no modification to suit different problems; therefore, solution time for each problem is much shorter than it would be using optimal control.

One of the most important observations about the optimization results relates to the differences in steering input between the three optimization methods. Despite differences in steering input values, the tracking is extremely good, which suggests that there may be many ways of steering through a manoeuvre to produce acceptable tracking. If this is true, then care must be taken in any future studies not to rely too heavily on a single steering control history as an indicator of vehicle control or performance characteristics.

This work is an attempt at applying optimization methods to the simulation of the driver. Effective simulation, as demonstrated here, allows for improved methods of simulation, design, and control of road vehicles. The future holds further study in this area, both to strengthen the correlation between driver and optimal control methods, and to develop tools to utilize the methods in vehicle and roadway design.

References

1. Whitcomb, D.W. and W.F. Miliken, Jr., "Design Implications of a General Theory of Automobile Stability and Control', *Proc. I. Mech. E.* (A.D.), 1956

2. Ellis J.R., "Oversteer and Understeer", *Automobile Engineer*, May, 1963

3. Ellis, J.R., *Vehicle Dynamics*, Ellis, 1989

4. Legouis, T., Laneville, P., Bourassa, P. and Payre, G., "Vehicle/Pilot System Analysis: A New Approach Using Optimal Control With Delay", *Vehicle System Dynamics*, 16 (1987), pp. 279-295

5. McRuer, D.T. and Klein, R., "Mathematical Models of Human Pilot Behavior", *N.A.T.O. AGARDograph*, No. 188, 1974

6. Weir, D.H. and McRuer, D.T., "Dynamics of Driver Vehicle Steering Control", *Automatica*, Vol. 6, 1970, pp. 87-98

7. Garrot, W.R. et al., "Closed Loop Automobile Maneuvers Using Describing Function Models", SAE paper no. 820306

8. McLean, J.R. and Hoffman, E.D., "The Effect of Restricted Preview on Driver Steering Control and Performance", *Human Factors*, vol. 15, no. 4, August, 73, pp. 367-378

9. Kondo, M. and Ajimine, A., "Driver Sight Point and Dynamics of the Driver-Vehicle System Related to it", SAE paper no. 680104

10. Yoshimoto, K., "Simulation of Man-Automobile System by the Driver's Steering Model With Predictability", *Bulletin of J.S.M.E.*, 12(51), 1969, pp. 495-500

11. Thomas. R.E., "Development of New Techniques for Analysis of Human Controller Dynamics", *USAF, MRL*, TDR-62-65, 1962

12. MacAdam, C.C., "Applications of and Optimal Preview Control for Simulation of Closed-Loop Automobile Driving", *IEEE Transactions of Systems, Man, and Cybernetics*, Vol SMC-11, No 6, June 1981, pp. 393-399

13. Delp, P., Crossman, E.R.F.W. and Szostak, H., "Estimation of Automobile-Driver Describing Function From Highway Tests Using the Double Steering Wheel", *Seventh Conference on Manual Control*, pp. 223-236

14. Carson, J.M. and Wierwille, W.W., "Development of a Strategy Model of the Driver in Lane Keeping", *Vehicle System Dynamics*, 7 (1978), pp. 233-253

15. Hayhoe, G.F., "A Driver Model Based on the Cerebellar Model Articulation Controller", *Vehicle System Dynamics*, 8 (1979), pp. 49-72

16. Van Zanten, A.T., "*Optimal Control of the Tractor-Semitrailer Truck*", Ph.D. Thesis, Cornell University, Ithaca, 1974

17. Van Zanten, A.T. and A.I. Krauter, "Optimal Control of the Tractor-Semitrailer Truck", *Vehicle System Dynamics*, 7 (1978), pp. 203-231

18. Hatwal, H. and Mikulcik E.C., "An Optimal Control Approach to the Path Tracking Problem for an Automobile", *Transactions of the CSME*, Vol 10, No. 4, 1986, pp. 233-241

19. Hatwal, H. and Mikulcik E.C., "Some Inverse Solutions to an Automobile Path Tracking Problem with Input Control of Steering and Brakes", *Vehicle System Dynamics*, 15 (1986), pp 61-71

20. Press, W.H., Flannery, B.P., Teukolsky, S.A. and Vetterling, W.T., *Numerical Recipes in C*, Cambridge University Press, 1988, pp. 290-352

21. Nelder, J.A. and Mead,R., *Computer Journal,* 1965, vol 7, p.308

22. Kirk, D.E., *Optimal Control Theory*, Prentice-Hall, 1970, pp. 371-409

23. Radt Jr., H.S. and W.F. Miliken Jr., "Non-Dimensionalizing Tyre Data for Vehicle Simulation", *Road Vehicle Handling, Institution of Mechanical Engineers Conference Publications*, 1983, pp. 229-240

24. Moore, D.F., *The Friction of Pneumatic Tyres*, Elsevier Scientific Publishing Company, 1975

Appendix 1: The Derivation of the Equations of Motion Used

The equations used in this thesis to model the test vehicle's motion are quite simple and are equivalent to those used in other studies [3,18,19]. They allow for three degrees of freedom: two directional relative to the plane of travel, and one rotational about the vertical axis. The objective in choosing a simple model was to minimize computation while retaining sufficient complexity to allow for realism in the movements.

The base equations to describe the accelerations of the vehicle are

$$\begin{aligned} m(\ddot{x} - \dot{\theta}\dot{y}) &= \sum F_x \\ m(\ddot{y} + \dot{\theta}\dot{x}) &= \sum F_y \\ I\ddot{\theta} &= \sum T_\theta \end{aligned} \qquad \text{(A1.1)}$$

where m is mass

I is the moment of inertia about the vertical axis through the center of gravity

F_x and F_y are the longitudinal and lateral forces and

T_θ is torque about the vertical axis.

The x and y are measured relative to a coordinate system attached to the vehicle's center of gravity. The rotational angle, θ, is the rotation of the vehicle's coordinate system relative to the fixed reference, XY. The coordinate systems are shown in Figure A1.1.

The velocity components of the vehicle are

$$\begin{aligned} \dot{X} &= \dot{x}\cos\theta - \dot{y}\sin\theta \\ \dot{Y} &= \dot{x}\sin\theta + \dot{y}\cos\theta \end{aligned} \qquad \text{(A1.2)}$$

where X and Y are the axes on the fixed coordinate system.

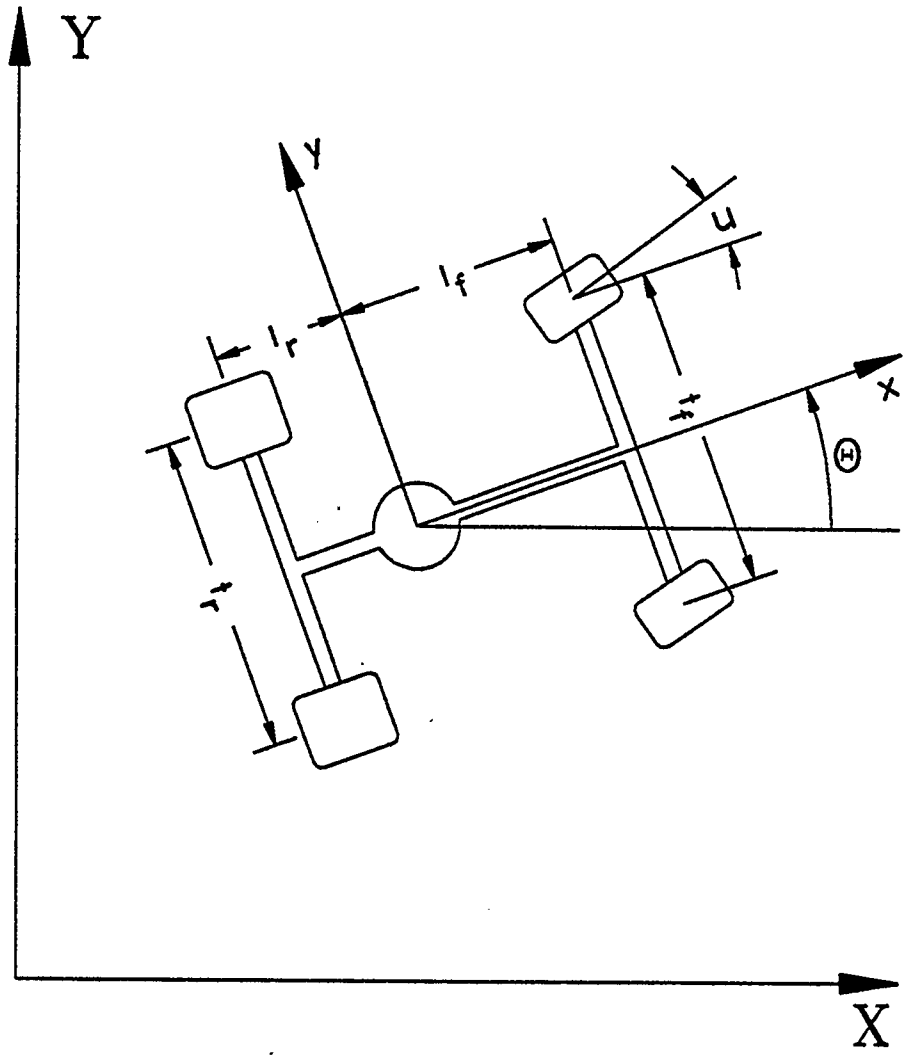

Figure A1.1: Vehicle Coordinate Systems

The equations may be written in state-space format with

$$\dot{X} = \dot{x}_1 = x_2 \cos x_5 - x_4 \sin x_5$$

$$\ddot{x} = \dot{x}_2 = x_6 x_4 + \frac{1}{m} \sum F_x$$

$$\dot{Y} = \dot{x}_3 = x_2 \sin x_5 + x_4 \cos x_5 \qquad \text{(A1.3)}$$

$$\ddot{y} = \dot{x}_4 = -x_6 x_2 + \frac{1}{m} \sum F_y$$

$$\dot{\theta} = \dot{x}_5 = x_6$$

$$\ddot{\theta} = \dot{x}_6 = \frac{1}{I} \sum T_\theta \quad .$$

The motion of the vehicle is found by integrating the state equations given the initial state vector, $\mathbf{x}_o$. The forces still remain to be defined.

Neglecting aerodynamic forces, the tires are the only mechanisms for generating force on the vehicle. The tire model considers only forces which act perpendicular to the plane of rotation of the tire; therefore rolling resistance and other tractive forces are neglected. The tire forces generated are

$$\sum F_y = (F_{fr} + F_{fl}) \cos u + (F_{rr} + F_{rl}) \qquad \text{(A1.4)}$$

where u is the steer angle. The tire forces longitudinally are

$$\sum F_x = -(F_{fr} + F_{fl}) \sin u \quad . \qquad \text{(A1.5)}$$

The torque about the vertical axis relative to the center of gravity of the vehicle is

$$\sum T_\theta = (F_{fr} + F_{fl}) l_f \cos \delta - (F_{rr} + F_{rl}) l_r + (F_{fr} + F_{fl}) \frac{t_f}{2} \sin \delta \quad . \qquad \text{(A1.6)}$$

The tire forces were calculated from the equations given by Radt and Miliken [23] and used in [18] and [19]. The forms of these equations are presented in Section 5 of this thesis.

Appendix 2: Description of the Test Instrumentation Used for Vehicle Testing

In the experimental work's early planning stages, it was decided that a computer controlled instrumentation system would be required. The design goals identified were that the system must be light, compact and rugged, and that due to the electrically noisy environment created by the engine, the equipment must be designed and shielded correctly. Financial restrictions, and a general inability to find a commercially available system exactly suited to the need, led to the decision to design and build it.

The variables to be measured were the vehicle's speed and the steer angle. Also needed was some method for indicating the beginning of the manoeuvre. Jack Dyck, of Valmet Automation (Canada) Ltd., designed an instrumentation card based upon specifications given by the author. The printed circuit board for the instrumentation was built and assembled by the author. Valmet Automation provided the microprocessor, a Hitachi HD64180 based CPU card approximately 10 cm X 16 cm. It had an input/output bus with 19-bit address space and 8-bit data bus. A backplane board attached the instrumentation card to the CPU card.

The instrumentation card was equipped with the following:

1) Hewlett-Packard HCTL-2000 Quadrature Decoder/Counter Interface IC: This chip was used for determining steering angle. It is the standard interface chip for Hewlett-Packard shaft encoders. A HP HEDS-5000 shaft encoder was attached to the steering column and measured steering wheel angle. The shaft encoder has a resolution of 500 counts per revolution.

2) Intel 8254 Programmable Interval Timer: Used in conjunction with an optical switch and slotted disk attached to the rear axle, this determined the rotational velocity of the rear wheels.

3) ADC 1210 Analog to Digital Converter: This 12 bit analog to digital converter was not used in these tests, but was intended for use in future experiments, most likely with strain gauges or accelerometers.

5) Digital Input: Eight digital input lines were available for use; only one was used in testing. It was attached to a switch to be activated when initiating the collection of data. The switch was mounted on the steering wheel.

Data collection commenced at the beginning of each manoeuvre when the driver depressed the switch mounted to the steering wheel. The data was collected at a rate of 100 samples per second for a period of about 10 seconds, after which the vehicle was stopped and the data transferred from the on-board computer to the floppy disk of a portable computer.

Appendix 3: A Method for Estimating the Cornering Stiffness of a Tire

A fundamental operating characteristic of pneumatic tires is cornering stiffness, defined as the change in lateral force generated by the tire with change in slip angle, the slip angle being the angle between the plane of the rotation of the tire and its direction of travel. The cornering stiffness may be determined experimentally using an apparatus which holds a tire on a moving surface and measures the forces generated by the tire. However, these tire-testers were too expensive to be built for this project, and existing ones are usually too large for kart tires. Because tire data was otherwise not available, an inexpensive method for estimating a tire's cornering stiffness was devised. The method employs a mathematical tire model similar to the taut string models and beam models [3].

Rubber is a visco-elastic material with some unusual frictional properties [24]. On the molecular level, its long polymer chains do not appear to slide over a surface as with most materials; instead, the ends of the molecules will attach to the surface. If a force is applied, a molecule will stretch and not detach from a particular point, unless the molecule chain or the contact breaks. This has the effect on a rolling tire that as the tire surface enters the contact patch, the rubber molecules will attach to the road unstretched. This will create a boundary condition for calculation of the forces in the contact patch, namely that all forces are zero at the beginning. For low cornering forces, the bonds between the road and the tire surface will not break at any point in the contact patch. The lateral forces produced will increase in an approximately linear manner until the end of the contact patch, where the molecular bonds break as the tire leaves the road surface. The deflection caused by the stretching of the molecules is assumed to be very small compared to deflections of the tire which are due to the elasticity of the tire body.

A tire is shown rolling on a surface in Figure A3.1, where the rotation angle of the axle $\alpha = 0$ is zero. In Figure A3.2, the tire is shown with its axle rotated at an angle of α about the vertical axis. The coordinate system $x'\,y'$ is attached to the axle and will also rotate about the vertical axis. As this model is concerned with predicting the tire characteristics near $\alpha = 0$, this angle will be assumed to be very small.

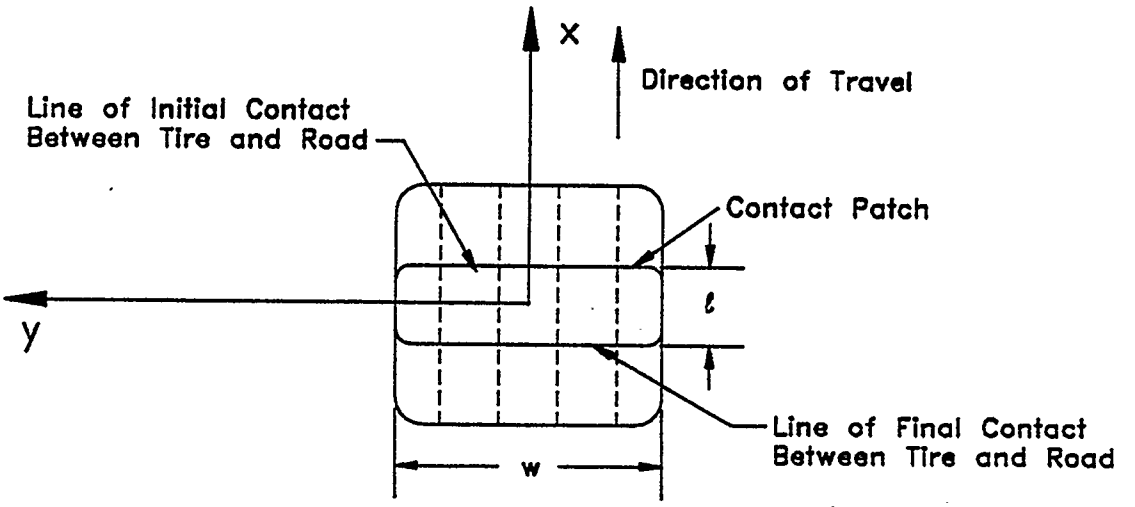

FIGURE A3.1: Tire in No Slip Condition

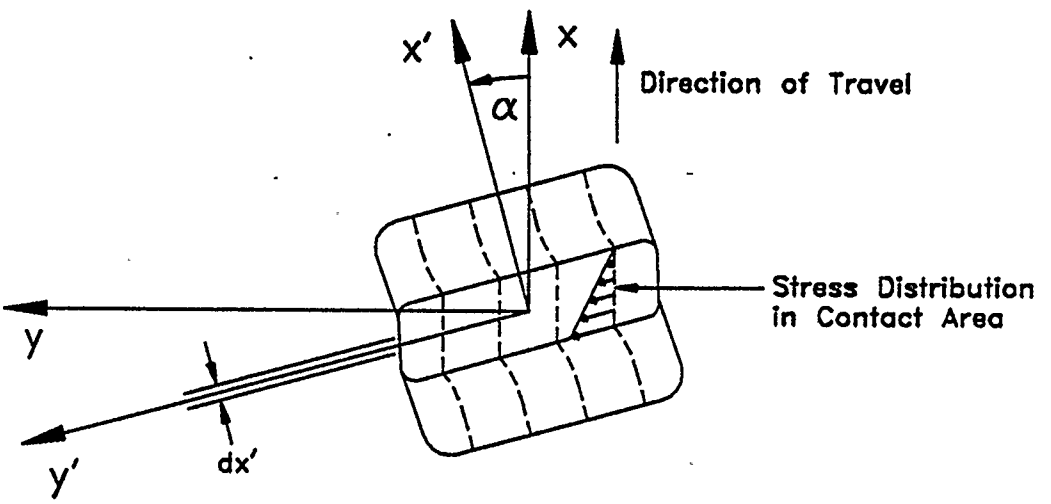

FIGURE A3.2: Tire with Slip Angle Applied

Because there is no slip in the contact patch, the twisting of the contact area of the tire relative to the axle creates a moment about the vertical axis. The tire body is considered to have a torsional stiffness of K_α.

A strip along the contact patch has the area $w \cdot l$ where w is its width and l the length where both are measured relative to the rotating axis. The shear stress in the y' direction is

$$\tau_y = \left(\frac{l}{2} - x'\right)\frac{\tau_m}{l} \tag{A3.1}$$

where τ_m is the maximum shear stress, found at the rear of the contact patch. If the axle is rotated an angle α about the vertical axis, summing the moment about the center of the tire would, neglecting dynamic effects, give

$$\Sigma M = 0 \tag{A3.2}$$

so

$$0 = K_\alpha \alpha - \int_{-\frac{l}{2}}^{\frac{l}{2}} \left(\frac{l}{2} - x'\right)\frac{\tau_m}{l} w x' dx' . \tag{A3.3}$$

Performing the integration and solving for α gives

$$\alpha = \frac{-\tau_m \left(\frac{l^2}{12}\right) w}{K_\alpha} . \tag{A3.4}$$

In equilibrium, the force in the y' direction, $F_{y'}$, is obtained from

$$F_{y'} = \int_{-\frac{l}{2}}^{\frac{l}{2}} \left(\frac{l}{2} - x' \right) \frac{\tau_m}{l} w \, dx' \qquad \text{(A3.5)}$$

from which

$$F_{y'} = \tau_m w \frac{l}{2}. \qquad \text{(A3.6)}$$

As mentioned earlier, the cornering stiffness is the change in lateral force produced by a change in the slip angle. Therefore, combining equations A3.4 and A3.6 gives the cornering stiffness

$$c = \frac{F_{y'}}{\alpha} = \frac{6K_\alpha}{l}. \qquad \text{(A3.7)}$$

Equation A3.7 shows that for small slip angles, the cornering stiffness depends upon K_α, the torsional stiffness of the tire, and l, the length of the contact patch. To measure these values for the experimental tires, a small test apparatus was constructed, consisting mainly of a yoke which rigidly held the axle but did not touch the tire body. A down-force equal to the static load from the test vehicle was applied to the yoke through a thrust bearing which allowed free rotation of the yoke about the vertical axis. An epoxy based adhesive held the contact patch of the tire to a rigid surface, first ensuring that the desired vertical loading was applied before the adhesive could set. Torque was applied to the yoke using a torque wrench attached to the bottom of the thrust bearing. Dial gauges were used to measure the yoke's rotational deflection. Using these torque and deflection measurements, the torsional stiffness, K_α, was determined to be 310 *Nm* for the front and 1200 *Nm* for the rear; after the tire was removed, the contact patch length was found by

measuring the length of the epoxy contact area. The patch length was 0.08 m for the front and 0.09 m for the rear. Therefore, the front and rear cornering stiffnesses were estimated to be 23000 N and 81000 N, respectively.

Appendix 4: A Coefficient of Understeer/Oversteer as an Indicator of a Vehicle's Control Characteristics

Understeer and oversteer are commonly used to describe a vehicle's dynamic characteristics. The formal definition of understeer is that the slope of the plot of steady-state lateral acceleration versus steer angle is positive. A negative value indicates an oversteer and an infinite slope indicates neutral steer. As an example, an understeer vehicle will have to increase its steer angle in order to travel at a higher speed through a circle of a certain radius. The driver will likely feel that the vehicle's front end tends to lose its grip, while the rear tires adhere very well. The oversteer vehicle will have a decrease in steer angle as speed increases. The vehicle will feel as if the rear tires have insufficient grip, so the vehicle wants to 'spin out'.

For a planar linear vehicle model of the type discussed in Appendix 1, understeer, oversteer and neutral steer vehicles have the following properties [2,3].

$$\begin{aligned} c_f l_f < c_r l_r \quad & \textit{understeer} \\ c_f l_f = c_r l_r \quad & \textit{neutral steer} \\ c_f l_f > c_r l_r \quad & \textit{oversteer} \end{aligned} \tag{A4.1}$$

where l_f and l_r are the distances from the center of gravity to the front and rear axles, and c_f and c_r are the front and rear cornering stiffnesses, respectively. The cornering stiffness is defined by the change in lateral force for a change in tire slip angle. A planar linear vehicle will maintain the same degree of understeer or oversteer at all times. This is not likely to be the case for vehicles with nonlinear tire characteristics.

A simple method of showing any changes to the degree of understeer or oversteer for nonlinear vehicles is useful. While equation A4.1 is exact only for linear vehicles, the type of steer be approximated by this equation. The method of representing this graphically shown below will be referred to as the coefficient of understeer/oversteer $C_{u/o}$.

$$if\begin{cases} c_f l_f < c_r l_r & \mathbf{C}_{u/o} = \dfrac{c_f l_f - c_r l_r}{c_r l_r} \\ c_f l_f > c_r l_r & \mathbf{C}_{u/o} = \dfrac{c_f l_f - c_r l_r}{c_f l_f} \\ c_f l_f = c_r l_r & \mathbf{C}_{u/o} = 0 \end{cases} \qquad \text{(A4.2)}$$

The coefficient may take on any value between 1.0 and -1.0. A value of 0.0 indicates a neutral steering vehicle. As the coefficient approaches 1.0 the understeer becomes more severe. The oversteer becomes more extreme as the value approaches -1.0.

This is a simple method of approximating a vehicle's instantaneous control characteristics. It does not, however, indicate how the vehicle operates over the entire operating range or how close it might be to reaching its limits of controllability. For example, it does not necessarily indicate the proximity to side-force saturation of the tire; if a vehicle is very close to saturating both front and rear tires, then the understeer/oversteer coefficient will mean very little, as the response from the tires at that moment will also be very small.